

The Function of Synaptotagmin 7 in Mouse Cytotoxic T Lymphocytes

Dissertation

zur Erlangung des Grades

des Doktors der Naturwissenschaften

der Naturwissenschaftlich-Technischen Fakultät

der Universität des Saarlandes

von

Marwa W. Sleiman

Saarbrücken

2019

Tag des Kolloquiums: 19.06.2020

Dekan: Prof. Dr. Guido Kickelbick

Berichterstatter/in: Prof. Dr. Jens Rettig

Prof. Dr. Frank Schmitz

Vorsitz: Prof. Dr. Adolfo p. Cavalie´

Akad. Mitarbeiter: Dr. Jens Neunzig

Disclosure:

This work was funded by:

The **Sonderforschungsbereich** 894 SFB894:

Calcium Signals: Molecular Mechanisms and Integrative Functions
from April 14, 2014 till July 31, 2018

All experiments were executed in the department of Cellular Neurophysiology, Prof. Dr. Jens Rettig Laboratory, CIPMM – University of Saarland, 66421 Homburg, Germany.



UNIVERSITÄT
DES
SAARLANDES



Anlage I

Erklärung gemäß § 7 Abs. 1 Nr. 4

Ich erkläre hiermit an Eides statt, dass ich die vorliegende Arbeit ohne unzulässige Hilfe Dritter und ohne Benutzung anderer als der angegebenen Hilfsmittel angefertigt habe. Die aus anderen Quellen direkt oder indirekt übernommenen Daten und Konzepte sind unter Angabe der Quelle gekennzeichnet.

Bei der Auswahl und Auswertung folgenden Materials haben mir die nachstehend aufgeführten Personen in der jeweils beschriebenen Weise unentgeltlich/entgeltlich geholfen:

1. Chairman: Prof. Adolfo. Cavalie´
2. Examiner 1: Prof. Jens Rettig
3. Examiner 2: Prof. Frank Schmitz
4. Academic member: Dr. Jens Neunzig

Weitere Personen waren an der inhaltlich-materiellen Erstellung der vorliegenden Arbeit nicht beteiligt. Insbesondere habe ich nicht die entgeltliche Hilfe von Vermittlungs- bzw. Beratungsdiensten (Promotionsberater/innen oder anderer Personen) in Anspruch genommen. Außer den Angegebenen hat niemand von mir unmittelbar oder mittelbar geldwerte Leistungen für Arbeiten erhalten, die im Zusammenhang mit dem Inhalt der vorgelegten Dissertation stehen.

Die Arbeit wurde bisher weder im Inland noch im Ausland in gleicher oder ähnlicher Form in einem anderen Verfahren zur Erlangung des Doktorgrades einer anderen Prüfungsbehörde vorgelegt.

Ich versichere an Eides statt, dass ich nach bestem Wissen die Wahrheit gesagt und nichts verschwiegen habe.

Vor Aufnahme der vorstehenden Versicherung an Eides Statt wurde ich über die Bedeutung einer eidesstattlichen Versicherung und die strafrechtlichen Folgen einer unrichtigen oder unvollständigen eidesstattlichen Versicherung belehrt.

Ort, Datum

Unterschrift der/des Promovierenden

Unterschrift der die Versicherung an Eides statt aufnehmenden Beamtin bzw. Des aufnehmenden Beamten.

Dedicated to
Mom and Dad

ACKNOWLEDGEMENTS

Foremost, I would like to thank my Chef Professor Jens Rettig with sincere gratitude and respect for his great knowledge and continuous support and motivation. You have been a great leader.

My appreciation goes as well to my supervisor Dr. David R. Stevens for his unceasing care, support, understanding and great scientific input throughout my PhD.

I would like to give a lot of thanks to Dr. Ute Becherer for her continuous support and great contribution to my project.

I appreciate and thank the help and support of Prof. Olaf Pongs, Prof. Roy Lancaster, Dr. Elmar Klause, Dr. Claudia Schirra, Dr. Varsha Pattu, and Dr. Ulrike Hahn. Scientific advice and discussions were always fruitful.

I truly appreciate the help of our sweet technicians Anja Bergsträßer, Margarete Klose, Katrin Sandmeier, Anne Weinland, Jacqueline Vogel, Tamara Paul, Nicole Rothgerber, and Silke Bruns-Engers.

Thanks a lot to the nice help of Bernadette Schwarz, Andrea Berger, and Josephine Kretschmer from the secretary, and Holger Frisch from the IT department.

I would like to acknowledge Marina Wirth for her amazing and appreciated organization and handling of mouse breeding.

I am grateful to the amazing company of my colleagues Olga Ratai, Angelina Staudt, Praneeth Chitirala, Keerthana Ravichandran, Hsin Fang Chang, Mazen Makke, Dalia Ansary, and former colleagues Hawraa Bzeih, Ali Shaib, Ali Harb, and Ahmad Shaaban. You made this journey remarkable. I would like to thank Dalal Haidar and Ibrahim Haidar as well for being my Lebanese family in Germany.

After all, what I have achieved today would have been impossible without my family. Dad and Mom, your pure love, guidance, and support were key in every step in my life. I love you beyond words. Maysa and Maya, you are not only my sisters, you are my dearest friends. You've been and will always be idols. Ali, my other half, you've been endlessly amazing with your love and care. You've been a true survivor through five years of distance relationship. I am proud of who you are. Thank you.

Marwa

TABLE OF CONTENTS

Disclosure	Page 3
Anlage I	Page 4
Dedication	Page 5
Acknowledgements	Page 6
Table of Contents	Page 7
List of Figures	Page 11
List of Tables	Page 13
List of Abbreviations	Page 14
Abstract	Page 20
Zusammenfassung	Page 21
I. INTRODUCTION	Page 22
I.1 The Immune System	Page 22
I.1.1 Innate and adaptive immunity	Page 22
I.1.2 Cytotoxic T lymphocytes	Page 24
I.1.2.1 The immunological synapse	Page 26
I.1.2.2 Store-operated calcium entry	Page 27
I.2 Exocytosis	Page 29
I.2.1 The SNARE protein machinery	Page 29
I.2.2 Docking, priming, and fusion of cytotoxic granules	Page 30
I.2.2.1 Docking	Page 30
I.2.2.2 Priming	Page 31
I.2.2.3 Fusion	Page 32
I.3 Synaptotagmins	Page 33
I.3.1 Synaptotagmin 7: The ubiquitous protein with multiple functions	Page 34
I.3.1.1 Syt7 expression	Page 34

I.3.1.2 Syt7 localization	Page 35
I.3.1.3 Syt7 functions	Page 36
I.3.1.4 Functional properties of C2 domains of Syt7	Page 36
I.4 Aim of the Thesis	Page 38
II. MATERIALS AND METHODS	Page 39
II.1 Materials	Page 39
II.1.1 Chemicals	Page 39
II.1.2 Solutions for cell culture	Page 41
II.1.2.1 RPMI 1640 (10% FCS)	Page 41
II.1.2.2 IMDM (10% FCS)	Page 41
II.1.2.3 Isolation buffer	Page 42
II.1.2.4 Erythrolysis buffer	Page 42
II.1.3 Solutions for cell fixation and staining	Page 42
II.1.3.1 Paraformaldehyde (15% PFA)	Page 42
II.1.3.2 Permeabilization solution	Page 42
II.1.3.3 Blocking solution	Page 42
II.1.3.4 Mounting medium	Page 43
II.1.4 Solutions for Cloning	Page 43
II.1.4.1 LB medium	Page 43
II.1.4.2 Loading buffer	Page 43
II.1.5 Solutions for TIRF experiments	Page 43
II.1.5.1 T cell extracellular solution (no CaCl ₂ added)	Page 43
II.1.5.2 T cell extracellular solution (10 mM Ca ²⁺)	Page 44
II.1.5.3 NH ₄ Cl (40 mM)	Page 44
II.1.6 Solutions for Calcium Imaging	Page 45
II.1.6.1 Fura-2ff calibration solutions	Page 45
II.1.7 Solutions for Western Blotting	Page 45
II.1.7.1 Lysis buffer	Page 45

II.1.7.2 TBS (10x)	Page 46
II.1.7.3 TBST (0.1%)	Page 46
II.1.8 Kits	Page 46
II.1.8.1 Kits for cloning	Page 46
II.1.8.2 Kits for cell culture	Page 46
II.1.9 Antibodies	Page 47
II.1.10 Bacteria	Page 47
II.1.11 Mouse Strains	Page 47
II.1.12 Plasmids	Page 47
II.1.12.1 Syt7 α -pMAX-IRES-GFP	Page 47
II.1.12.2 D227N mutant	Page 50
II.1.12.3 3DN mutant	Page 50
II.1.13 siRNA	Page 50
II.1.14 Software	Page 50
II.1.14.1 Primer Design	Page 50
II.1.14.2 Cloning	Page 51
II.1.14.3 Image Analysis	Page 51
II.1.14.4 Statistics and Figures	Page 51
II.2 Methods	Page 51
II.2.1 Positive isolation of CD8⁺ T lymphocytes	Page 51
II.2.2 Cell splitting and transfection	Page 52
II.2.3 RNA extraction	Page 52
II.2.4 CDNA synthesis: reverse transcription	Page 54
II.2.5 Polymerase Chain Reaction PCR	Page 54
II.2.6 Preparation of anti-CD3 coated coverslips	Page 55
II.2.7 Immunocytochemistry	Page 55
II.2.8 Western blotting	Page 56
II.2.9 Structured Illumination Microscopy (SIM)	Page 57

II.2.10 Total Internal Reflection Fluorescence Microscopy (TIRF)	Page 58
II.2.11 Calcium imaging	Page 59
II.2.11.1 Measurement of intracellular free calcium using Fura-2	Page 59
II.2.11.2 Measurement of extracellular free calcium using Fura-2ff	Page 61
II.2.12 NH ₄ Cl treatment	Page 61
III. RESULTS	Page 62
III.1 The experimental setup	Page 62
III.2 The expression profile of synaptotagmins in mouse CTLs	Page 64
III.3 The localization of Syt7 in mouse CTLs	Page 66
III.4 CG fusion in WT and Syt7 KO cells	Page 67
III.4.1 The secretion probability is similar between WT and Syt7 KO CTLs	Page 68
III.4.2 A second round of secretion is not possible in Syt7 KO CTLs	Page 70
III.4.3 Rescue of Syt7 KO cells with Syt7 overexpression	Page 73
III.5 The cytosolic calcium concentration is unchanged in Syt7 KO cells	Page 76
III.6 Syt7 promotes CG trafficking to the immunological synapse	Page 78
III.7 Syt7 regulates the fusion pore opening of cytotoxic granules in mouse CTLs	Page 81
III.8 Synaptotagmin 2 in mouse cytotoxic T lymphocytes	Page 86
IV. DISCUSSION	Page 89
IV.1 Cytotoxic granule release is regulated by Syt2 and Syt7	Page 91
V. CONCLUSION and OUTLOOK	Page 93
Bibliography	Page 95
Resume	Page 107

LIST OF FIGURES

Figure 1: The innate and adaptive immune systems

Figure 2: Three killing pathways by cytotoxic T lymphocytes (CTLs)

Figure 3: The immunological synapse

Figure 4: The major TCR-mediated signaling pathways in T cells

Figure 5: Description of the SNARE proteins

Figure 6: Vesicle docking, priming, and fusion by SNAREs and SNARE-associated proteins

Figure 7: General structure of a synaptotagmin

Figure 8: Syt7 domains and calcium-binding loops

Figure 9: Syt7 α -pMAX-IRES-GFP map and Syt7 α forward and reverse primers

Figure 10: Cloning Syt7 α into pMAX-IRES-GFP vector

Figure 11: Checking RNA quality by denaturing RNA gel electrophoresis

Figure 12: Verification of cDNA quality

Figure 13: Principle of TIRF microscopy

Figure 14: The fluorescence excitation spectra of Fura-2 under different free calcium concentrations from 0 to 39.8 μ M

Figure 15: CG fusion in TIRF microscopy

Figure 16: The expression profile of the synaptotagmin family in mouse activated CTLs and brain cells

Figure 17: The localization of Syt7 in mouse CTLs

Figure 18: Fura-2ff calibration curve

Figure 19: No difference in the fusion probability nor the fusion latency between WT and Syt7 KO cells

Figure 20: CG fusion in WT and Syt7 KO cells

Figure 21: CG secretion after WT and mutant Syt7 overexpression

Figure 22: The cytosolic free calcium concentration is unchanged in Syt7 KO cells

Figure 23: The mean number of granules in TIRF field over time (s) in low and high Ca²⁺

Figure 24: The mean number of CGs in TIRF field over time (s) in low Ca^{2+} only

Figure 25: CG count in whole cell

Figure 26: Syt7 overexpression leads to slower emptying of GranzymeB from cytotoxic granules

Figure 27: Syt7 regulates the fusion pore expansion

Figure 28: Syt2 protein expression in day3 activated WT and Syt7 KO cells

Figure 29: Cytotoxic granule fusion is reduced as Syt2 expression is downregulated by siRNA

LIST OF TABLES

Table 1: Composition of Fura-2ff calibration solutions

Table 2: Duration and applied temperatures of PCR

Table 3: The list of primers, annealed exons, annealing temperatures, and the PCR band sizes

LIST OF ABBREVIATIONS

°C	Degrees Celsius
α	alpha
A	Adenine
am	acetoxymethyl
APC	Antigen presenting cell
ATP	Adenosine triphosphate
a.u.	arbitrary units
β	beta
BCR	B cell receptor
BH3	Bcl-2 homology domain 3
BID	BH3 interacting-domain death agonist
β ME	β -mercaptoethanol
bp	Base pair
BSA	Bovine serum albumin
C	Cytosine
$[Ca^{2+}]_i$	Intracellular calcium concentration
CD	Cluster of differentiation
cDNA	Coding DeoxyriboNucleic Acid
CG	Cytotoxic granule
CO ₂	Carbon dioxide
CRAC	calcium release activated channels
cSMAC	central supramolecular activation cluster
CTL	Cytotoxic T Lymphocyte
DAG	diacylglycerol

DH5 α	<i>Escherichia coli</i> competent cells: F ⁻ endA1 glnV44 thi-1 recA1 relA1 gyrA96 deoR nupG purB20 ϕ 80dlacZ Δ M15 Δ (lacZYA-argF)U169, hsdR17(rK ⁻ mK ⁺), λ ⁻
DISC	death-inducing signaling complex
DMEM	Dulbecco's modified eagle medium
DMSO	Dimethyl sulfoxide
DNA	DeoxyriboNucleic Acid
dNTP	DeoxyriboNucleotide TriPhosphate
DPBS	Dulbecco's phosphate buffered saline
DPTA	Diethylenetriaminepentaacetic acid
DR	Death receptor
dSMAC	distal supramolecular activation cluster
DTT	1,4-Dithiothreitol
<i>E. coli</i>	<i>Escherichia coli</i>
EDTA	Ethylenediaminetetraacetic acid
EGTA	Ethylene glycol tetra-acetic acid
Em	Emission
EMCD	Electron magnetic circular dichroism
ER	Endoplasmic reticulum
EtBr	Ethidium Bromide
FADD	Fas-associated death domain
Fas	First apoptosis signal
FCS	Fetal calf serum
FHL	familial hemophagocytic lymphohistiocytosis
γ	gamma
G	Guanine
g	gram
GAPDH	Glyceraldehyde 3-phosphate dehydrogenase

GFP	Green fluorescent protein
GLUT4	Glucose transporter 4
GS2	Griscelli syndrome type 2
GTPase	Guanosine Triphosphate hydrolase
GzmB	GranzymeB
h	hour
H ⁺	Hydrogen ion
HEPES	4-(2-Hydroxyethyl)-1-piperazineethanesulfonic acid
HPLC	High performance liquid chromatography
HRPT	Hypoxanthine Guanine Phosphoribosyl Transferase
Hz	Hertz
IFN	Interferon
IP3	Inositol triphosphate 3
IRES	Internal Ribosomal Entry Site
IS	Immunological synapse
ITAM	Immune-receptor tyrosine-based activation motifs
K ⁺	Potassium
Kb	Kilo base
KCl	Potassium chloride
Kd	Dissociation constant
KHCO ₃	Potassium bicarbonate
KO	Knockout
λ	Lambda
L	Liter
LAT	Linker for activation of T-cells family member 1
LB	Loading buffer
LB-medium	Lysogeny Broth-medium

LFA-1	Lymphocyte function-associated antigen 1
M	Mol/L
m	meter
m-	milli
M-	Mega
MAPK	mitogen-activated protein kinase
MES	2-(<i>N</i> -morpholino)ethanesulfonic acid
Mg ²⁺	Magnesium ion
MHC	Major Histocompatibility Complex
min	minute(s)
MIP	maximal intensity projection
MOPS	(3-(<i>N</i> -morpholino)propanesulfonic acid)
MTOC	microtubule organization center
MW	Molecular weight
n	number of experiments
n-	nano
NaCl	Sodium chloride
NaCHO ₃	Sodium bicarbonate
NH ₃	Ammonia
NH ₄ Cl	Ammonium chloride
NK	Natural Killer cell
Ori	Origin of replication
P	Probability value
p-	Pico
PBS	Phosphate buffer saline
PCR	Polymerase chain reaction
Pen/Strep	Penicillin/Streptomycin

pH	Potential Hydrogen
PFA	Paraformaldehyde
<i>Pfu</i>	<i>Pyrococcus furiosus</i> polymerase
PIP2	phosphatidylinositol-(4,5)-bisphosphate
pKa	the acid dissociation constant at logarithmic scale
PKC	Protein kinase C
PLC γ 1	phospholipase C gamma 1
PM	Plasma membrane
PMSF	Phenylmethylsulfonyl fluoride
PS	phosphatidylserine
pSMAC	peripheral supramolecular activation complex
Rcf	Relative centrifugal force
RNA	Ribonucleic Acid
ROI	Region of interest
rpm	round per minute
RPMI	Roswell Park Memorial Institute
RRP	Readily releasable pool
rRNA	Ribosomal Ribonucleic acid
RT	Room temperature
s	second(s)
SDS	Sodium dodecyl Sulfate
sem	standard error of the mean
SNAP-25	Synaptosomal-associated protein-25
SNARE	Soluble N-Ethylmaleimide-sensitive factor attachment receptor
SOCE	Store-operated calcium entry
STIM	stromal-interacting molecule
Syt	Synaptotagmin

T	Tau
T	Thymine
TAE	Tris-Acetate-EDTA
<i>Taq</i>	<i>Thermus aquaticus</i>
TCR	T cell receptor
T _h	T helper
TIRFm	Total internal reflection fluorescence microscopy
TM	Trademark
TMD	Transmembrane domain
TMR	Transmembrane region
TNF	Tumor necrosis factor
TRAIL	TNF-related apoptosis inducing ligand
Tris	Tris(hydroxymethyl)aminomethane
t-SNARE	target-SNARE
U	Units
UV	Ultra Violet
V	Volts
VAMP	Vesicle-associated membrane protein
v-SNARE	vesicular-SNARE
WT	Wild type
ZAP-70	Zeta-associated protein tyrosine kinase (70 kDa)

ABSTRACT

Cytotoxic T lymphocytes (CTLs) kill tumor cells and virus-infected cells by secreting lytic components like perforin and granzymes contained in cytotoxic granules (CGs). Exocytosis of cytotoxic granules is calcium-dependent and might be regulated by synaptotagmins. Synaptotagmin 7 (Syt7) is a calcium-dependent isoform of synaptotagmins which has been shown to regulate multiple functions in different types of tissues. Its ubiquitous expression and extremely high calcium sensitivity made it to be further investigated as the candidate calcium sensor for cytotoxic granule exocytosis. We determined the expression profile of the synaptotagmin family in mouse CTLs; four isoforms are expressed: Syt2, Syt7, Syt11, and Syt16; only Syt2 and Syt7 are calcium-dependent. Since cytotoxic granules are lysosome-related organelles, and Syt7 has been shown to regulate lysosomal exocytosis as well as to influence killing in T cells, we studied the function of Syt7 in CTLs. We found that Syt7 is localized on cytotoxic granules and on the plasma membrane. We compared GranzymeB-mCherry secretion in WT and Syt7 KO cells at low and high (10 mM) extracellular calcium and we found that Syt7 is not required for early CG fusion at low calcium however its absence abolishes regenerated secretion at high calcium. Overexpression of WT Syt7 in Syt7 KO cells rescued secretion at high calcium. Expression of Syt7 mutants which lack the calcium binding aspartate residues in the C2A domain of Syt7 produced limited CG fusion at high calcium. We checked the availability of granules at the synapse and we found that granule counts were compromised in cells lacking Syt7 or expressing mutated Syt7. Yet, differences in granule numbers were modest and do not account to the lack of secretion at high calcium. Hence, we think that Syt7 promotes granule replenishment at the synapse in response to elevated calcium and regulates their fusion. By comparing the fusion kinetics in WT and Syt7 KO cells, we found that Syt7 prolongs and stabilizes fusion pore openings. To examine the role of Syt2 in CTLs, we downregulated its expression by siRNA. This resulted in reduced probability of secretion to comparable levels of protein downregulation. According to our results, we propose Syt2 as a major regulator of CG fusion in mouse CTLs, and Syt7 as a regulator of regenerated secretion under elevated calcium conditions.

ZUSAMMENFASSUNG

Zytotoxische T-Lymphozyten (CTLs) töten Tumorzellen und virusinfizierte Zellen, indem sie lytische Komponenten wie Perforin und Granzyme, die in zytotoxischen Granulaten (CGs) enthalten sind, absondern. Die Exozytose von zytotoxischen Granulaten ist calciumabhängig und kann durch Synaptotagmine reguliert werden. Synaptotagmin 7 (Syt7) ist eine kalziumabhängige Isoform von Synaptotagminen, die nachweislich mehrere Funktionen in verschiedenen Gewebearten reguliert. Aufgrund seiner allgegenwärtigen Expression und seiner extrem hohen Kalziumempfindlichkeit wurde er als geeigneter Kalziumsensor für die zytotoxische Granulatoxozytose weiter untersucht. Wir haben das Expressionsprofil der Synaptotagminfamilie in Maus-CTLs bestimmt; vier Isoformen werden exprimiert: Syt2, Syt7, Syt11 und Syt16; nur Syt2 und Syt7 sind calciumabhängig. Da zytotoxische Granulate lysosomenbezogene Organellen sind und Syt7 nachweislich die lysosomale Exozytose reguliert und das Töten in T-Zellen beeinflusst, haben wir die Funktion von Syt7 in CTLs untersucht. Wir fanden heraus, dass Syt7 auf zytotoxischen Granulaten und auf der Plasmamembran lokalisiert ist. Wir verglichen GranzymeB-mCherry-Sekretion in WT- und Syt7-KO-Zellen bei niedrigem und hohem (10 mM) extrazellulärem Kalzium und wir fanden heraus, dass Syt7 nicht für die frühe CG-Fusion bei niedrigem Kalziumgehalt erforderlich ist, aber seine Abwesenheit beseitigt regeneriertes Sekret bei hohem Kalziumgehalt. Die Überexpression von WT Syt7 in Syt7 KO-Zellen rettete das Sekret bei hohem Kalziumgehalt. Die Expression von Syt7-Mutanten, denen die calciumbindenden Aspartatreste in der C2A-Domäne von Syt7 fehlen, führte zu einer begrenzten CG-Fusion bei hohem Calciumgehalt. Wir überprüften die Verfügbarkeit von Granulaten an der Synapse und fanden heraus, dass die Granulatzahl in Zellen ohne Syt7 oder mit mutiertem Syt7 beeinträchtigt war. Die Unterschiede in der Granulatzahl waren jedoch bescheiden und erklären nicht den Mangel an Sekretion bei hohem Kalziumgehalt. Daher denken wir, dass Syt7 die Granulatauffüllung an der Synapse als Reaktion auf erhöhtes Kalzium fördert und deren Fusion reguliert. Durch den Vergleich der Fusionskinetik in WT- und Syt7-KO-Zellen fanden wir heraus, dass Syt7 die Porenöffnungen der Fusion verlängert und stabilisiert. Um die Rolle von Syt2 in CTLs zu untersuchen, haben wir seine Expression durch siRNA heruntergeregelt. Dies führte zu einer reduzierten Wahrscheinlichkeit der Sekretion auf ein vergleichbares Niveau der Protein-Downregulation. Gemäß unseren Ergebnissen schlagen wir Syt2 als Hauptregulator der CG-Fusion in Maus-CTLs und Syt7 als Regulator der regenerierten Sekretion unter erhöhten Kalziumbedingungen vor.

I. INTRODUCTION

I.1 The Immune system

I.1.1 Innate and adaptive immunity

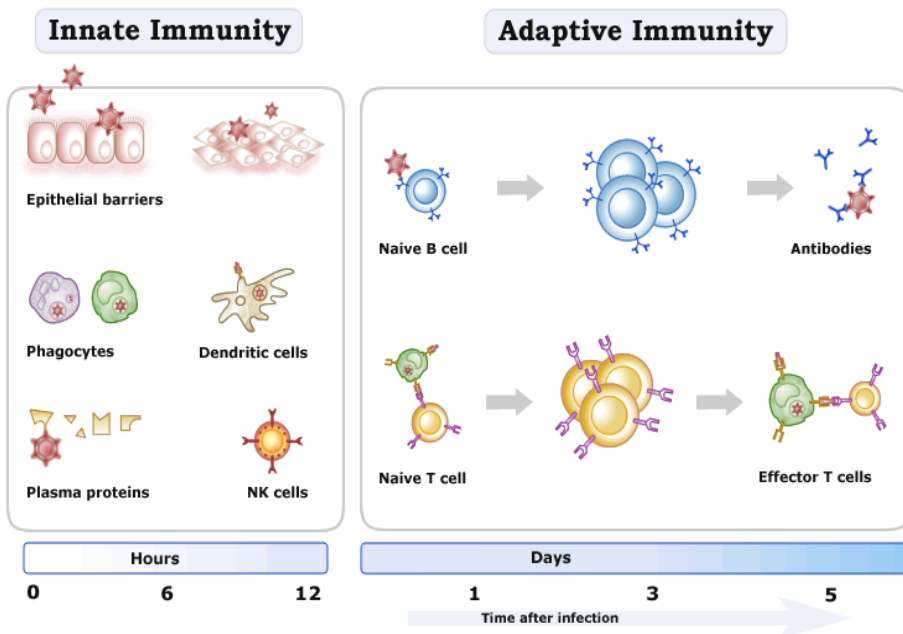
The immune system which protects our bodies against foreign microorganisms and invading pathogens is composed of innate and adaptive immune components.

The innate immune system is the immune system we are born with. It acts as the first line of defense against bacteria and microbes. It consists of the physical barriers on or in our bodies like our skin, skin oils, stomach acid, mucus lining, and the enzymes in our tears. If pathogens are able to penetrate these barriers, they will be encountered by the innate immune cells, which are phagocytes (e.g. macrophages, neutrophils, dendritic cells) and Natural Killer (NK) cells. These cells recognize bacteria or microbes by common structural patterns expressed on their surface and eliminate them immediately on site (Molnar and Gair, 2013; Bennett et al., 2018).

If the innate immune system fails to eradicate the infection, the more specialized adaptive immune system is alerted to prepare a more specific response. Cells from the innate immune system such as dendritic cells migrate from the infected tissue to the secondary lymphoid organs (e.g. lymph nodes), where antigen-specific B and T cells reside. Here they present fragments of the digested pathogen on their surface as antigens. These antigen-presenting cells (APCs) also secrete cytokines that drive the differentiation of activated lymphocytes. The pattern of cytokine release determines the phenotype of the adaptive immune reaction (Medzhitov and Janeway, 2000).

The adaptive immune response is based on two components: the cell-mediated immune response carried out by T cells, and the humoral immune response executed by B cells via antibodies. Both immune responses are initiated by activating CD4⁺ T helper (T_h) lymphocytes upon a specific interaction between the MHC-II/antigen complex located on an APC and the matching T cell receptor (TCR) of a naïve T cell. Depending on the nature of the presented antigen and the nature of the cytokines being secreted by cells of the innate immune system, the T_h cell reaction can take two different routes: T_h1 pathway where a T_h cell secretes cytokines to activate cytotoxic T lymphocytes and macrophages, and T_h2 pathway where B cells are stimulated to produce specific antibodies. In the T_h1 pathway, macrophages are stimulated by specific cytokines to enhance their

digestive capabilities in order to get rid of engulfed yet resilient bacteria. Besides this, cytotoxic T lymphocytes (CTLs) are activated by T_h1 cells via direct interaction or via cytokine stimulation to kill virus-infected or tumor cells. Hence, the T_h1 pathway is dedicated to controlling intracellular infections. In the second branch of the T_h pathway, T_h2 cells activate B lymphocytes to take the control over extracellular pathogens. The B lymphocyte binds the pathogen with its B cell receptor (BCR), engulfs it, and acts as an APC by presenting fragments of the pathogen on its MHC-II complex. T_h2 cells interact with the MHC-II/antigen complex and secrete cytokines which induce the B cell to mature, proliferate, and secrete antigen-specific antibodies to neutralize the pathogen (Shedlock and Shen., 2003; Murphy and Reiner, 2002; Molnar and Gair, 2013).



Patrick Fisher, Immunology Module 2011, University of California San Francisco

Figure 1: The innate and adaptive immune systems.

Immune cells belong to two different immune system branches; the innate and the adaptive immune systems. The two systems differ mainly in their specificity and time course of action. Components of the innate immune system (epithelial barriers, phagocytic cells, complement proteins, NK cells) are always available and react immediately at the site of infection. They are not target-specific and they execute their function within a few hours. In contrast, the adaptive immune system is composed of highly specialized and organized immune cells that are activated by signals and interactions with innate immune cells when the infection is not successfully controlled and a target-specific reaction is needed. There are 2 types of adaptive immune responses: the humoral immune response (by antibodies secreted by B lymphocytes), and the cellular immune response by T lymphocytes. It takes several days for target-specific lymphocytes to be activated and proliferate before they eliminate the pathogen.

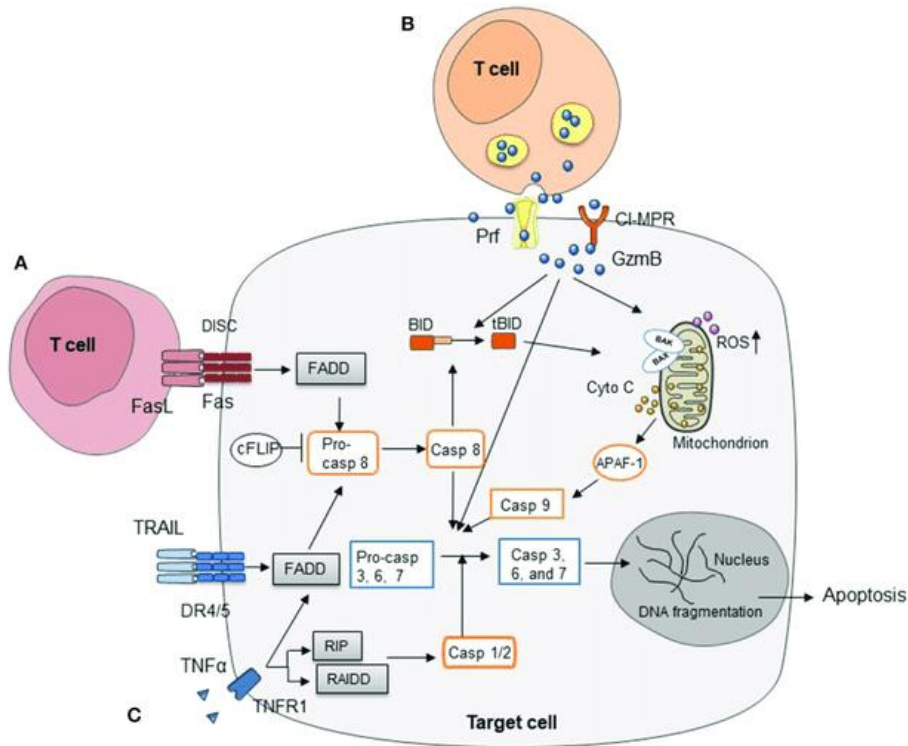
I.1.2 Cytotoxic T lymphocytes

Cytotoxic T cells (CTLs) are CD8⁺ T lymphocytes tasked with eradicating infected host cells and tumor cells. CTLs interact with the pathogen indirectly via an interaction of their T-cell receptor/cluster of differentiation 3 complex (TCR/CD3) with the pathogen's processed remnants presented on the MHC-I complex on the surface of infected cells or tumor cells. Once a CTL recognizes its target, it induces programmed cell death of the target cell by either secreting lytic proteins, death-inducing ligands (Fas Ligand-FasL), or TNF-related apoptosis inducing ligand (TRAIL) (Luis-Martinez Lostao et al., 2015).

Lytic proteins are packaged in cytotoxic granules (CGs). These granules are lysosome-related organelles which are acidic in nature, carry lysosomal membrane markers and luminal hydrolases, and contain cytolytic proteins such as perforin and granzymes in its dense core (Peters et al., 1991). Perforin is a pore-forming glycoprotein, homologous to the pore-forming complement proteins C6, C7, C8 and C9 (Osinska et al., 2014). At its C-terminus lies a C2 domain which binds Ca²⁺ via its acidic residues. Calcium facilitates the interaction of perforin with the membrane phospholipids of the target cell upon release from cytotoxic granules. While in the acidic lumen of the granule, perforin is inactive due to neutralization of the anionic moieties of the acidic residues at low pH (Voskoboinik et al., 2005). It has been shown that perforin is a key element in CTL cytotoxicity. Upon exocytosis, perforin molecules polymerize in target cell membrane to form a channel which allows the passive access of ions, water, and cytolytic proteases, and causes the target cell death. Perforin deficiency causes severe immune dysregulation such as familial hemophagocytic lymphohistiocytosis (FHL), B cell lymphoma, inability to clear infection, and autoimmune diseases (Osinska et al., 2014).

The other key element of cytotoxicity is granule enzymes or granzymes. Granzymes are proteases stored in the dense core of cytotoxic granules. Once released into the target cell cytosol, they activate pro-caspases by cleaving them into caspases. Caspases are endo-proteases that cleave nuclear proteins, plasma membrane proteins, mitochondrial proteins, and viral proteins, and activate DNA fragmentation leading to cell death (McIlwain et al., 2013). Perforin is key to the activity of granzymes as it allows their access to the target cell. In organisms lacking granzymes, cytotoxic cells can still kill target cells. This is not the case with perforin deficiency (Janeway et al., 2001).

The alternate pathway by which CTLs induce target cell death is by the surface expression or secretion of death ligands (e.g. FasL and TRAIL). Death ligands bind to death receptors expressed on the host cell surface. Cross-linking of these receptors activates the caspase pathway, leading to target cell death (Mellwain et al., 2013).



Du and Cao, 2018

Figure 2: Three killing pathways by cytotoxic T lymphocytes (CTLs).

Three major pathways are used by CTLs to eradicate tumor or virus-infected cells. **(A)** is the Fas/FasL or the TRAIL/Death Receptor (DR) pathway where the Fas Ligand (FasL)/TRAIL expressed on the surface of activated T cells engages with the Fas receptor (CD95) /DR 4/5 receptor on the surface of the target cell and induces the formation of the death-inducing signaling complex (DISC). Subsequently, the Fas-associated death domain (FADD) protein is activated. This leads to the catalytic cleavage of pro-caspase 8 to caspase 8 and the activation of the apoptotic pathway via DNA fragmentation or activation of the mitochondrial cell death pathway. **(B)** is the pathway through which T cells secrete lytic granules containing perforin and granzymes after TCR engagement. Upon secretion, perforin forms pores in the target cell membrane which compromises its integrity. Granzymes are proteases that enter the target cell cytosol via the pores formed by perforin or via receptor-mediated endocytosis. Granzymes are believed to be key effectors in CTL cytotoxicity due to their ability to activate different caspases and to induce mitochondria-mediated apoptosis either directly or through the action of BID (BH3 interacting-domain death agonist). **(C)** Cytokines such as TNF (Tumor-Necrosis Factor) and IFN (Interferon) are secreted by activated T cells and activate the various apoptotic pathways in target cells.

I.1.2.1 The immunological synapse

The immunological synapse (IS) is the zone of contact between the cytotoxic T lymphocyte and its target. Tight contact between the lymphocyte and the target cell limits exposure to toxins to the APC and requires the establishment of a focused interaction zone. Following recognition of a target cell, F actin accumulates at the center of the contact zone. F actin then clears to a distal area called the distal supramolecular activation cluster or dSMAC. T cell Receptor (TCR) molecules cluster in the center of the synapse, along with other signaling molecules (e.g. PKC θ and Lck kinases), to form the central supramolecular activation cluster or cSMAC. A ring of adhesion molecules surrounds the cSMAC to ensure a tight contact of the T cell with its target, and to spare any neighboring healthy cells from exposure to cytotoxic molecules. This ring is mainly formed of LFA-1 protein, its adaptor talin, and other selectin molecules. This area is known as the peripheral supramolecular activation complex or pSMAC. Between the cSMAC and the pSMAC lies the secretory domain where cytolytic molecules are released into the synaptic cleft. The delivery of cytotoxic granules to the IS occurs after cytoskeleton reorganization. The microtubule organization center or MTOC polarizes from the rear of the cell to the synapse and docks next to the cSMAC in an actin-depleted region. Granules are transported on the microtubules, in the direction of the MTOC, and fuse at the secretory domain. Following this lethal hit, the CTL detaches from its dying target and searches for another target (Fooksman et al., 2010; Dustin, 2014; Dieckmann et al., 2016).

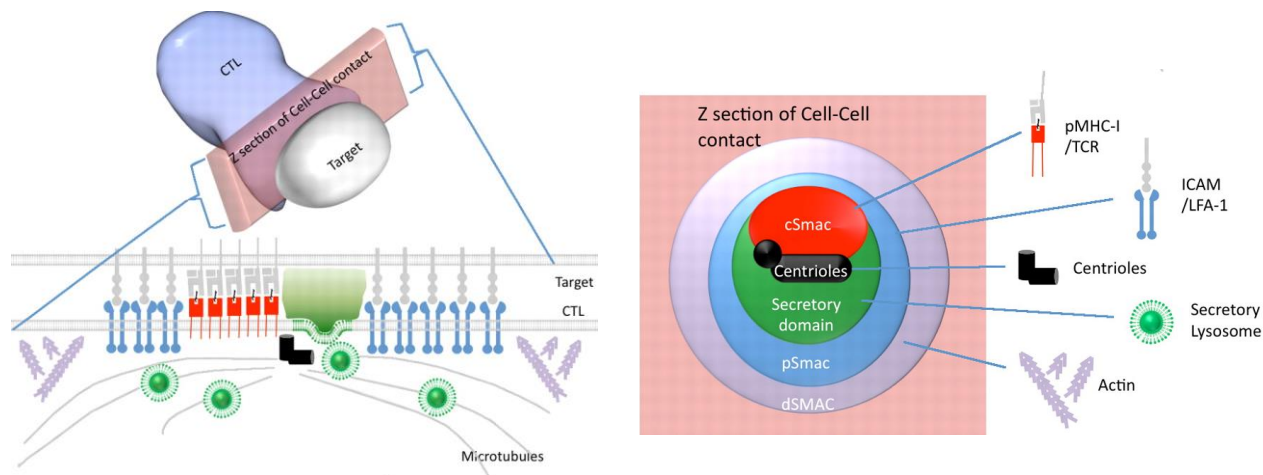
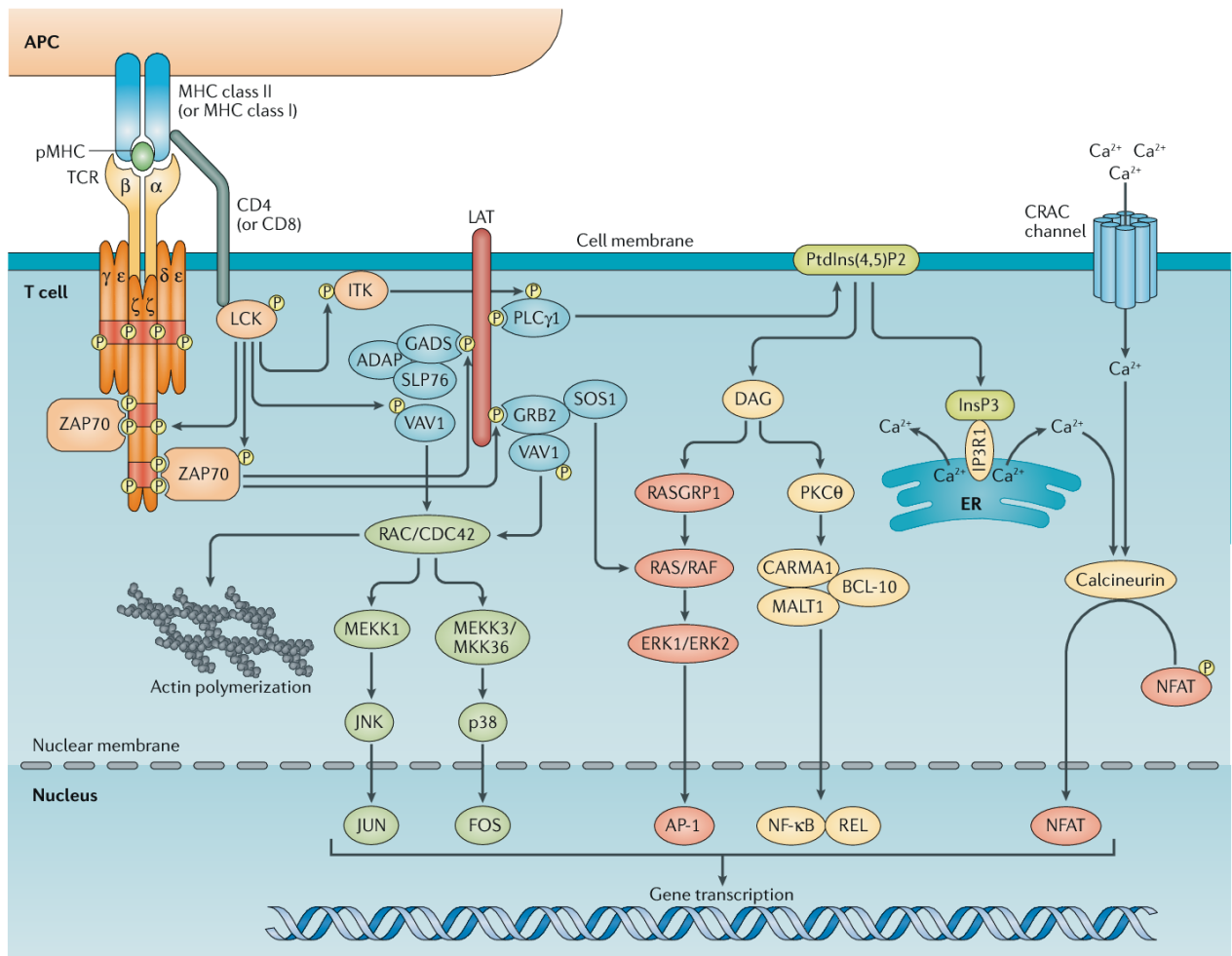


Figure 3: The immunological synapse.

After a T cell-target cell contact, the organization of the immunological synapse (IS) starts with the accumulation of actin at the center of the contact zone and its clearance afterwards to the dSMAC (in gray). The MTOC or centrioles (in black) move towards the secretory domain to allow the recruitment of the cytotoxic granules along microtubules to the secretory domain (in green). To establish a tight and specific lethal hit, specific TCRs and other kinases accumulate in the cSMAC (in red), and adhesion molecules like LFA-1 and selectins form a ring (pSMAC, in blue) surrounding the cSMAC and the secretory domain. The right panel shows a Z-section of the contact zone between a T cell and a target cell. The left panel shows the relative positions of the different specialized zones in an IS.

I.1.2.2 Store-operated calcium entry

In addition to cytoskeletal reorganization and the formation of an immune synapse between the CTL and its target, cytotoxic T lymphocytes require a sustained increase in cytosolic Ca^{2+} to execute their immune function. A sustained influx of extracellular calcium is indispensable for lytic granule fusion (Lancki et al., 1987; Lyubchenko et al., 2001). In T cells, this occurs by the process of store-operated calcium entry (SOCE) through the calcium-release activated channels (CRAC). CRAC channels are the main and most selective source of extracellular calcium in T cells. The CRAC channel pore is composed of ORAI protein subunits and it is activated via the interaction with the ER Ca^{2+} sensor STIM (Zhang et al., 2005; Hogan et al., 2010; Qu et al., 2011). As the TCR binds the peptide-MHC I complex on APC/target cell, intracellular signaling starts with the tyrosine phosphorylation of immune-receptor tyrosine-based activation motifs (ITAMs) in the cytosolic domain of the zeta chain of the CD3 complex. Protein tyrosine kinases are recruited and activated at the plasma membrane (PM), leading to the phosphorylation and activation of phospholipase C gamma 1 (PLC γ 1). PLC γ 1 acts on membrane phosphatidylinositol 4,5-bisphosphate, generating inositol triphosphate (IP3) and diacylglycerol (DAG). IP3 binds to its receptor which is a Ca^{2+} channel on the ER membrane, and DAG activates protein kinase C (PKC). Binding of IP3 to its receptor activates ER store depletion. As the calcium concentration in the ER decreases, STIM proteins oligomerize in the ER membrane. Subsequently, STIM oligomers translocate to puncta at the ER-PM junctions, and activate SOCE through an interaction with ORAI proteins (Liou et al., 2007; Vig and Kinet, 2009). Mutations in ORAI or STIM proteins abolish Ca^{2+} entry into the cell and lead to a severe immunodeficiency disease called CRAC channelopathy (Shaw et al., 2012).



Gaud et al., Nature Reviews Immunology, 2018

Figure 4: The major TCR-mediated signaling pathways in T cells.

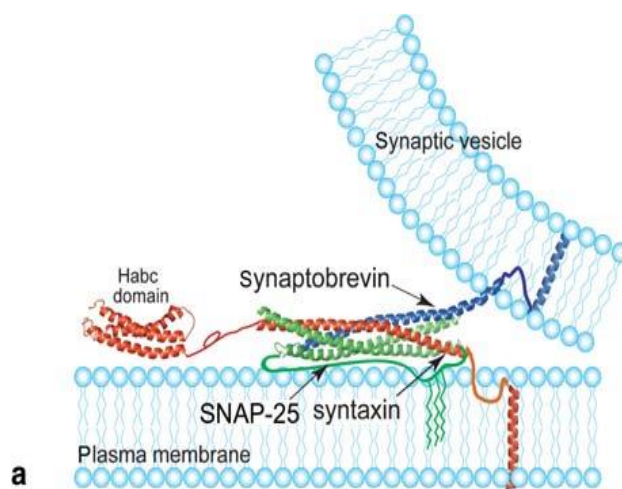
Crosslinking of TCR/CD3 complex of the T cell with the MHC/antigen complex on the APC leads to the recruitment of the LCK protein tyrosine kinase. LCK interacts with the cytoplasmic domain of the CD4/CD8 co-receptor which is already interacting with the MHC protein of the target cell. LCK phosphorylates the immuno-receptor tyrosine-based activation motifs (ITAMs) in the zeta chain of the CD3 complex, hence creating a docking site for ZAP-70, which is the Zeta-associated protein tyrosine kinase. ZAP-70 is subsequently phosphorylated by LCK. Once activated, ZAP-70 phosphorylates the transmembrane adaptor protein Linker of activation of T cells. As an adaptor protein, LAT recruits different effector protein, generating multiple signaling pathways. The major activated signaling pathways lead to: 1)- efflux of calcium from the ER stores and subsequent activation of the store-operated calcium entry (SOCE) through CRAC channels, 2)- activation of the mitogen-activated protein kinase (MAPK) pathway that allows actin polymerization and activation of gene transcription through the JUN and FOS transcription factors, and 3)- activation of the DAG pathway which leads activation of gene transcription through AP-1 and NF- κ B/REL transcription factors. Calcium entry and activation of gene transcription allows T cell proliferation, migration and cytokine production.

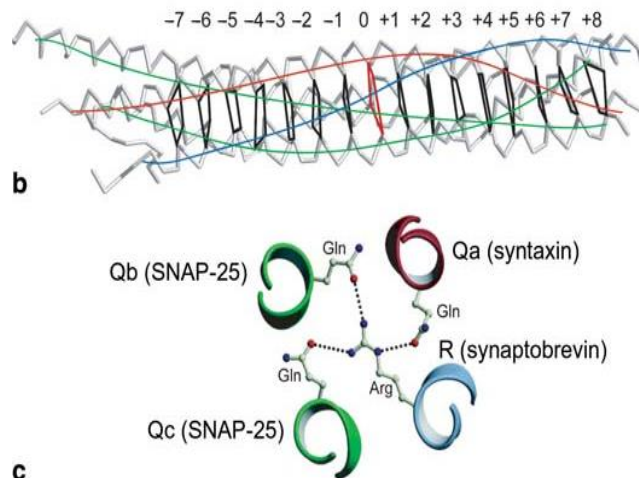
I.2 Exocytosis

The lethal hit by CTLs follows the polarization of cytotoxic granules to the T cell/target cell contact zone and their subsequent fusion with the plasma membrane. The fusion of vesicles is catalyzed by the SNARE proteins, which are an evolutionarily conserved superfamily of proteins that regulate the fusion process in most cell types from yeast to human. The soluble N-ethylmaleimide sensitive factor attachment protein receptors (SNAREs) exert their function by breaking the energy barrier created mainly by the negative charges of the opposing phospholipid leaflets (Jahn and Südhof, 1999; Han et al., 2017).

I.2.1 The SNARE protein machinery

SNAREs are divided into two categories: v-SNAREs which are found on the vesicular (donor) compartment, and t-SNAREs which are localized on the target compartment. The v-SNARE on the vesicular compartment carrying cargo proteins interacts with two t-SNAREs on the plasma membrane forming the functional SNARE complex required for fusion. (Hong, 2005). SNARE proteins share a SNARE motif comprised of 60-70 amino acid residues in their cytoplasmic domains. SNARE motifs from v- and t-SNAREs from adjacent membranes interact and form a tight coiled-coil alpha-helical complex, known as the trans-SNARE complex or the core complex. In neurons, a trans-SNARE complex is formed between one SNARE motif from VAMP (Vesicle-associated membrane protein) which is a v-SNARE, one SNARE motif from syntaxin and 2 SNARE motifs from SNAP-25 (Synaptosomal-nerve associated protein-25 kDa) which are t-SNAREs (Jahn and Scheller, 2006; Kloepper et al., 2007; Han et al., 2017).





Palfreyman and Jorgensen, *Molecular Mechanisms of Neurotransmitter Release*, 2008

Figure 5: Description of the SNARE proteins.

(a) As a model for neuronal SNAREs, syntaxin (red) and SNAP-25 (green) reside in the target membrane (plasma membrane), and synaptobrevin 2 (blue) extends from the synaptic vesicle membrane. They form a SNARE complex by sharing their 60-70 aa SNARE motif: syntaxin and synaptobrevin share one SNARE motif each, while SNAP-25 contributes 2 SNARE motifs to the SNARE complex. Syntaxin has an additional Habc domain composed of three α -helices. Both syntaxin and synaptobrevin are transmembrane proteins; however, SNAP-25 is linked to the plasma membrane via its palmitoylated linker region. (b) This wire model illustrates the inner core of the SNARE motif where the amino acids facing toward the center (numbered from -7 to +8) are largely hydrophobic. Only amino acids are layer 0 are an exception. (c) The amino acids contributed by the 4 SNARE motifs at the 0 layer are charged: Glutamines by syntaxin (Qa) and SNAP-25 (Qb and Qc), and arginine by synaptobrevin (R).

I.2.2 Docking, priming, and fusion of cytotoxic granules

I.2.2.1 Docking

As a prerequisite for granule fusion, CGs first dock at the target membrane, whereby they are ‘trapped’ by molecular players localized near to the plasma membrane. Docking is an intermediate step in which a partial formation of the SNARE complex occurs and precedes the generation of a release-ready granule (de Wit, 2010). The details of this process are still not clear. Several proteins are thought to regulate granule docking. The most likely candidates for docking regulation are Sec1/Munc18 and the syntaxin family. These two family proteins interact

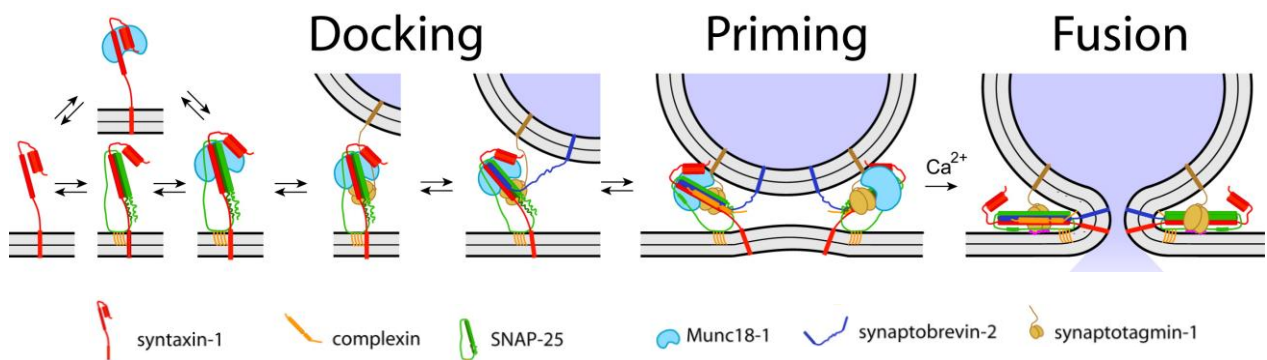
with high affinity (Jahn, 2000; Verhage and Sorensen, 2008). Null mutations or proteolytic cleavage of Munc18-1 and syntaxin-1 in different types of tissues cause dramatic reductions in the number of docked vesicles (without affecting their total number in the cell), and consequently produced strong secretion defects (Voets et al., 2001; de Wit et al., 2006; Toonen et al., 2006). Munc18-2 deficient CTLs showed a marked decrease in syntaxin 11 expression, which is believed to be a main partner in mediating granule docking in CTLs and NK cells (de Saint Basile et al., 2010). The mechanism of action of syntaxin 11 in cytotoxic granule docking was further demonstrated by Halimani et al (2014). Knockdown of endogenous syntaxin 11 caused a reduction in CG dwell time at the synapse and a subsequent inhibition in granule fusion (Halimani et al., 2014). Another prominent candidate for regulation of granule docking in cytotoxic lymphocytes is the small GTPase Rab27a. Electron microscopy experiments showed a docking failure at the immunological synapse by polarized CGs in Rab27a-deficient CTLs and NK cells (Stinchcombe et al., 2001; Haddad et al., 2001). Immunodeficiency diseases associated with expression defects in Munc18-2 (FHL-5), syntaxin 11 (FHL-4), and Rab27a have been demonstrated in humans (Familial Hemophagocytic Lymphohistocytosis-FHL). In Grischelli syndrome type 2 (GS2), patients exhibit defective cytotoxic activity (de Saint Basile et al., 2010). Equivalent mouse models like ashen mice (Rab27a defect) showed comparable immune defects (Haddad et al., 2001).

I.2.2.2 Priming

Priming is the step where the granule is rendered to be fusion-competent (Jahn et al., 2003; Karatekin et al., 2008). At this stage the four-helical SNARE-motif bundle that drives fusion is generated and fusion can proceed. The Unc13 family of proteins are well established priming factors which appear to permit the interaction of syntaxins with V-SNARES resulting in the primed state. Individuals that have Munc13-4 deficiency suffer from FHL-3 immunodeficiency. Mouse CTLs lacking Munc13-4 exhibit docking but lack fusion of lytic granules, consistent with a role of Munc13-4 in granule priming. Consequently, these patients exhibit cytotoxicity defects and severe autoimmune responses (Feldmann et al., 2003; de Saint Basile et al., 2010).

I.2.2.3 Fusion

Membrane fusion is the step at which the granule membrane merges with the plasma membrane, allowing the release of cytotoxic proteins. The positioning of the v-SNARE and the t-SNARE proteins in the respective membranes via their trans-membrane domains renders the granule and the target membrane in close apposition (Sutton et al., 1998). The tight bundle of the four helices starts at the N-termini of the SNARE-motifs and progresses towards the membrane-proximal C-termini by a process described as ‘zippering’ (Gao et al., 2012). The opposing outer lipid leaflets first fuse, while the other inner leaflets are intact. This intermediate state is called ‘hemifusion’. The full zippering of the trans-SNARE complex generates a fusion pore (Wu et al., 2017). The expansion of the fusion pore is followed by the complete merging of the two membranes, so all components of the SNARE complex are eventually residing in the plasma membrane (Südhof and Rizo, 2011). In mouse CTLs, synaptobrevin 2 is believed to be the v-SNARE driving CG fusion, and syntaxin 11 and SNAP-23 are the core t-SNARE proteins (Matti et al., 2013). Though fusion is often constitutive, some fusion events are highly regulated and dependent on calcium sensing proteins of the synaptotagmin family (Yoshihara et al., 2003; Südhof, 2004). Synaptotagmins are generally vesicle-associated proteins that interact with the SNARE complex and the plasma membrane phospholipids. After Ca^{2+} influx, calcium binds synaptotagmins and allows its insertion into the phospholipid bilayer. The insertion of Syt into the plasma membrane induces curvature, decreasing the energy barrier of fusion pore formation. To drive the last step of fusion, Syt allows the force transfer to the opposing membranes in a calcium-dependent manner (Han et al., 2017).



De Wit et al., Cell, 2009 (modified)

Figure 6: Vesicle docking, priming, and fusion by SNAREs and SNARE-associated proteins.

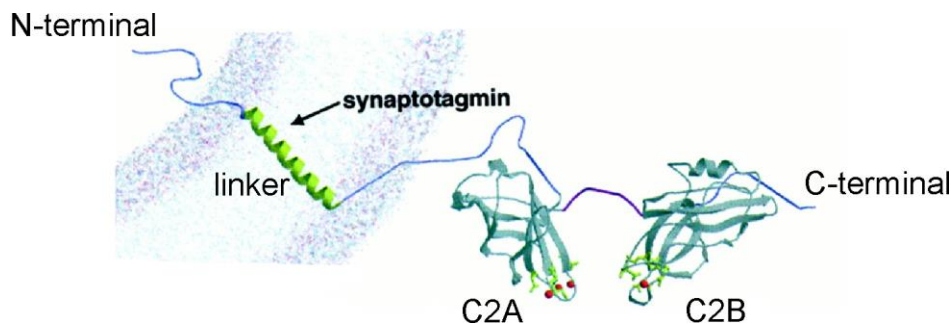
In the shown model from chromaffin cells, and prior to granule docking, the cytosolic Munc 18-1 (in light blue) interacts with the closed conformation of the transmembrane protein syntaxin-1 (in red). In the following step, SNAP-25 (in green) binds to the Munc/syntaxin complex. This complex is ready to receive the membrane-proximal vesicles, where the vesicle bound-synaptotagmin 1 supports vesicle docking through interacting with the Munc/syntaxin/SNAP complex. Munc 18-1 supports the binding of synaptobrevin2 (in dark blue) with the docking complex and the subsequent SNARE complex formation. Interaction of complexin (in orange) with the four-helix SNARE bundle follows and prepares the vesicle for synchronous release. The entrance of Ca^{2+} allows the synaptotagmin-membrane phospholipid interaction and induces membrane curvature. Merging of the opposing membranes allows fusion pore opening and egress of vesicle cargo to the extracellular space.

I.3 Synaptotagmins

How the fusion machinery works is not completely understood. Regulated fusion is highly calcium-dependent in neurons and neuroendocrine cells (Katz and Miledi, 1965; Baker and Knight, 1978; Barclay et al., 2005) and the fusion of cytotoxic granules appears to be calcium dependent as well (Lyubchenko et al., 2001). Synaptotagmins, which are evolutionarily conserved Ca^{2+} -binding proteins, have been shown to transduce the calcium signal to membrane fusion events in many different cell types (Brose et al., 1992; Goda and Stevens, 1994; Gao et al., 2000; Martinez et al., 2000; Michaut et al., 2001; Earles et al., 2001; Fernandez-Chacon et al., 2001; Falkowski et al., 2011; Chen et al., 2017). Synaptotagmins constitute a family of 17 members that share a common molecular architecture: they have a transmembrane N-terminal domain which anchors the protein to lipid membranes, a linker region of variable length, and two cytoplasmic tandem C2-domains (C2A and C2B) at the C-terminal. C2 domains were first characterized in protein kinase C (PKC) isoforms as the second constant sequence (hence C2), and they are found in a variety of proteins (Südhof, 2002). Crystallization experiments revealed that C2 domains adopt an eight-stranded β -barrel structure, with the Ca^{2+} -binding acidic residues in the protruding loops (Sutton et al., 1995; Sutton et al., 1999; Ubach et al., 1998; Chang et al., 2017). Other than binding Ca^{2+} , C2 domains in synaptotagmins are known to interact with SNARE proteins (syntaxin and SNAP23/25) and membrane phospholipids (Nalefski et al., 2001; Bhalla et al., 2006; Zhang et al., 2010). The ability of synaptotagmins to bind anionic phospholipids such as phosphatidylserine (PS) and phosphatidylinositol-(4,5)-bisphosphate

(PIP₂) in adjacent membranes after Ca²⁺ binding supports their insertion into target membranes (Davletov and Südhof, 1993; Chapman and Jahn, 1994). This phenomenon led to the idea that synaptotagmins might be the trigger for Ca²⁺ regulated exocytosis.

Eight out of the 17 Syt isoforms (Syt1, Syt2, Syt3, Syt5, Syt6, Syt7, Syt9, Syt10) showed the ability to interact with membranes due to Ca²⁺ binding, with Syt7 showing the highest calcium affinity (Sugita et al., 2002; Südhof, 2002).



Littleton et al., Journal of Neuroscience, 2001 (modified)

Figure 7: General structure of a synaptotagmin.

A synaptotagmin is a transmembrane protein through its N-terminal domain. A linker sequence extends between the transmembrane domain and the C2 domains at the C-terminal. C2A and C2B domains have an eight-stranded β -barrel structure and bind Ca²⁺ ions (red balls) through their surface loops.

I.3.1 Synaptotagmin 7: A ubiquitous protein with multiple functions

I.3.1.1 Syt7 expression

Synaptotagmin 7 expression is ubiquitous in all metazoans (Barber et al., 2009). It is widespread in neuronal and non-neuronal tissues, with the highest expression level being in the brain (Fagerberg et al., 2014; Chen and Jonas, 2017). Syt7 is known for the extensive alternative splicing of its gene primary transcript in the linker region. Three isoforms have been addressed in mouse brain: the canonical Syt7 α isoform (403 amino acids, 45 kDa) which is dominant, and the two alternate isoforms Syt7 β and Syt7 γ which have 44 and 116 amino acid insertions in their linker regions, respectively (Fukuda et al., 2002).

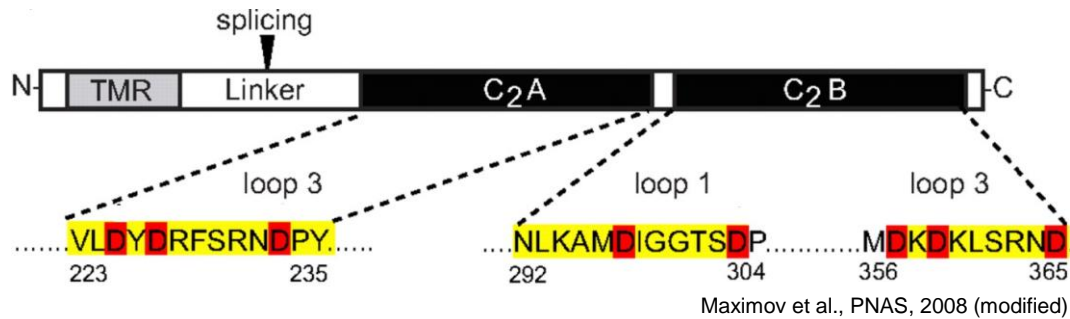


Figure 8: Syt7 domains and calcium-binding loops.

Syt7 structure comprises an N-terminal transmembrane (TMR) domain, a linker region, and 2 C2 domains, C2A and C2B, at the C-terminus. The linker region is alternatively spliced which gives rise to three main Syt7 isoforms (alpha, beta, and gamma). Syt7 binds calcium through its aspartate residue lying in the surface loops of its C2 domains.

I.3.1.2 Syt7 localization

Syt7 is present in different compartments of different tissues. Using light and electron microscopy, Syt7 was detected on the plasma membrane in neurons (Virmani et al, 2003; Weber et al., 2014); however, in neuroendocrine cells, neuroendocrine cell lines, and non-neuronal tissue, Syt7 was found on large dense-core vesicles (Fukuda et al., 2002; Wang et al., 2005) and lysosomes (Martinez et al., 2000; Reddy et al., 2001). In systems where Syt7 was tagged and overexpressed, it was mainly present on large dense-core vesicles and lysosomes, and to a lesser extent co-localized with the plasma membrane (Wang et al., 2005).

In other studies on Syt7 localization, it was shown that the post-translational modifications of Syt7 may affect its targeting to intracellular organelles. Flannery et al. (2010) showed that palmitoylation of the three cysteine residues of Syt7 within and next to its transmembrane domain (TMD) is critical to its localization to lysosomes (Flannery et al., 2010). Phosphorylation of Syt7 at serine 103 between the TMD and the C2A domain was shown to be key for its function in potentiating insulin secretion from pancreatic β cells (Wu et al., 2015).

I.3.1.3 Syt7 functions

One of the initially characterized functions of synaptotagmin 7 is its activity as a Ca^{2+} sensor for regulated exocytosis of lysosomes in normal rat kidney fibroblasts by Martinez et al. (2000). They showed that Syt7 is localized to lysosomes and requires its Ca^{2+} binding of the C2A domain to perform its function (Martinez et al., 2000). The importance of Syt7 activity in lysosomal exocytosis was demonstrated as well in membrane repair (Reddy et al., 2001), neurite extension (Arantes and Andrews, 2006), macrophage phagocytosis (Czibener et al., 2006; Becker et al., 2009), and in release of bone-degrading molecules or bone resorption by osteoclasts (Zhao et al., 2008). Bone remodeling and maintenance is also mediated by Syt7, which is localized on secretory vesicles containing bone matrix proteins in osteoblasts and promotes their secretion (Zhao et al., 2008).

Furthermore, Syt7 has an important role in glucose homeostasis. It was identified by Gustavsson et al. as a positive regulator of Ca^{2+} -stimulated insulin secretion by pancreatic β cells (Gustavsson et al., 2008) and Ca^{2+} -stimulated glucagon secretion by pancreatic α cells (Gustavsson et al., 2009). It has been shown also that Syt7 regulates the integration of the GLUT4 glucose transporter into the plasma membrane of adipose and skeletal muscle cells which is important for glucose tolerance (Li et al., 2007).

Although Syt7 was initially studied in non-neuronal cells (fibroblasts, pancreatic cells, bone cells, macrophages, dendritic cells, etc.), in neuronal cells and neuro-endocrine cells, where its expression levels are high and Ca^{2+} -dependence of neurotransmission is prominent, Syt7 may play a role in asynchronous release, facilitation, docking, fusion pore opening, and vesicle pool replenishment.

I.3.1.4 Functional properties of C2 domains of Syt7

Syt7 binds 3 Ca^{2+} ions per each of its C2 domains; however, the C2A and C2B domains of Syt7 do not contribute equally to its function (Voleti et al., 2017). It has been shown by Segovia et al. (2010) that the C2A domain activity is sufficient to prompt fusion pore opening; however, it's not sufficient for its stability and expansion. The role of the C2B domain of Syt7 lies in

stabilizing the fusion pore and supporting its expansion rather than its collapse which leads to kiss and run events (Segovia et al., 2010). Asynchronous release in hippocampal neurons was partly impaired upon Syt7 ablation, and totally suppressed in Syt1/Syt7 deficient cells. It could be rescued by WT Syt7 but not C2A mutated Syt7 at its Ca²⁺ binding sites. Mutations in Ca²⁺ binding sites in C2B domain did not affect asynchronous release (Bacaj et al., 2013). Overexpression of Syt7 in Syt1 KO neurons decreased the frequency of spontaneous mini-release events. This effect was blocked upon Syt7 mutation in its C2A domain but not its C2B domain (Bacaj et al., 2013). In a later study on the readily releasable pool (RRP) size, Bacaj et al (2015) showed that Syt1 and Syt7 redundantly maintain the size of the RRP, where either one of the isoforms was able to rescue the RRP in a double knockout background. Mutations in Ca²⁺ binding sites of the C2A domain but not the C2B domain of Syt7 abolished the rescue of the RRP in Syt1/Syt7 double KO cells (Bacaj et al., 2015).

I.4 Aim of the Thesis

Fowler et al. (2007) have shown that Syt7 is involved in immune function in mouse CTLs. They showed that clearance of the intracellular infection in Syt7 KO mice was compromised and that Syt7 KO cells were less effective in target cell killing in specific peptide-based killing assays, though the IS formation, CG biogenesis, and CG polarization were normal. When they tested GranzymeA release after CD3 cross-linking, they found that it is equivalent in Syt7 KO cells and WT cells. Knowing that the stimulation is different, and that stimulation via CD3 cross-linking leads to higher levels of cytosolic calcium, there could be two explanations to their results: either there is an alternative synaptotagmin with a lower Ca^{2+} affinity regulating CG exocytosis in CTLs, and/or Syt7 is mediating another function(s) in CTLs that affect(s) CG exocytosis. To address this, we carried out our experiments by using the CD3-crosslinking system to stimulate activated CTLs, used live-cell imaging to look at the different stages of GranzymeB exocytosis in WT and Syt7 KO cells, and challenged the cells with different levels of extracellular calcium in order to determine which role Syt7 plays in CG exocytosis.

II. MATERIALS AND METHODS

II.1 Materials

II.1.1 Chemicals

Product	Company
Agar	Roth
BSA	Sigma-Aldrich
Bradford	Bio-Rad
β -Mercaptoethanol	Roth
CaCl ₂ x 2H ₂ O	Merck
Chloroform	Sigma-Aldrich
dNTP-Mix	Fermentas
DPBS	Life Technologies
DPTA	Sigma Aldrich
Ethanol 100%	Roth
EtBr	Life Technologies
EDTA	Sigma-Aldrich
EGTA	Sigma-Aldrich
FCS	Life Technologies
Formaldehyde	PolyScience
Fura-2 am	Invitrogen
Fura-2 ff (K ⁺ salt)	Santa Cruz Biotechnology
Glucose	Merck
Glutamax	Life Technologies

Product	Company
Glycine	Roth
HEPES	Sigma-Aldrich
HPLC water	Life Technologies
Isopropanol	Roth
Kanamycin K-1377	Sigma-Aldrich
KCl	Merck
λ Marker	Roche
Methanol 100%	Roth
MgATP	Sigma-Aldrich
NaCl	Merck
NaCHO ₃	Merck
Nonfat dried milk powder	AppliChem Panreac
NuPAGE 10% Bis-Tris Gel 1.0mm	Fisher scientific
NuPAGE LDS sample buffer 4x	Invitrogen
NuPAGE MES SDS Running Buffer 20x	Fisher scientific
NuPAGE Transfer Buffer	Fisher scientific
PCR-buffer	Sigma-Aldrich
Pen/strep	Gibco
Peptone	Roth
<i>pfu</i> -Polymerase Buffer	Fermentas
Phenol	Sigma-Aldrich
Polyornithine	Sigma-Aldrich
Ponceau S solution 0,1%	Sigma-Aldrich
Protein G agarose	Thermo scientific

Product	Company
Restore Western Blot Stripping Reagent	Fisher scientific
RPMI	Sigma-Aldrich
Roti Nanoquant 5x	Roth
RNA Ladder	PEQGOLD high range
Spectra Multicolor Broad Range LAD	Fisher scientific
Streptomycin	Life Technologies
Sucrose	Merck
Super Signal West Dura Extended	Fisher scientific
Triton X-100	Roth
Tris-hydrochloride	Roth
TRIzol	Life Technologies
Tween 20	Roth
Water	Sigma-Aldrich

II.1.2 Solutions for cell culture

II.1.2.1 RPMI 1640 (10% FCS)

500 ml RPMI

50 ml FCS (10%)

5.5 ml Pen/Strep (1%)

5.5 ml HEPES from 1 M stock (10 mM)

II.1.2.2 IMDM (10% FCS)

500 ml IMDM

50 ml FCS (10%)

2.75 ml Pen/Strep (0.5%)

1.936 μ l 2-mercaptoethanol (50 μ M)

II.1.2.3 Isolation buffer

500 ml PBS

0.5 g BSA (0.1%)

2 ml EDTA

II.1.2.4 Erythrolysis buffer

0.829 g NH_4Cl (155 mM)

0.1 g KHCO_3 (10 mM)

260 μ l EDTA from 50 mM stock pH 7.3 (0.1 mM)

II.1.3 Solutions for cell fixation and staining

II.1.3.1 Paraformaldehyde (15% PFA)

PFA, 1.5 g

Sigma H_2O , 10 ml

NaOH, 20 μ l

pH 7.4

II.1.3.2 Permeabilization solution

Triton x-100, 50 μ l

PBS 1x, 50 ml

II.1.3.3 Blocking solution

BSA, 1 g

Triton x-100, 50 μ l

PBS, 50 ml

II.1.3.4 Mounting medium

Mowiol 4-88, 2.4 g

Glycerol, 6 g

H₂O double distilled, 6 ml

Tris-Buffer, 12 ml

pH 8.5

II.1.4 Solutions for Cloning

II.1.4.1 LB medium

Peptone, 8g

Yeast extract, 4g

NaCl, 4 g

H₂O, 800 ml

II.1.4.2 Loading buffer

Sucrose, 4g

Bromophenol blue

Sigma H₂O, 10 ml

II.1.5 Solutions for TIRF experiments

II.1.5.1 T cell extracellular solution (no CaCl₂ added)

NaCl, 155 mM

KCl, 4.5 mM

HEPES, 5 mM

MgCl₂.6H₂O, 3 mM

Glucose, 10 mM

Osmolarity: 300-310 mOsm, pH = 7.4 (adjusted with NaOH)

II.1.5.2 T cell extracellular solution (10 mM Ca²⁺)

NaCl, 140 mM

KCl, 4.5 mM

HEPES, 5 mM

MgCl₂.6H₂O, 2 mM

CaCl₂, 10 mM

Glucose, 10 mM

Osmolarity: 300-310 mOsm, pH = 7.4 (adjusted with NaOH)

II.1.5.3 NH₄Cl (40 mM)

NH₄Cl, 40 mM

NaCl, 105 mM

KCl, 2.4 mM

MgCl₂, 1.2 mM

CaCl₂, 2.5 mM

HEPES, 10 mM

10 mM Glucose

II.1.6 Solutions for Calcium Imaging

II.1.6.1 Fura-2ff calibration solutions

[Ca ²⁺] _i	[CaCl ₂] (mM)	[Ca ²⁺ -buffer] (mM)	[MgCl ₂ .6H ₂ O] (mM)	[HEPES] (mM)	[KCl] (mM)	[Fura-2ff] (μM)	pH
10 nM	0	[EGTA]= 2	3	5	4.5	100	7.25
1.2 μM	2.6	[EGTA]= 3	3	5	4.5	100	7.31
23.4 μM	1	[DPTA]= 5	3	5	4.5	100	7.30
108 μM	0.4	[DPTA]= 0.5	3	5	4.5	100	7.30
518 μM	1	[DPTA]= 0.5	3	5	4.5	100	7.35
9.4 mM	10	[DPTA]= 0.5	3	5	4.5	100	7.30

Table 1: Composition of Fura-2ff calibration solutions

NaCl was added after pH calibration and osmolarity check; its concentration ranged between 130 and 150 mM.

II.1.7 Solutions for Western Blotting

II.1.7.1 Lysis Buffer

Tris-Cl, 50 mM

NaCl, 150 mM

PMSF, 250 μl

Triton x-100, 1%

Deoxycholic acid, 1 mM

EDTA, 1 mM

DTT, 1 mM

H₂O, up to 5 ml

1 tablet protease inhibitor cocktail

II.1.7.2 TBS (10x)

NaCl, 87.7 g

1 M Tris-Cl (pH 7.5), 100 ml

H₂O, up to 1 L

II.1.7.3 TBST (0.1%)

10x TBS, 100 ml

Tween 20, 1 ml

H₂O, 900 ml

II.1.8 Kits

II.1.8.1 Kits for cloning

EndoFree Plasmid Maxi Kit, Qiagen

EndoFree Plasmid Mini Kit, Qiagen

QIAprep Spin Miniprep Kit, Qiagen

QIAquick Gel Extraction Kit, Qiagen

QIAquick PCR Purification Kit, Qiagen

II.1.8.2 Kits for cell culture

Dynabeads FlowComp mouse CD8 kit, Thermo Fisher

Dynabeads mouse T-activator CD3/CD28 for T-cell expansion and activation, Thermo Fisher

II.1.9 Antibodies

Antibody against Syt7 was from Synaptic Systems (Cat. No. 105 173). We pre-cleared the antibody on CTL lysate from Syt7 KO mouse. Other used antibodies were commercial as well: rabbit anti-mouse anti-Syt2 (ab113545), anti-CD3e (Cell Sciences, b-n11), anti-CD3-Alexa 647 (BD Biosciences-17A2), goat anti-Rabbit-Alexa 405 (Life Technologies), goat anti-rabbit-HRP (Millipore Sigma), and rabbit anti-mouse GAPDH (Cell Signaling).

II.1.10 Bacteria

DH5 α : F⁻ endA1 glnV44 thi-1 recA1 relA1 gyrA96 deoR nupG purB20
 ϕ 80dlacZ Δ M15 Δ (lacZYA-argF) U169, hsdR17(rK-mK⁺), λ ⁻. Invitrogen, Life Technologies

II.1.11 Mouse Strains

C57Bl/6N (Black 6), Stock No: 005304, The Jackson Laboratory

Syt7 KO mouse: Stock No: 004950, The Jackson Laboratory

II.1.12 Plasmids

II.1.12.1 Syt7 α -pMAX-IRES-GFP

Syt7 α was cloned into pMAX-IRES-GFP vector by amplifying Syt7 α from total brain cDNA using the following primers:

forward primer: 5'-TATAGGATCCGCCACCATGTACCCATACGATGTTCCAGATTA
CGCTTACCGGGACCCGGACGCG-3'

reverse primer: 5'-TATAGCGCGCTCAGGCTTTCAGCTGGTGCC-3'

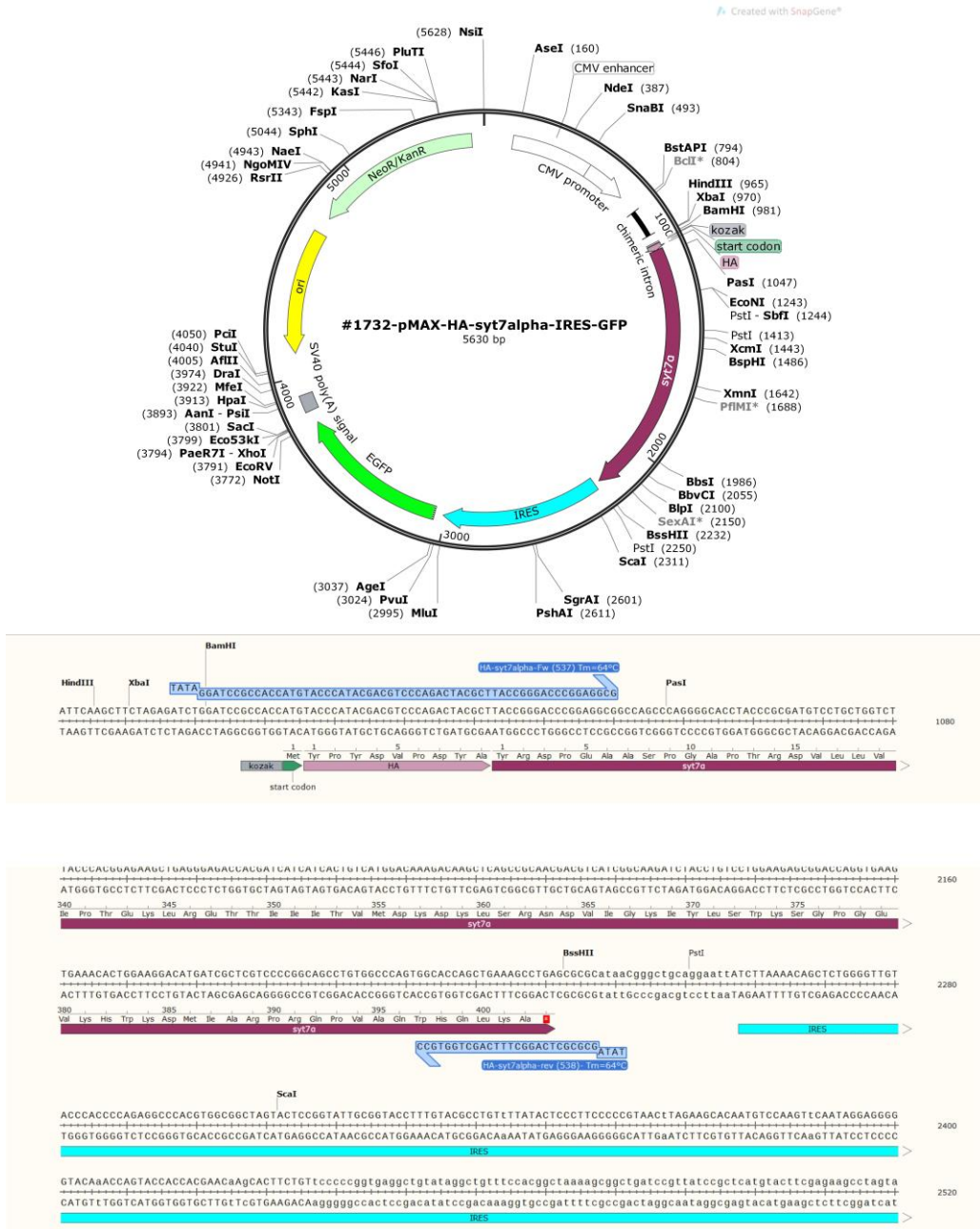


Figure 9: Syt7 α -pMAX-IRES-GFP map and Syt7 α forward and reverse primers.

Top panel: The pMAX-IRES-GFP vector map into-which the Syt7 α cDNA was inserted. The map shows the composition of pMAX vector and the restriction enzymes that were used to cleave it. **Bottom panel:** The forward primer was designed to contain a TATA box as a transcription initiation site, BamHI restriction site, Kozak sequence as a translation initiation site, ATG as the start codon, HA-tag (Human Influenza Hemagglutinin) to be able to detect the Syt7 protein with the highly specific anti-HA antibody, and the first 18 nucleotides of Syt7 sequence as a complementary stretch to the reverse strand. The reverse primer contains a TATA box as a transcription initiation site of the reverse strand, BssHIII restriction site, and the last 20 nucleotides as a complementary stretch to the forward strand.

The designed primers could detect the Syt7 α and Syt7 β isoforms at 1267 bp and 1399 bp, respectively (figure 1-A). Since running the gel for extra time did not help separate the two bands, we cut out the two bands together from the gel, purified them using the Gel Extraction kit from Invitrogen (see Materials), and digested them with SmlI restriction enzyme from NEB. This enzyme cuts only in Exon 4 of the β isoform of Syt7 (giving two products at 386 bp and 1011 bp), and does not cut neither in Syt7 α nor in the overhangs of the amplified PCR products. Syt7 α and pMAX-IRES-GFP vector were then digested with BamHI and BssHII restriction enzymes to generate their compatible ends and allow their ligation (figure 10-B, C). After ligation with the T4 DNA ligase kit (NEB) and transformation into bacteria (see Materials), clones were extracted by the EndoFree Plasmid Mini Kit (Qiagen) and digested by the same restriction enzymes. The clone that gave the right band size of the plasmid and insert was chosen for a Maxi prep (EndoFree Plasmid Maxi Kit, Qiagen) to amplify its concentration and purity. Afterwards, the produced construct was sequenced.

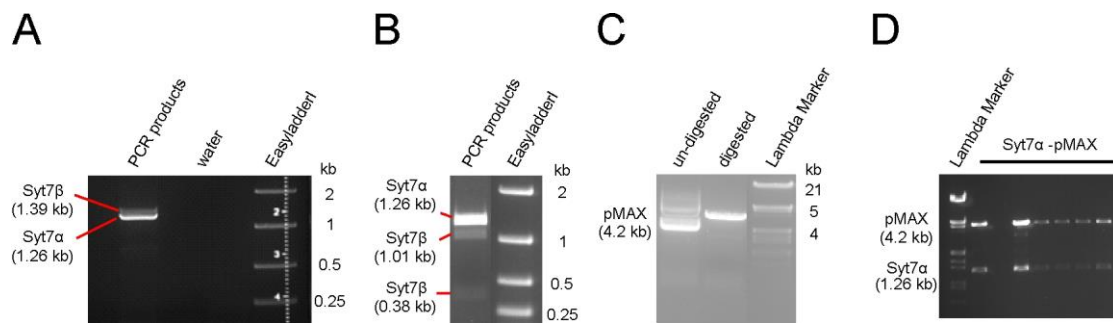


Figure 10: Cloning Syt7 α into pMAX-IRES-GFP vector.

(A) Syt7 α (1.26 kb) and Syt7 β (1.39 kb) isoforms were amplified with the designed primers (right lane). cDNA was replaced with water for a negative control (middle lane). **(B)** Syt7 α and Syt7 β isoforms were digested with SmlI restriction enzyme that cleaves Syt7 β only. Syt7 α was further cleaved with BamHI and BssHII restriction enzymes to produce sticky ends for ligation with the vector. **(C)** pMAX-IRES-GFP vector was digested with BamHI and BssHII restriction enzymes to produce compatible ends with the digested insert (Syt7 α) (middle lane). A control for digestion is shown in the right lane where the undigested plasmid takes the coiled (upper band) and supercoiled (lower band) forms. **(D)** Different clones of the transformed construct were digested with BamHI and BssHII to check for the clone with the right insert and plasmid size.

II.1.12.2 D227N mutant

One aspartate residue at position 227 in C2A domain of Syt7 was mutated to asparagine using the following primers on the original Syt7 α -pMAX-IRES-GFP vector:

- forward primer: 5'-CTGGATTATAACCGTTTCAGC-3'
- reverse primer: 5'-GCTGAAACGGTTATAATCCAG-3'

II.1.12.3 3DN mutant

Two more aspartate residues in the C2A domain of Syt7 α were mutated to asparagines by using the following vectors on the D227N mutant.

D225N mutation:

- forward primer: 5'-CAGGTCCTGAATTATGACCG-3'
- reverse primer: 5'-CGGTCATAATTCAGGACCTG-3'

D233N mutation:

- forward primer: 5'-CAGCCGCAATAACCCCATTGG-3'
- reverse primer: 5'-CCAATGGGGTTATTGCGGCTG-3'

II.1.13 siRNA

Control (scrambled) and silencing siRNA sequences (Mm_Syt2_1 and Mm_Syt2_2, designated later as siRNA1+2) against mouse Syt2 (NM_009307) were ordered from Qiagen. They were diluted in RNase-free water to a final concentration of 20 μ M and stored at -20°C for further use.

II.1.14 Software

II.1.14.1 Primer Design

NCBI Primer Blast: <https://www.ncbi.nlm.nih.gov/tools/primer-blast/>

Primer3 Plus: <http://www.bioinformatics.nl/cgi-bin/primer3plus/primer3plus.cgi>

NCBI blastn: <https://blast.ncbi.nlm.nih.gov/Blast.cgi>

Ensembl: <https://www.ensembl.org/index.html>

Clustal w: <https://www.genome.jp/tools-bin/clustalw>

Sequence Manipulation Suite:

- Reverse Complement: http://www.bioinformatics.org/sms2/rev_comp.html

- Primer properties: http://www.bioinformatics.org/sms2/pcr_primer_stats.html

II.1.14.2 Cloning

SnapGene: <https://www.snapgene.com/>

II.1.14.3 Image Analysis

ImageJ: <https://imagej.nih.gov/ij/>

- JACoP Plugin: <https://imagej.nih.gov/ij/plugins/track/jacop.html>

- Time Series Analyzer Plugin: <https://imagej.nih.gov/ij/plugins/time-series.html>

iLastik: <https://www.ilastik.org/>

II.1.14.4 Statistics and Figures

Microsoft Excel 2016

CorelDRAW X5

II.2 Methods

II.2.1 Positive isolation of CD8⁺ T lymphocytes

CD8⁺ T cells were isolated from the spleen by means of ‘Dynabeads FlowComp Mouse CD8’ kit according to the manufacturer's instructions. 8-12 weeks old mouse was sacrificed by keeping it in a CO₂ chamber followed by cervical dislocation. The spleen was isolated from the sacrificed mouse and smashed into 70 µm filter into fresh and warm RPMI medium. Splenocytes were then

collected into a fresh falcon tube and spun down. Red blood cells were then lysed by treating the cell pellet with 1 ml of erythrolysis buffer for 30 s, after which the lysed cells were diluted in RPMI medium and then centrifuged. The cell pellet was then washed with ice-cold isolation buffer and 50×10^6 splenocytes were then re-suspended in 0.5 ml of isolation buffer with 25 μ l of mouse anti-CD8 antibody and kept on ice for 10 min. The cell suspension was then washed in isolation buffer at 1300 rpm for 8 min at 4°C to get rid of unbound antibody. After the wash, the cells were re-suspended in 1 ml of isolation buffer with 75 μ l of magnetic FlowComp Dynabeads, and kept to rotate at 4°C for 15 min. The cells were then exposed to the magnet for 2-3 min to replace the Dynabeads solution with 2 ml of fresh isolation buffer. After another 2-3 min in the magnet, the isolation buffer was replaced with 1 ml of Release Buffer and the cells were kept on the rotator for 10 min at RT. The cells were exposed to the magnet again to separate them from the magnetic beads, and CD8⁺ T cells were collected in the supernatant. Cells were then centrifuged at 1300 rpm for 8 min at RT and re-suspended in IMDM medium at a concentration of 1×10^6 /ml in a 24-well plate. Cells were activated with mouse CD3/CD28 mouse Activation Dynabeads and incubated for 2 days at 37°C/5% CO₂.

II.2.2 Cell splitting and transfection

After 2 days of activation, CD8⁺ T cells were transferred to a 12-well plate and supplemented with fresh IMDM medium and mouse IL-2 (50 U/ml). 12-16 h before measurements on day 3, cells were prepared for electroporation. Activation Dynabeads were removed by the magnet and cells were centrifuged and then washed in warm isolation buffer at 900 rpm for 8 min at RT. During this time, Transfection medium was prepared according to the manufacturer's instructions and incubated at 37°C/5% CO₂ to warm it and calibrate its acidity. After wash, 5×10^6 cells were re-suspended in 100 μ l of Nucleofection solution with 1 μ g of plasmid DNA, and cells were then electroporated using the Amaxa Nucleofection device. Cells were then immediately gently transferred to the warm transfection medium and incubated at 37°C/5% CO₂.

II.2.3 RNA extraction

5×10^6 CTLs were collected, pelleted, and re-suspended in 1 ml of TRIzol. The pellet was homogenized by thorough pipetting and then centrifuged at 13000 rpm for 10 min at 4°C. The supernatant was then moved to a fresh 1.5 ml tube and 200 μ l of chloroform (for 1 ml of TRIzol)

were added and mixed. The mixture is let to stand at RT for 2-3 min before centrifugation at 13000 rpm for 15 min at 4°C. A three-phase mixture resulted in: a top aqueous phase (contains RNA), an interphase (contains DNA), and a bottom organic phase (contains DNA and proteins). The aqueous phase was carefully transferred to a fresh 1.5 ml tube where RNA was precipitated with 500 µl of isopropanol (per 1 ml of TRIzol). The mixture was incubated for 10 min at RT and centrifuged at 13000 rpm for 10 min at 4°C. The supernatant was discarded and the precipitated RNA washed with 1 ml of 70% ethanol (per 1 ml of TRIzol) at 7500 g for 5 min at 4°C. The RNA pellet was then allowed to air-dry at RT for 15-20 min. Its color should change to transparent and the ethanol smell should disappear. RNA was then dissolved in 12 µl of DEPC-treated water.

To check the RNA quality, RNA was diluted in DNase/RNase-free water (1:100 and 1:200). The diluted RNA samples were incubated at 90°C for 10 min to linearize RNA, then cooled immediately on ice. Samples were then run on an RNA-denaturing gel (0.4 g agarose, 20 ml DEPC water, 5.3 ml 5x MOPS buffer, 4.7 ml Formaldehyde 37%) in order to detect the 18S and 28S ribosomal RNA (rRNA) bands. The running buffer contained 50 ml 5x MOPS buffer in 200 ml DEPC water, and the running time was 10 min at 80 V and 85 min at 100 V.

Absence of higher molecular weight bands on the gel showed that RNA was pure and not contaminated with genomic DNA. Absence of smearing indicated that RNA was not degraded.

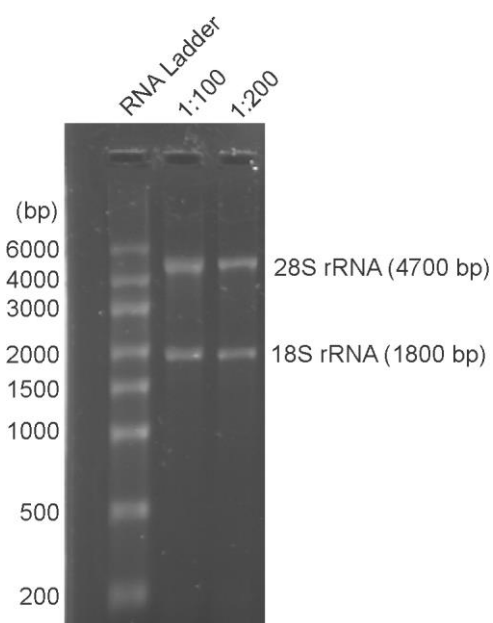


Figure 11: Checking RNA quality by denaturing RNA gel electrophoresis.

Two dilutions of extracted RNA (1:100 and 1:200) were prepared and run on denaturing gel to check for the quality and purity of total RNA. The two bands in lanes 2 and 3 at 4.7 and 1.8 kb correspond to the 28S and 18S ribosomal RNA (rRNA) subunits. Absence of smears and other bands showed that RNA was not degraded nor contaminated with genomic DNA. RNA ladder was from PEQGOLD high range RNA Ladder.

II.2.4 CDNA synthesis: reverse transcription

SuperScript™ II Reverse Transcriptase kit was used to synthesize cDNA (coding DNA) out from RNA. 1 µg of RNA was collected and mixed with 1 µl of dNTP mix (10 mM), 1 µl of random primers (1 µM), and complemented with RNase-free water to a volume of 12 µl. The mixture was heated in the thermocycler at 65 °C for 5 min to linearize the RNA secondary structure, and then incubated on ice for 5 min to preserve the linearized structure. After incubation, 4 µl of first strand buffer (5x), 2 µl DTT (0.1 M), 1 µl of RNaseOUT (RNase inhibitor), and 1 µl of SuperScript™ II reverse transcriptase was added. The total mixture was run in the thermocycler for 1 h at 42°C.

II.2.5 Polymerase Chain Reaction PCR

For detection of synaptotagmin isoforms expression at the mRNA level in day 3 activated mouse CTLs versus adult mouse brain as a positive control, highly specific primers were designed to bind the corresponding cDNA sequences but not genomic DNA. For this purpose, forward and reverse primers were designed to bind to two different exons of the same transcript. The set of used primers, bound exons, applied melting temperatures and expected PCR product length are displayed in Table 3.

In general, for a 50 µl PCR, 1 µl of each primer (25 pmol/L) were mixed with 100 ng of CTL cDNA (25 ng of brain cDNA), 1 µl dNTPs (10 mM), 5 µl of reaction buffer (10x), 1 µl of REDTaq DNA polymerase, and water till a total volume of 50 µl. The reaction was run according to the following protocol:

	Step	Duration	Temperature
1	Initial Denaturation	5 min	94°C
2	Denaturation	30 sec	94°C
3	Primer Annealing	30 sec	Listed in Table 3
4	Extension	30 sec-1min	72°C
5	Final Extension	10 min	72°C
6	Hold		4°C

Table 2: Duration and applied temperatures of PCR.

The cDNA quality was always checked with each cDNA synthesis for contamination with genomic DNA. The produced cDNA was run in a PCR with primers for the house-keeping gene Hypoxanthine Guanine Phosphoribosyl Transferase (HPRT), where the primers bind exons 1 and 2. The forward primer sequence is: GTT ATG ACC TAG ATT TGT TTT G, and the reverse primer sequence is: ATG GAT CTA TCA CTA TTT CTA TTC. The expected PCR product length from cDNA was 232 bp. Results are shown in the following gel picture.

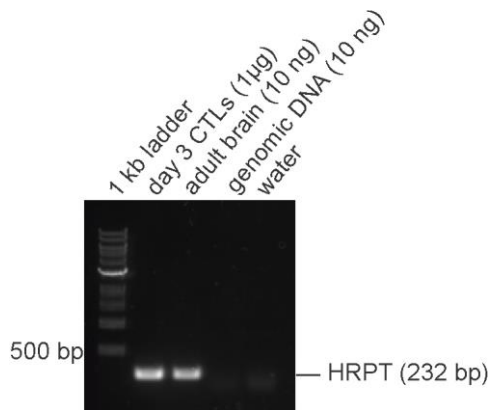


Figure 12: Verification of cDNA quality.

1 µg of CTL cDNA, 10 ng of brain cDNA, and 10 ng of genomic DNA were run in PCR reactions with primers for the house keeping gene HRPT to check for the production of cDNA after reverse transcription from RNA and the absence of genomic DNA from the produced samples. Water replaced cDNA for a negative control. A single band for the amplified HRPT was detected at the right size (232 bp) from activated CTLs and brain cDNA but not in genomic DNA and water.

II.2.6 Preparation of anti-CD3 coated coverslips

25 mm glass coverslips were used to apply the anti-CD3 coating. 40 µl of diluted 0.1 mg/ml polyornithine (10%) were applied to the center of the coverslip and let on RT for 30 min to settle. The whole volume was then sucked out and replaced with 40 µl of 30 µg/ml of mouse anti-CD3. Coverslips were then incubated for 2 h at 37°C. The solution was then sucked out and the coated coverslips were stored at 4°C before use.

II.2.7 Immunocytochemistry

To check the localization of Syt7 in mouse CTLs, day 3 activated CTLs were transfected with GranzymeB-mCherry. Eight hours' post-transfection, cells were spun down and then seeded onto anti-CD3 coated coverslip where they were allowed to attach for 10 min at RT. Ice-cold PFA (4%) was added carefully afterwards to fix seeded cells and allowed to stand at 4°C for 20 min. Later, PFA was sucked out and cells were washed gently with PBS (1X) for 3 times. Cells were

then permeabilized by replacing PBS with PBS containing 0.1% TritonX-100 for 20 min at RT. Cells were then blocked with a blocking solution containing PBS with 0.1% TritonX-100, 2% BSA for another 20 min-40 min at RT. After blocking, rabbit anti-Syt7 primary antibody diluted in blocking solution (1:200) was applied and kept for 2 h at RT. Cells were then washed with PBS (1X) with 0.1% Triton-X every 5 min for 5 times to remove excess antibody. Cells were incubated afterwards with the secondary goat anti-rabbit antibody conjugated with Alexa-405 diluted in blocking solution (1:2000) for 1 h at RT. Unbound antibody was then washed away with PBS (1X) with 0.1% TritonX-100 every 5 min for 5 times at RT. Coverslips were then mounted on glass slides using the 20 µl of mounting medium and allowed to dry for 15 min at RT. Glass slides were kept at 4°C until image acquisition by SIM microscopy.

The same protocol was applied to compare the localizations of Syt7 and CD3 where Rat anti-CD3-Alexa 647 primary antibody (1:200) was applied.

II.2.8 Western blotting

Lysate Preparation: To detect Syt2 expression level after transfection with siRNA, cells were collected from culture after 24 h and 48 h post-transfection and washed with ice-cold PBS. Pellets were re-suspended in 50 µl of SDS sample buffer (1x) (Invitrogen) + 10% β-mercaptoethanol. Cells were then sheared by sonication. Cell homogenates were spun down at 13000 rpm speed for 10 min at 4°C then supernatants were collected and denatured at 70°C for 20 min. In case of endogenous Syt2 protein detection, day3 activated CTLs were collected from culture, washed in ice-cold PBS, and re-suspended in 50-150 µl (for 10 million cells) of fresh ice-cold lysis buffer. Cells were then homogenized with 1 ml syringe on ice and incubated on a rotator for 30 min at 4°C. Cell homogenates were spun down at 13000 rpm speed for 10 min at 4°C and supernatants were collected into fresh tubes. Protein concentrations were measured via the Bradford Assay (Sigma Aldrich) and 100 µg of protein were aliquoted. For lysate denaturation, protein aliquots were mixed with sample buffer containing 1x SDS+10 % β-mecraptoethanol along with water till a maximum volume of 35 µl. Protein samples were then denatured at 70°C for 20 min.

Blotting: Denaturing gradient 4-12% Bis-Tris gel (Fischer Scientific) was used to run and separate protein lysates. Electrophoresis was done by running the gel for 2-2.5 h at 100 V. Proteins were then transferred onto a nitrocellulose membrane (Fischer Scientific) with 0.45 µm

pore diameter for 3 h at 300 mA. The membrane was then blocked with 5% non-fat dry milk (AppliChem Panreac) in 1X TBS-T (0.1%) buffer for 1.5 h at RT, and then incubated with rabbit anti-Syt2 antibody (1:1000) (ab113545) in 5% BSA in 1X TBS-T (0.1%) for overnight at 4°C. The blot was then washed for 5 times with 1X TBS-T (0.1%) at RT to remove unbound antibody and incubated with the HRP-conjugated goat anti-rabbit secondary antibody (1:5000) (Millipore Sigma) for 2 h at RT. The blot was washed again 5 times in 1X TBS-T (0.1%) at RT. For chemiluminescent detection of proteins, the membrane was developed with Pierce western blot signal enhancer and then images were taken by FluorChem E Imaging System (ProteinSimple).

For loading control, the blot was stripped using stripping buffer (Fischer Scientific) for 11 min at RT and then washed 3 times with 1X TBS-T (0.1%). Further the blot was blocked with 5 % non-fat dry milk in 1X TBS-T (0.1%) buffer for 1 h at RT and then incubated with rabbit anti-GAPDH antibody (Cell Signaling) for 1 h at RT, washed 5 times with 1X TBS-T (0.1%), and incubated with HRP-conjugated goat anti-rabbit secondary antibody (1:5000) for 1 h at RT. Washing 5 times with 1X TBS-T (0.1%) followed before treating the membrane for chemiluminescent detection again with the same procedure stated above.

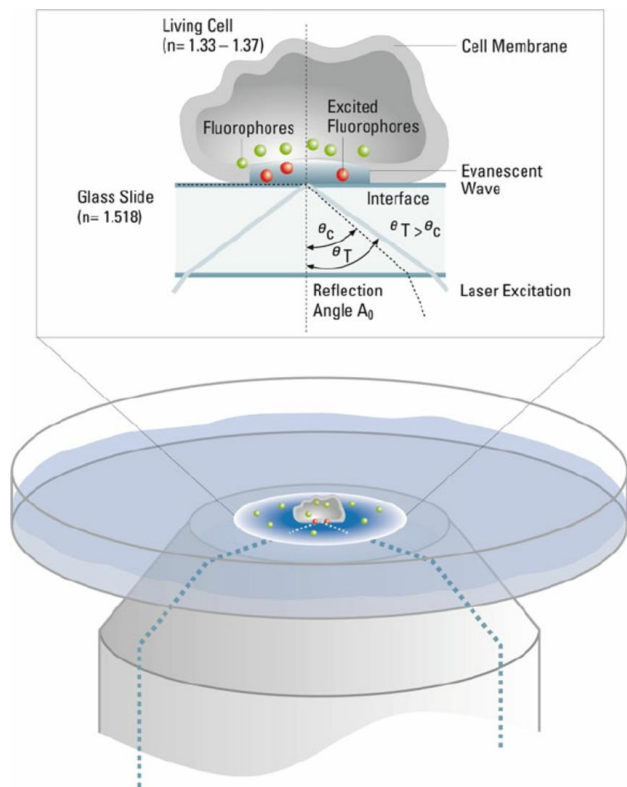
II.2.9 Structured Illumination Microscopy (SIM)

We used this super-resolution technique to determine and compare the localization of different proteins in the cell. The SIM microscope is a widefield microscope that defies the diffraction limit of light discovered by Ernst Abbe in 1873 under the law: $d = \lambda / 2NA$, where d is the diffraction limit of light, λ is the wavelength of light, and NA is the numerical aperture of the objective (Abbe, 1873). SIM uses stripes-patterned light illumination to excite the sample. The pattern orientation is changed by rotation and the emitted fluorescence is collected and recorded for each rotation. The interference between the striped excitation pattern and the resulting diffraction in the sample emission ends in a Moiré effect. These Moiré patterns enclose high frequency spatial information which are deciphered using a specialized algorithm. After processing, a final image is reconstructed from the multiple images into a final image that has lateral resolution between 100 and 130 nm. The SIM microscope we used has an oil-immersion 63x objective with a NA of 1.4 Plan Apochromat. The setup has several lasers, out of which we

used an HR Diode 405, 488, and 642 nm lasers, in addition to an HR DPSS 561 nm lasers. Cells were imaged using ZEN software by acquiring multiple stacks with a step of 0.2 μm .

II.2.10 Total Internal Reflection Fluorescence Microscopy (TIRF)

TIRF microscopy is an advantageous technique for imaging cellular structures or organelles located at or close to synapses with high axial resolution below 100 nm. The principle of TIRF is explained in figure 13. TIRF Recordings were performed using the TIRF microscope setup from Visitron, Puckheim, Germany. It consisted of an inverted Optical IX microscope (Olympus, Hamburg), solid-state lasers (Visitron Systems) emitting at a wavelength of 561 nm and 488 nm. The TIRF condenser was based on the iLAS² (Roper Scientific, Evry, France) that allows even TIRF illumination and multiband filter set (AHF, Tübingen, Germany). The camera was a back-illuminated EMCD Evolve 512 (Photometrics, Tucson, AZ, USA). Acquisition rate was set to 10 Hz and the exposure time to 100 ms.



Leica Tutorial, 2012

Figure 13: Principle of TIRF microscopy.

This technique was developed by Daniel Axelrod in 1980. It is based on exciting fluorophores using an evanescent wave instead of a direct illumination. The evanescent wave is created when an incident laser light is totally internally reflected at the interface between glass and cell media that have different refractive indices. The electromagnetic field generated at this interface excites fluorophores localized at a close proximity to the cell membrane. The energy of the electromagnetic field decays exponentially as we go deeper into the cell and hence only fluorophores within 100-200 nm away from the interface are excited. This leads to images with outstanding signal to noise ratio as distant fluorophores are hardly excited.

II.2.11 Calcium imaging

II.2.11.1 Measurement of intracellular free calcium using Fura-2 am

Fura-2 is a widely used fluorescent calcium indicator that shows a shift in excitation wavelength upon binding calcium. This fact allows us to determine the concentration of free calcium regardless of the dye loading efficiency, specimen thickness, change in focus, variation in laser intensity, bleaching, etc. the acetoxymethyl (am) form of Fura-2 is membrane-permeable. Once it crosses the plasma membrane, the acetoxymethyl group is cleaved by cellular esterases, rendering Fura-2 in the cytosol. The K_d of Fura-2 for calcium is between 135 nM and 224 nM, depending on pH, temperature, and ionic composition of the medium (Grynkiewicz et al., 1985). When Ca^{2+} -free, the absorption maximum of laser light by Fura-2 is at 380 nm. When it's Ca^{2+} -bound, its absorption maximum shifts to 335 nm. The emission maximum is 510 nm in both states.

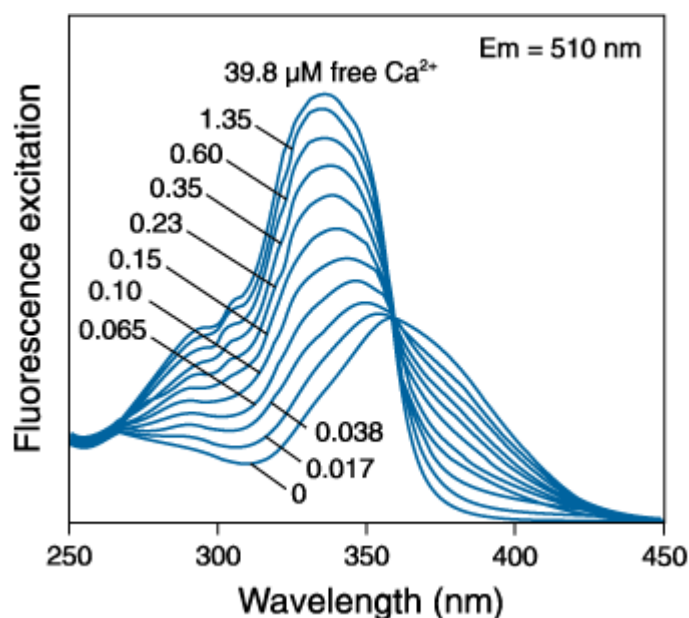


Figure 14: The fluorescence excitation spectra of Fura-2 under different free calcium concentrations from 0 to 39.8 μM (Thermofischer Scientific).

In our experiment, 350 nm and 380 nm were chosen as the excitation wavelengths for the Ca^{2+} -bound and Ca^{2+} -free forms of Fura-2. A ratio of the emission fluorescence intensities after

excitation at these wavelengths was calculated to determine the real calcium concentration using the Grynkiewicz equation: $[Ca^{2+}]_i = Kd \cdot \beta \cdot ((R - R_{min}) / (R_{max} - R))$, where:

* $[Ca^{2+}]_i$: the concentration of free intracellular calcium

* Kd: the dissociation constant of Fura-2 under our measurement conditions (RT, pH = 7.2)

* β : the ratio of (maximum fluorescence intensity of Fura-2 at 380 nm in the Ca^{2+} -free conditions) / (maximum fluorescence intensity of Fura-2 at 380 nm in the saturating conditions)

* R: the experimental Fura-2 350/380 ratio

* R_{min} : the minimum Fura-2 ratio obtained in Ca^{2+} -free conditions

* R_{max} is the maximum Fura-2 350/380 ratio obtained in Ca^{2+} saturating conditions.

These constants were determined previously by Dr. Ute Becherer who patched Jurkat cells on the same setup with 3 intracellular solutions (+ Fura-2) with known free calcium concentrations: 0, 268 nM, and 10 mM, representing Ca^{2+} -free, 'around the Kd', and saturated conditions, respectively.

To determine the concentration of free calcium in WT and Syt7 KO cells under my conditions in the TIRF experiments, we collected day 3 activated CTLs and removed the activation magnetic beads. We washed the cells in PBS (1X) and re-suspended the cells in 500 μ l of 2 μ M Fura-2 am medium (Fura-2 am + serum-free IMDM medium). We incubated the cells with Fura-2 am for 30 min at RT and washed them afterwards twice with IMDM medium. After washing, we re-suspended the pellet in 0 mM Ca^{2+} Ringer's solution and loaded the cells onto anti-CD3 coated glass coverslips. By applying this protocol, the cells were under the same conditions as the TIRF experiments. We recorded in low Ca^{2+} for 7 min, and then in 10 mM extracellular Ca^{2+} Ringers solution for another 7 min.

II.2.11.2 Measurement of extracellular free calcium using Fura-2ff

Fura-2ff is a di-fluorinated derivative of Fura-2 where it has similar fluorescence properties to Fura-2 but a lower affinity to Ca^{2+} (Hyrc et al., 2000). We used this calcium indicator to measure the concentration of extracellular calcium under residual/low conditions.

In order to do so, we prepared 6 different calibration solutions with known free calcium concentration (10 nM, 1.33 μM , 23.4 μM , 108 μM , 518 μM , and 9.4 mM). We measured the emitted fluorescence intensity of Fura-2ff when excited at 350 nm and 380 nm and plotted the 350/380 ratio as a function of the known concentrations to generate a calibration curve.

To determine the concentration of residual calcium under our measurement conditions, we pelleted day 3 activated cells, collected the supernatants, and combined them with Fura-2ff (100 μM). From each supernatant, we did three measurements and averaged them. In each measurement, we added 1.5 μl of the (supernatant+Fura-2ff). We did this experiment 3 times.

II.2.12 NH_4Cl treatment

Cells were treated with 1 ml of 40 mM NH_4Cl . NH_4^+ dissociates to NH_3 and H^+ . NH_3 diffuses to the acidic lumen of the granule and sequesters H^+ inside and therefore the granule pH increases (Lazarenko et al., 2017). The fluorescence intensity was recorded in epifluorescence mode and the mean fluorescence intensity of individual granules was quantified. The maximal values from individual traces were averaged.

III. RESULTS

III.1 The experimental setup

CG fusion in cytotoxic T lymphocytes takes place at the immunological synapse (Grakoui et al., 1999; Dustin and Long, 2010). We imaged fluorescently labelled CGs of CTLs seeded on anti-CD3 coated coverslips. These cells build the immune synapse at the plasma membrane-coverslip interface in response to the anti-CD3 which allowed us to monitor fusion using TIRF illumination (Mattheyses et al., 2010; Pattu et al., 2013; Ming et al., 2015). CD8⁺ T cells contain very few granules under resting conditions, so we activated the cells for 2 days in culture with CD3/CD28 Dynabeads (Thermofischer) to trigger cell proliferation and CG biogenesis (Olsen et al., 1998). After activation in culture, we transfected the cells by electroporation with a GranzymeB-mCherry fusion protein construct to specifically label cytotoxic granules (Pattu et al., 2013). TIRF measurements were carried out 12-16 h post-transfection. For each measurement, 600×10^3 cells were collected from culture, centrifuged, and re-suspended in a nominally 0 Ca²⁺ Ringer's solution. Cells were then seeded on anti-CD3 coated coverslips to induce IS formation at the cell-coverslip interface and to prompt the subsequent recruitment of CGs to the newly formed synapse.

The TIRF images were acquired at 10 Hz (10 frames/second). A fusion event was recognized as a rapid decrease in the fluorescence intensity of GranzymeB-mCherry and a rapidly dispersing cloud of fluorescence around the site of fusion. Intensity-over-time recordings were analysed in image J after drawing a region of interest (ROI) around the fusing granule, a second ROI in close proximity to the fusing granule, and a third ROI at a moderate distance from the fusing granule. In this way we could track the cloud's dispersion after GranzymeB-mCherry release and confirm that the disappearance of the fluorescent granule was due to its fusion and not due to movement from the plasma membrane. Figure 15 illustrates a series of representative TIRFm images of a CG fusion event (panel A) and the described analysis (panel B).

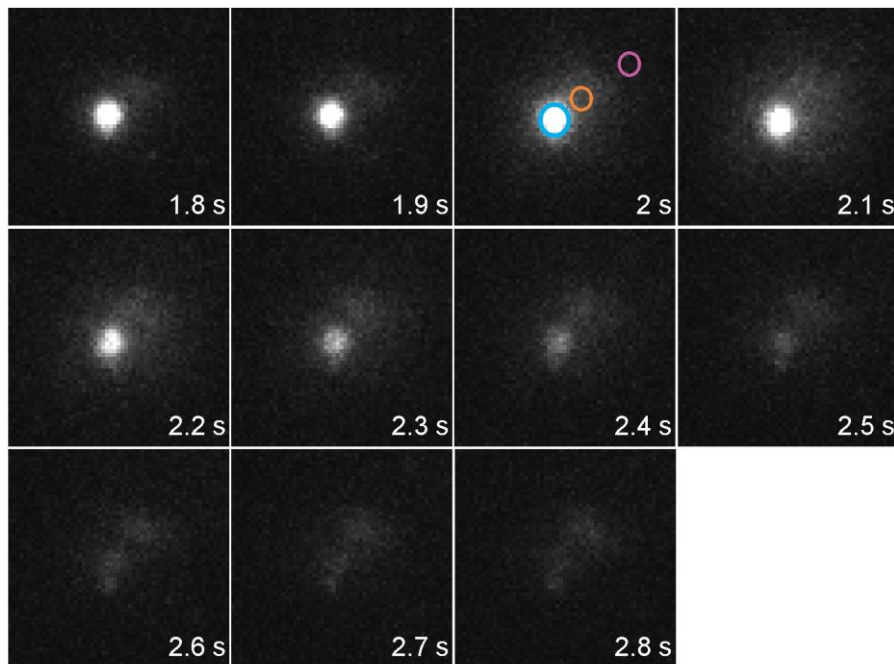
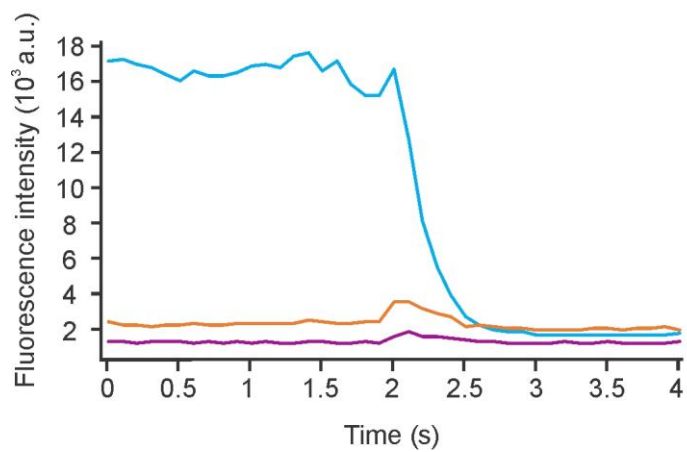
A**B**

Figure 15: CG fusion in TIRF microscopy.

(A) Individual frames of a fusion event of a GranzymeB-mCherry loaded cytotoxic granule. ROIs are drawn around the fusing granule (in blue), next to the granule (in orange), and at a distance from the granule (in purple) to confirm GranzymeB-mCherry release and cloud propagation. **(B)** Fluorescence intensity change (10^3 a.u.) over time (s) of the three regions of interest shown in (A).

III.2 The expression profile of synaptotagmins in mouse CTLs

To examine which synaptotagmin isoforms are expressed in activated CTLs, we designed specific primers for the 17 isoforms of synaptotagmins using the software listed in the Methods (II.1.14). Primers were designed to bind only exons in order to exclude genomic DNA binding. The list of primers, annealed exons, annealing temperatures, and PCR band sizes are shown in Table 3.

Syt isoform	Forward primer	Reverse primer	Exons	Tm (°C)	PCR product size (bp)
Syt1	AACTTGAGGCTGTAACCGGG	TTCCTTGGATGCAGAGGAGAC	Exon1-Exon2	59.5	364
Syt2	TCACCTGTTGCTTCTGCATC	ATGTCTCATTGAAGGCTGGGT	Exon2-Exon4	57.5	392
Syt3	ATCACGTGGCCACTATGTCTG	CCAGAACCTGTTCCACCCTC	Exon3-Exon4	60	609
Syt4	AAGCGAGACCTCAATGGCAAC	ACCAACCGTCCAATCACCTC	Exon2-Exon4	59.5	884
Syt5	GATGGGGTGGCATAACAGAGG	CCCAGCTCCTTCACTTCTG	Exon1-Exon2	60.5	463
Syt6	ATGGGGATGATGCAAGTCG	AACTCCAGTGGCTGTGCTC	Exon3-Exon7	59.5	927
Syt7	AAAGCCATCAAGTTGCCTGC	GGATGGACACCTCCCAATG	Exon3/4-Exon6	57.5	534
Syt8	ATCCCAGACCTCATCACCAG	CAGGGTTCTAGGCAGTCCAC	Exon2-Exon4	59.5	248
Syt9	CTCTGTGAGCCTGCTAACC	GTCCCAGAGAAGTCTTGGC	Exon2-Exon3	61	615
Syt10	GGGCATCTTCCAGCCGATAG	GGAAGGACACTGAGGTTGGG	Exon1-Exon2	61	185
Syt11	GTCATCGGAGAGGTCATGGT	TGACAAGGAACCTCGATGCTG	Exon3-Exon5	57.5	376
Syt12	CCGTGGACGTGACAGAATATC	CGATGTCCAGAGCTTCCATAG	Exon2-Exon3	59.5	131
Syt13	GACACATGCACCCCAAGAAG	CTCCTCTGTGGTCTCCAAGG	Exon1-Exon2	59.5	232
Syt14	ACCACCAATGGACTGTTCTG	GGCTGCTGAGCATTAAAGGAC	Exon7/8-Exon8	59	576
Syt15	GGGACCACCACCGTATCATC	CCACGGGTGTACATGTAGGG	Exon5-Exon8	61	403
Syt16	GCCACAACAGGGCGATTATC	AATGGGGTGGCAGAGGATTG	Exon6-Exon7	59	849
Syt17	CTGAACGTGGACATCATTG	GCGTTTTCCAGTCTTCTG	Exon6-Exon7	57	200

Table 3: The list of primers, annealed exons, annealing temperatures, and PCR band sizes.

We collected total RNA from day3-activated CTLs by the TRIzol method and synthesized total cDNA by reverse transcription using the SuperScript™ II Reverse Transcriptase kit. Adult mouse brain cDNA was used as a positive control and was replaced with water for a negative control. Figure 16 shows the expression profile of the synaptotagmin family in mouse activated cytotoxic T lymphocytes.

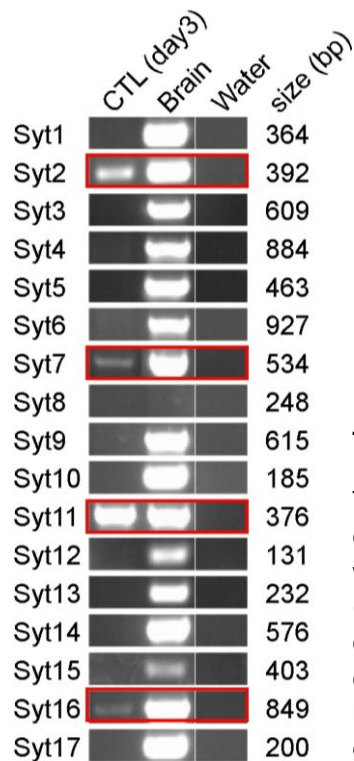


Figure 16: The expression profile of the synaptotagmin family in mouse activated CTLs and brain cells.

Total RNA was collected from day3-activated CTLs and converted to total cDNA by reverse transcription. PCR reactions were applied on total cDNA from CTLs and adult mouse brain (positive control) using complementary primers. 100 ng of CTL cDNA and 25 ng of brain cDNA were used for each reaction. cDNA was replaced with water for negative controls. PCR reactions were carried out 3 times. Syt isoforms which are expressed in activated CTLs are indicated by red boxes.

We found 4 synaptotagmin isoforms expressed in day3 activated mouse CTLs: Syt2, Syt7, Syt11, and Syt16 were present (figure 16-marked in red rectangles), and all the isoforms were detected in the brain except for Syt8 (we confirmed that the primers functioned by the presence of a band in the genomic DNA which ran at a higher size). Syt16 is a Ca^{2+} -independent member of the synaptotagmin family (Fukuda, 2003), hence it is an unlikely candidate for calcium sensing of cytotoxic granule fusion. Syt11 is a non-calcium binding Syt as well and has been shown to be implicated in inhibiting bulk endocytosis in neurons (Wang et al., 2016). Syt2 is a low affinity Ca^{2+} sensor, highly expressed in the brain, and shows high homology with Syt1 (Geppert et al., 1991; Xu et al., 2007; Sun et al., 2007; Craxton, 2010). Syt7 is a high affinity Ca^{2+} sensor shown previously to be localized to LDCVs in chromaffin cells (Fukuda et al., 2004; Matsuoka et al., 2011) and to lysosomes in fibroblasts (Martinez et al., 2000). Cytotoxic granules in CTLs are secretory lysosomes by nature (Burkhardt et al., 1990; Peters et al., 1991; Clark and Griffiths, 2003), and Syt7 has been reported to regulate lysosome fusion in fibroblasts (Martinez et al., 2000), macrophages (Czibener et al., 2006; Becker et al., 2009), and osteoclasts (Zhao et al., 2008). It has been shown that CTLs are able to carry out killing at a low intracellular Ca^{2+}

concentration (Lyubchenko et al., 2001). For these reasons, Syt7 is considered a good candidate for the Ca^{2+} - sensor for fusion of CGs in CTLs.

III.3 The localization of Syt7 in mouse CTLs

To determine if Syt7 is localized on CGs in mouse CTLs, we electroporated day3 activated CTLs with a GranzymeB-mCherry fusion protein to label CGs, knowing that GranzymeB is a highly specific marker of CGs in cytotoxic lymphocytes (Pattu et al., 2013). Eight hours after overexpression, we detected the fluorescence of GranzymeB-mCherry in some cells, so we fixed, permeabilized, and stained the cells with anti-Syt7 antibody (see Methods). Syt7 was not detected in western blots. This was surprising considering that Syt7 has been reported to be involved in CG release in lymphocytes (Fowler et al., 2007). The discrepancy is likely due to low expression levels of Syt7. We produced a Syt7-IRES-GFP construct and expressed it in day3 activated CTLs. Using SIM microscopy (Zen software), we scanned the cells and imaged 0.2 μm -thick stacks of each cell. GranzymeB-mCherry fluorescence (red) was punctate, consistent with cytotoxic granules (figure 17-top panel). Syt7 (green) showed two patterns: punctate staining and membrane-like staining. The yellow staining in the merged image and in the maximal intensity projection (MIP) image of the top panel show that Syt7 was associated with CGs. Statistical analysis of the Manders' overlap coefficients gave 0.198 ± 0.048 for M1 (Syt7 to GranzymeB) and 0.292 ± 0.058 for M2 (GranzymeB to Syt7) (figure17-top bar graph).

The relatively low Manders' coefficients of Syt7 versus GranzymeB are due to both a localization of Syt7 at the membrane and the fact that not all puncta stained for both Syt7 and GranzymeB. To confirm a membrane localization of Syt7 we overexpressed Syt7 in day3 activated CTLs and co-stained them for Syt7 (green) and CD3 (magenta), which is a membrane marker in T cells (Leong et al., 2003). Syt7 and CD3 co-localized (white staining in the merge and the MIP images) at the plasma membrane (M1= 0.617 ± 0.043 for Syt7 to CD3; M2= 0.436 ± 0.042 for CD3 to Syt7) (figure 17-bottom panel/bottom bar graph). Syt7 membrane localization is expected after CG fusion with the plasma membrane and may be exacerbated following overexpression (Virmani et al., 2003; Wang et al., 2005; Weber et al., 2014).

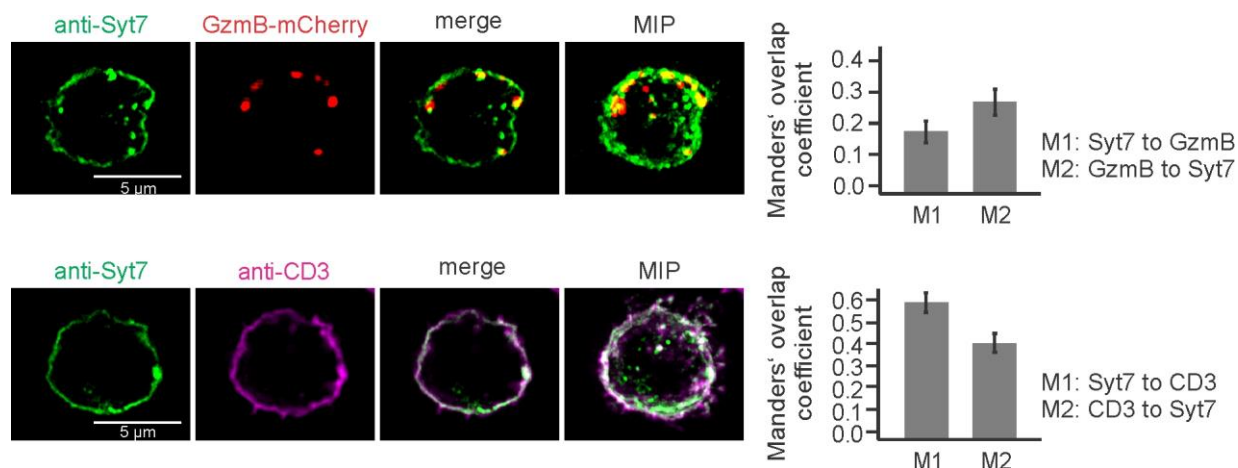


Figure 17: The localization of Syt7 in mouse CTLs.

Top Panel: Day3-activated CTLs overexpressing GranzymeB-mCherry (red) were fixed after 8 hours of electroporation, permeabilized, and stained with anti-Syt7 antibody (green). The yellow staining in the merge and MIP images show that Syt7 is associated with cytotoxic granules in CTLs. M1=0.198 ± 0.048 for Syt7 to GzmB; M2=0.292 ± 0.058 for GzmB to Syt7. Bar=5µm; n=13 cells. **Bottom Panel:** Day3-activated CTLs were co-stained for Syt7 and CD3 (membrane marker) and show a nice co-localization (white) at the plasma membrane as illustrated in the merge and the MIP images. M1= 0.617 ± 0.043 for Syt7 to CD3; M2= 0.436 ± 0.042 for CD3 to Syt7. Bar = 5µm; n=13 cells; error bars = ± sem values.

III.4 CG fusion in WT and Syt7 KO cells

To elucidate the role of Syt7 in mouse CTLs, we compared GranzymeB-mCherry secretion between WT and Syt7 KO cells. Based on the fact that T cells can secrete in low extracellular calcium (100 µM) (Lyubchenko et al., 2001), we decided to carry out TIRF measurements in low/residual extracellular calcium conditions which makes Syt7, due to its high Ca^{2+} affinity the likely calcium sensor. For this purpose, 600×10^3 cells were harvested from culture medium, pelleted by centrifugation, and re-suspended in nominal 0 calcium Ringer's solution without prior washing. Hence, residual calcium from the culture medium was left with the cells. To determine the concentration of residual calcium, we added the calcium indicator Fura-2ff (100 µM; apparent $K_d = 80$ µM) to six calibration solutions with known free-calcium concentration (10 nM, 1.33 µM, 23.4 µM, 108 µM, 518 µM, 9.4 mM), and measured the 350nm/380 nm Fura-2ff ratios (see Methods II.2.11.2). A calibration curve (figure 18) was generated and the residual Ca^{2+} concentration was calculated from 9 experimental measurements of supernatants from pelleted CTLs. The deduced residual concentration was equal to $56 \mu\text{M} \pm 5.8 \mu\text{M}$ (n=3

experiments). According to a recent publication by Zhou et al. (2018), optimal killing by CTLs conjugated with target cells was achieved when the extracellular calcium concentration ranged between 23 and 625 μM (Zhou et al., 2018). Hence, our low extracellular calcium condition was physiologically relevant.

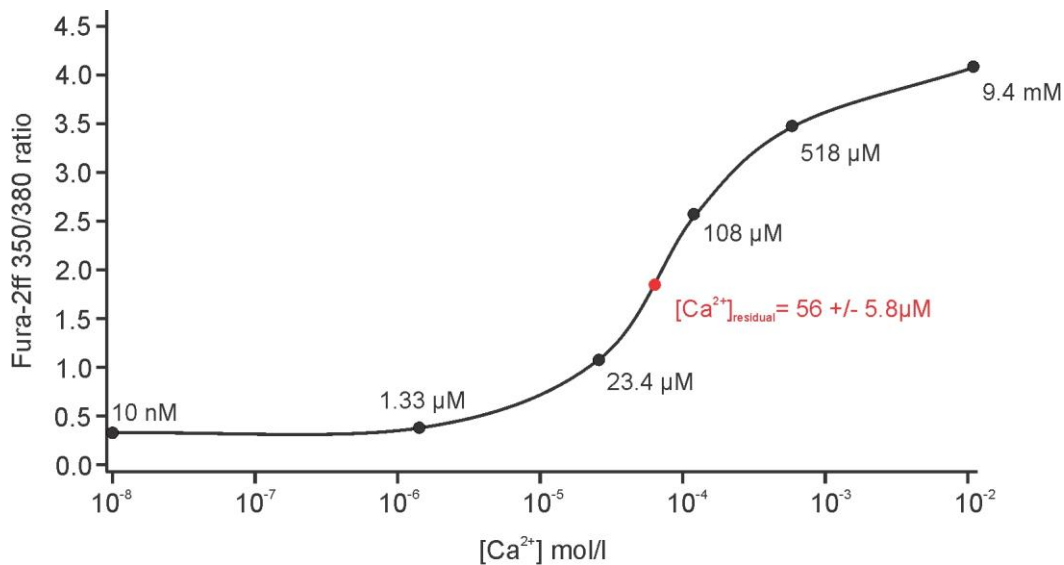


Figure 18: Fura-2ff calibration curve.

The residual free $[\text{Ca}^{2+}]$ was determined by extrapolating the average 350/380 Fura-2ff ratio deduced from 9 measurements (3 experiments) into the calibration curve. The calibration curve was generated by measuring the Fura-2ff ratio of 6 different calibration solutions with known free $[\text{Ca}^{2+}]$. The free residual Ca^{2+} concentration at which the TIRF measurements were performed was equal to $56 \mu\text{M} \pm 5.8 \mu\text{M}$.

III.4.1 The secretion probability is similar between WT and Syt7 KO CTLs

We compared CG fusion between WT and Syt7 KO cells at the residual calcium conditions and found no significant difference in the fraction of cells exhibiting CG fusion ($32.94\% \pm 2.49$ for WT; $38.69\% \pm 13.69$ for Syt7 KO; mean \pm sem; $P = 0.74$) (figure 19-B) nor in the mean number of fusion events per cell (2.04 ± 0.45 for WT; 2.23 ± 0.46 for Syt7 KO; $P = 0.77$) (figure 19-C). This could be because either Syt7 is replaced by a different Syt isoform in Syt7 KO cells, or that a Syt is not required for CG fusion.

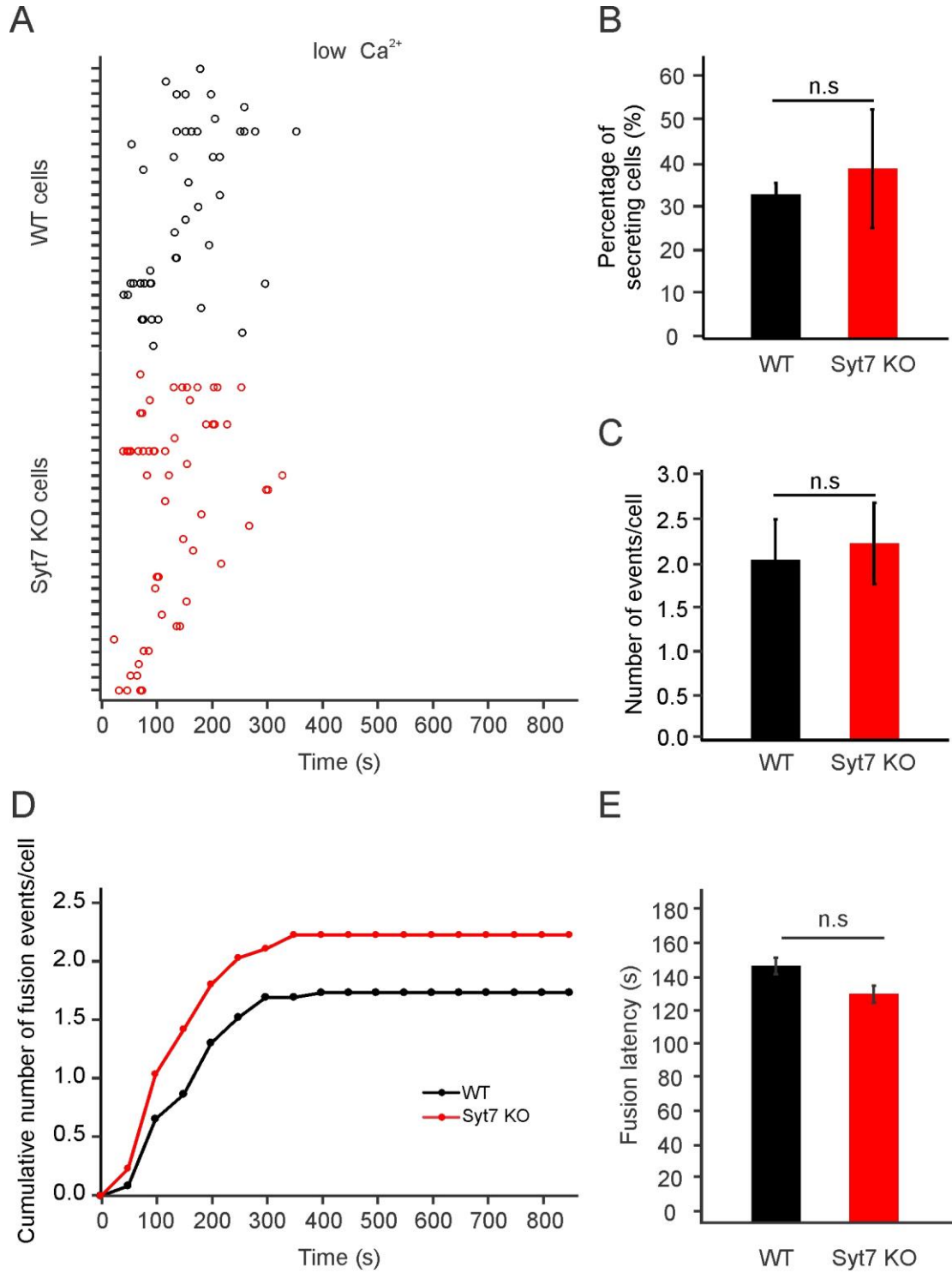


Figure 19: No difference in the fusion probability nor the fusion latency between WT and Syt7 KO cells.

(A) A scatter plot of the time latencies (s) of individual fusion events from WT and Syt7 KO cells incubated in low calcium for 14 min recording time. **(B)** Quantification of the mean percentage of secreting cells. **(C)** Quantification of the mean number of fusion events per cell. **(D)** The Cumulative number of fusion events per cell over time (s). **(E)** Quantification of the mean fusion latency of individual fusing granules. Data were collected from 3 experiments (68 WT cells, 81 Syt7 KO cells). Error bars = \pm sem. Non-significant, n.s via the unpaired Student's T test.

Both Syt7 KO cells and WT cells stopped secreting after 5 min (300 s) (figure 19-A). Although Syt7 KO cells show a faster accumulation of events over time (figure 19-D), we found no significant difference ($P = 0.28$) in the mean fusion latency (\pm sem) averaged from the latency of each fusing granule displayed in the scatter plot in panel A: WT cells ($146.017 \text{ s} \pm 10.89$); Syt7 KO cells ($130.067 \text{ s} \pm 9.93$). This experiment was done 3 times (68 WT cells; 81 Syt7 KO cells) and the unpaired Student's T-test was applied to determine P values.

III.4.2 A second round of secretion does not occur in Syt7 KO CTLs

It is possible that fusion of CGs was inhibited by the low ambient calcium concentration which would likely be reflected in low intracellular calcium concentration, so we added a higher concentration of extracellular calcium (10 mM) after 7 min of recording to determine if this led to further fusion. We carried out this protocol in TIRF over 14 min total recording time. The mean percentage of secreting cells (figure 20-B) was similar in the first 7 min in WT ($18.489\% \pm 2.757$) and Syt7 KO cells ($20.738\% \pm 2.885$). The mean number of fusion events per cell (figure 20-C) in the first 7 min was comparable as well (1.66 ± 0.38 for WT; 1.56 ± 0.15 for Syt7 KO). In the 7 min period after addition of 10 mM calcium, WT cells exhibited a second round of secretion ($9.18\% \pm 0.89$ secreting cells \pm sem; 1.69 ± 0.19 events/cell \pm sem) but Syt7-lacking cells did not (***, $P < 0.001$) (figure 20-A, B, C, D). Figure 20-E quantifies the mean fusion latency at low and high extracellular calcium. Fusion latency is the time taken for a fusion event to occur after the cell touches the anti-CD3 (at time = 0 s) or after the 10 mM Ca^{2+} is added (at 420 s). There is no significant difference in the fusion latencies in low calcium. The latency of

secretion in high calcium is similar in WT cells but Syt7 KO cells exhibited no fusion events after addition of high calcium (figure 20-E). The above result indicates that Syt7 is not required for CG fusion but may be necessary for a subsequent phase of fusion after addition of high calcium.

The lack of fusion in 10 mM Ca^{2+} could be due to an inhibition of secretion in Syt7 KO cells by high calcium or due to a failure of granule trafficking in the Syt7 KO cells. We incubated cells in a Ca^{2+} -free extracellular solution after rinsing the pellet to remove the residual calcium (0 mM Ca^{2+}). Fusion does not occur under these conditions. Recordings were carried out in TIRF for 7 min and then 10 mM Ca^{2+} was added. The CTLs showed no secretion in the first phase (0 mM Ca^{2+}) but both WT and Syt7 KO CTLs exhibit similar fusion after addition of the 10 mM Ca^{2+} medium. The percentage of secreting cells \pm sem was equivalent between WT (22.424% \pm 2.424) and Syt7 KO cells (21.25% \pm 0.93) at 10 mM extracellular Ca^{2+} (figure 20-F). So Syt7 KO cells could fuse under the high calcium conditions and the loss of secretion in Syt7 KO cells was not due to the increase in extracellular calcium. Hence, the loss of secretion in Syt7 KO cells is either due to a failure to resupply primed vesicles after the first bout of fusion and/or due to a regulatory role of Syt7 in late CG fusion.

Data in figure 20 A-E were collected from 3 different experiments: WT (n=99 cells), Syt7 KO (n=75 cells). Data in figure 20-F were collected from 3 different experiments (21 WT cells; 48 Syt7 KO cells). Error bars represent the standard error mean (sem). The two-tailed unpaired Student's T-test was applied to calculate the P values.

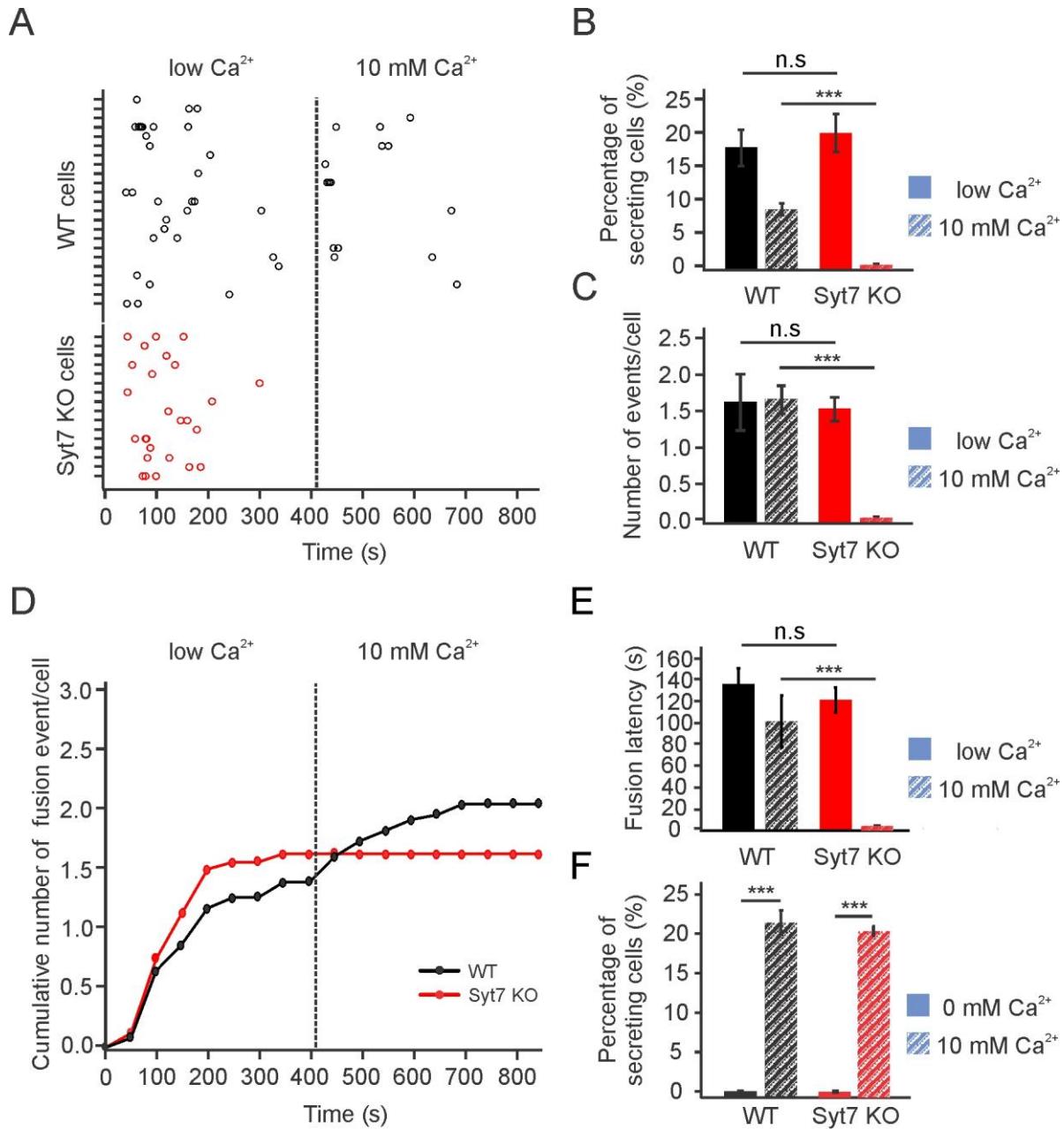


Figure 20: CG fusion in WT and Syt7 KO cells.

(A) The time course of individual fusion events (small circles) in scatter plot for WT (black) and Syt7 KO (red) cells in low Ca^{2+} and 10 mM extracellular Ca^{2+} . Ticks on the Y axis represent individual cells. Each circle corresponds to one fusion event. The dashed line stands at the switch between low calcium and 10 mM calcium. **(B)** The mean percentage of secreting cells in WT and Syt7 KO cells in low Ca^{2+} (uniform color) and 10 mM Ca^{2+} (patterned color). **(C)** The mean number of fusion events/cell in WT and Syt7 KO cells in low Ca^{2+} (uniform color) and 10 mM Ca^{2+} (patterned color). **(D)** The cumulative number of fusion events/cell in WT and Syt7 KO cells over time in low Ca^{2+} and 10 mM Ca^{2+} .

(E) The mean fusion latency (s) of fusing granules in WT and Syt7 KO secreting cells shown in panel A. Data in figures A-E were collected from 99 WT cells and 75 Syt7 KO cells in 3 different preparations. (F) Secretion in WT and Syt7 KO cells in Ca²⁺-free and 10 mM Ca²⁺ conditions. The experiment was done 3 times (21 WT cells; 48 Syt7 KO cells). Error bars are equivalent to sem values. P values (***, <0.001; n.s., non-significant) were determined by the unpaired Student's T-test.

III.4.3 Rescue of Syt7 KO cells with Syt7 overexpression

To determine if the absence of secretion under high calcium conditions in Syt7 KO cells was due to the lack of Syt7, we overexpressed a Syt7-IRES-GFP construct in Syt7 KO cells. The second round of secretion in Syt7 KO cells at 10 mM Ca²⁺ was rescued upon Syt7 overexpression, with the mean percentage of secreting cells \pm sem (24.407% \pm 2.733) and the mean number of events/cell \pm sem (2.4 \pm 0.2) significantly enhanced in comparison to Syt7 KO cells (***, P < 0.001) (figure 21-A, B, C-right panels). Compared to WT CTLs, KO+Syt7 cells showed a significant increase in the percentage of secreting cells (P = 0.006) and an almost significant (P = 0.06) increase in the number of events/cell in the second 7 min of recording. There was no change in numbers of secreting cells (20.231% \pm 1.927; P > 0.05) or numbers of events (2.361 \pm 0.518; P > 0.05) during the first 7 min of recording (figure 21- A, B, C-left panels). This shows us again that Syt7 is not involved in the early phase of secretion, rather it is necessary for the regeneration of CG secretion.

Since the second round of secretion was Syt7-dependent (figure 20-21) and required high calcium (figure 19-20), we tested the role of calcium binding to Syt7 C2A domain in this effect. For this purpose, we produced two Syt7 calcium-binding-deficient mutants. In one mutant we replaced one of the calcium binding aspartates (D227) with a neutral asparagine residue and in the second mutant we replaced all three aspartates (D225, D227, D233) involved in calcium binding with asparagine. These changes were made in the C2A domain of Syt7 since it has been shown to be required for the calcium sensing of Syt7 (Segovia et al., 2010; Bacaj et al., 2013; Bacaj et al., 2015). We co-expressed each mutant along with GranzymeB-mCherry in Syt7 KO cells and carried out TIRF experiments as before, to determine the effects of the expression of these mutants on CG fusion of Syt7 KO CTLs. Results in figures 21- B and C show that there was no significant difference in the percentage of secreting cells (P = 0.928 for KO+D227N vs. KO+Syt7; P = 0.343 for KO+3DN vs. KO+Syt7; P = 0.566 for KO+D227N vs. KO+3DN) nor in the number of fusion events/cell (P = 0.927 for KO+D227N vs. KO+Syt7; P = 0.108 for

KO+3DN vs. KO+Syt7; $P = 0.288$ for KO+D227N vs. KO+3DN) in the first 7 min (figure 21-B, C). The 3DN mutation had fewer fusion events than did the single aspartate mutation (D227N) (figure 21-A) but the differences with WT Syt7 and single mutant Syt7 (D227N) overexpression were not significant (figure 21-B, C-left panels). However, observed secretion was significantly lower in the second round after change to 10 mM extracellular calcium solution in both mutants (figure 21-A, B, C-right panels) (*, $P < 0.05$; **, $P < 0.01$). The traces of cumulative fusion events/cell (figure 21-D) showed increases for all three genotypes in the first 7 min. After addition of high calcium, fusion occurred in cells expressing mutated Syt7 isoforms but at lower levels than WT Syt7-expressing Syt7 KO cells. We quantified the fusion latency of occurring events at low and 10 mM Ca^{2+} and we found no significant difference between the three genotypes under low or high calcium conditions although disrupted calcium binding tended to reduce fusion (figure 21-E). The fact that secretion was not completely abolished in Syt7 KO cells expressing the triple mutant (3DN) points to a possible role of the C2B domain calcium sensing in the function of Syt7.

The lack of a significant effect of Syt7 overexpression on the early phase of secretion indicates that Syt7 is not involved in this phase. Results of this experiment confirm as well that Syt7 is necessary for the second round of secretion. It shows also that the role of Syt7 in the second round of secretion is dependent on Ca^{2+} binding via the aspartate residues in its C2A domain. Experiments were done 3 times (63 KO+syt7 cells; 80 KO+D227N cells, 51 KO+3DN cells). Error bars represent sem values. The unpaired two-tailed Student's T-test was done to determine P values.

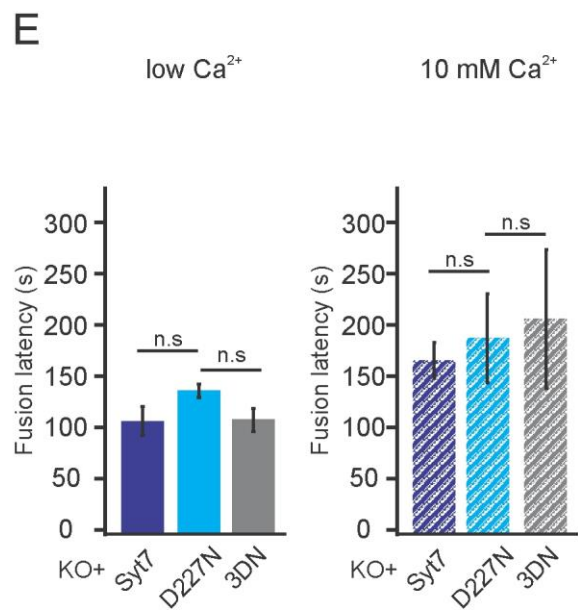
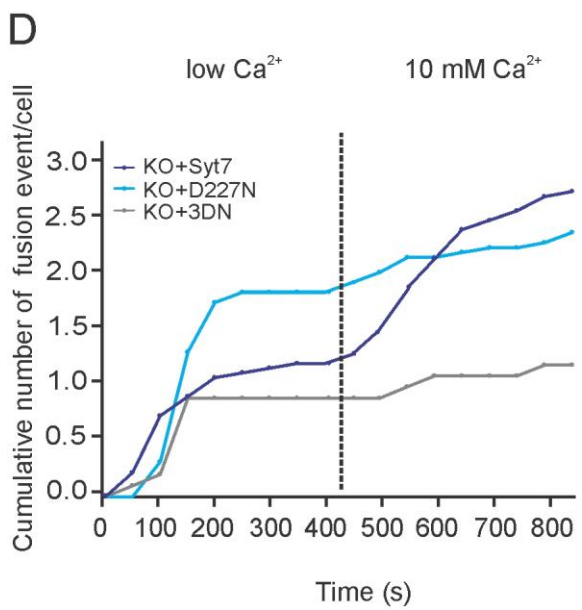
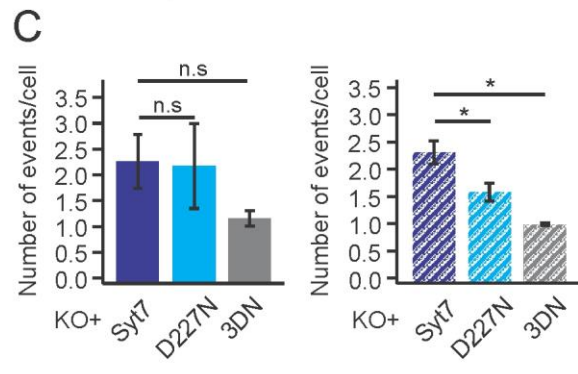
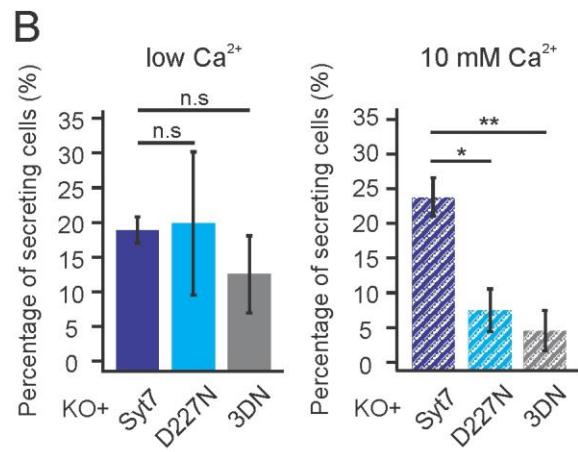
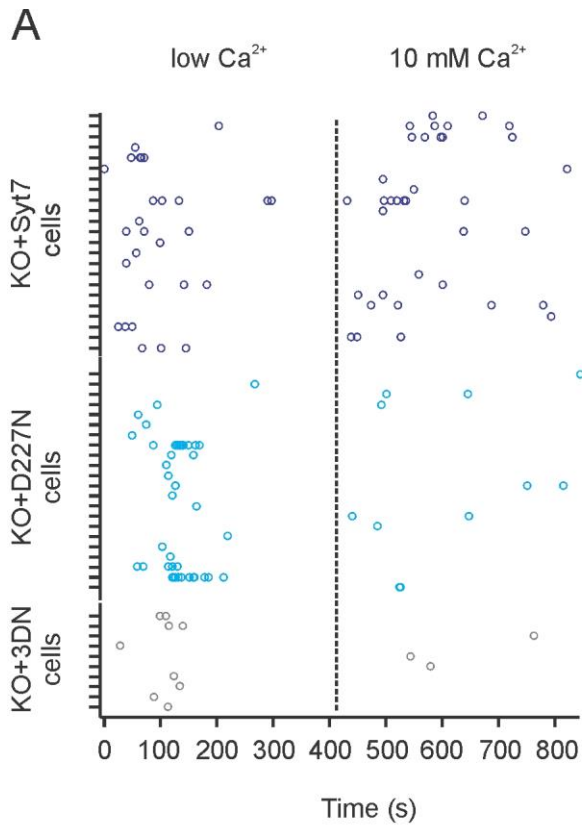


Figure 21: CG secretion after WT and mutant Syt7 overexpression.

(A) The time course of individual fusion events (small circles) in scatter plot for KO+Syt7 (navy blue), KO+D227N (cyan blue), and KO+3DN (gray) cells in low Ca^{2+} and 10 mM extracellular Ca^{2+} . **(B)** The mean percentage of secreting cells at low Ca^{2+} (left graph) and 10 mM Ca^{2+} (right graph). **(C)** The mean number of events per cell at low Ca^{2+} (left graph) and 10 mM Ca^{2+} (right graph). **(D)** The cumulative number of fusion events/cell over time (s). **(E)** The mean fusion latency of fusing granules at low Ca^{2+} (left graph) and 10 mM Ca^{2+} (right graph). Means in (B), (C), and (E) were deduced from 3 preparations (63 KO+Syt7 cells, 80 KO+D227N cells, 51 KO+3DN cells). Error bars = \pm sem. P value (* < 0.05; ** < 0.01; non-significant, n.s) via the unpaired two-tailed Student's T-test.

III.5 The cytosolic calcium concentration is unchanged in Syt7 KO cells

Since the fusion which occurs following the change from low to high calcium depends on the presence of Syt7 and on the increase in extracellular calcium, we tested whether there was a difference in cytosolic calcium concentration of WT and Syt7 KO CTLs using Fura-2 am. We incubated day3 activated cells with Fura-2 am (2 μM) for 30 min at room temperature. After Fura loading, the cells were washed to eliminate the excess Fura-2 am and then the cells were seeded on anti-CD3 coated coverslips. The fluorescence of the cells was measured sequentially at 350/380 nm UV light in our low Ca^{2+} and 10 mM Ca^{2+} conditions for 7 min each (same conditions as the original TIRF experiments) for ratiometric calcium determination. The mean Fura-2 350/380 fluorescence ratios were plotted over time (figure 22-A). The results showed that the Fura-2 ratio in Syt7 KO cells is not different from that observed in WT cells. Mean ratios were recorded from 34 WT cells and 31 Syt7 KO cells. Error bars represent sem values. The dashed line represents the time at which low Ca^{2+} was replaced with 10 mM Ca^{2+} . Figure 22-B shows the estimated intracellular free Ca^{2+} ion concentration (see Methods II.2.11.1). There was no difference between WT and Syt7 KO cells in the mean cytosolic calcium concentration either in the low calcium condition or in the high calcium condition.

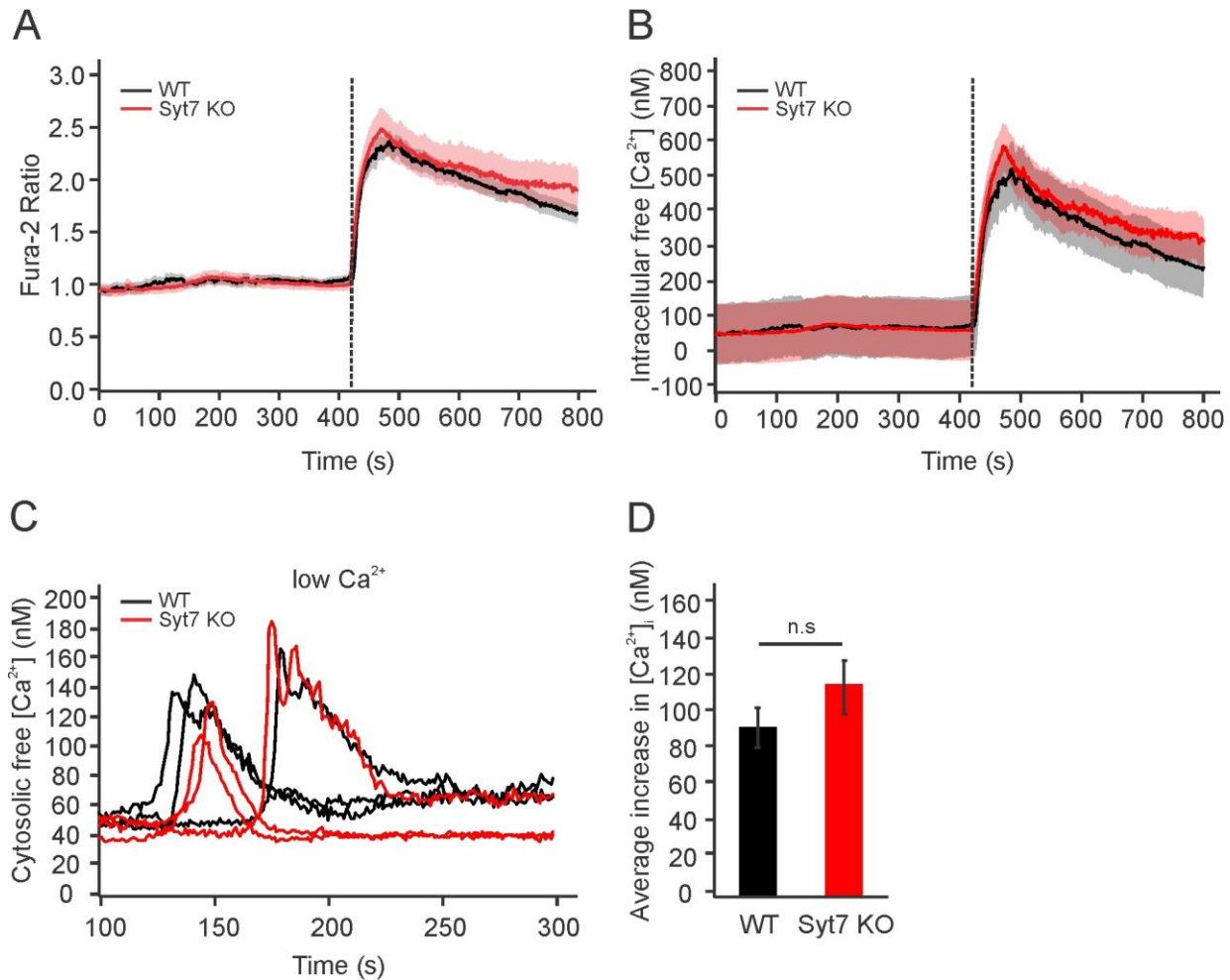


Figure 22: The cytosolic free calcium concentration is unchanged in Syt7 KO cells.

(A) The Fura-2 fluorescence intensity ratio at 350 nm and 380 nm UV light in WT (black) and Syt7 KO (red) cells over time under the low Ca^{2+} and 10 mM extracellular Ca^{2+} . **(B)** The concentration of free calcium in WT and Syt7 KO cells under the low and 10 mM Ca^{2+} conditions. Shades around the traces represent sem values. **(C)** Individual traces of cytosolic free $[Ca^{2+}]$ in WT and Syt7 KO cells during the low Ca^{2+} phase. **(D)** The mean increase in cytosolic free $[Ca^{2+}]$ (nM) in WT and Syt7 KO cells at low extracellular calcium. Error bars = \pm sem. P value was determined by unpaired two-tailed Student's T-test (non-significant, n.s).

Figure 22-C shows examples of individual traces of cytosolic free $[Ca^{2+}]$ in WT and Syt7 KO cells in the low extracellular Ca^{2+} condition. The results show that the transient calcium increases associated with release of calcium stores upon activation were similar in WT and Syt7 KO cells. Figure 22-D shows summary bar graphs of the mean amplitude of these calcium transients. There was no significant difference in the amplitudes of transients of WT or Syt7 KO cells (92.789 nM

± 14.526) and Syt7 KO cells ($116.33 \text{ nM} \pm 19.406$) (mean \pm sem) (figure 22-D). Although this method does not show the calcium concentration in micro-domains near the plasma membrane, it indicates that the access of calcium to the cytosol of Syt7 KO cells is comparable to that of WT cells and is not affected by the lack of Syt7.

III.6 Syt7 promotes CG trafficking to the immunological synapse

Since CG fusion was unaffected during the first round but the lack of Syt7 led to loss of the second round of secretion, we considered the possibility that Syt7 promotes granule trafficking. To test this hypothesis, we compared the numbers of granules in the TIRF field over time at low and 10 mM Ca^{2+} from the cells in our previous TIRF measurements. We plotted the mean granule counts from Syt7 KO cells in comparison with mean CG counts from WT cells (figure 23-A), KO+Syt7 cells (figure 23-B), KO+D227N cells (figure 23-C), and KO+3DN cells (figure 23-D).

The number of CGs at the IS in WT and Syt7 KO cells was quite similar during the first 5 min of the recording, when most secretion occurred (figure 23-A) with granule numbers modestly increasing over time. This indicates that the granules were being delivered to the IS. When low Ca^{2+} was replaced with 10 mM Ca^{2+} , the granule numbers at the IS dropped in both groups. This drop is not due to secretion since it was present in the Syt7 KO cells which did not secrete at all in high Ca^{2+} . The decrease is probably due to a cytoskeletal rearrangement that occurs after the increase in intracellular calcium which leads to movement of some granules away from the TIRF field. After the rapid decrease in granules, granule counts increase at the IS in WT cells is expected since polarization of granules is calcium dependent (Beal et al., 2009; Kabanova et al., 2018). In contrast, granule numbers remained low in Syt7 KO cells (figure 23-A). This is consistent with a role for Syt7 in granule trafficking to the synapse in response to elevation in cytosolic calcium.

When WT Syt7 was overexpressed in Syt7 KO cells, the number of granules at the beginning of the recording was higher than that of the Syt7 KO cells (and WT cells), and it remained high during the first 7 min of recording (figure 23-B). When 10 mM Ca^{2+} was added, CG numbers dropped in both genotypes and could be regenerated in KO+Syt7 cells only (figure 23-B). Hence, the re-introduction of Syt7 to Syt7 KO cells promotes the trafficking of granule to the synapse.

In KO cells overexpressing mutated Syt7, the starting number of granules at the IS was comparable to Syt7 KO levels and not to KO+Syt7 levels (figure 23-C, D). At the switch to 10 mM Ca²⁺, KO+D227N cells could moderately regenerate the granule numbers at the IS (figure 23-C) but KO+3DN cells acted worse than Syt7 KO cells (figure 23-D). In spite of the role of Syt7 in CG trafficking, the regenerated and enhanced secretion at 10 mM Ca²⁺ observed in the previous experiment upon WT Syt7 overexpression (figure 21) and the compromise in secretion upon Syt7 mutation (figure 21) can not be simply explained by the regeneration of granule pools at the IS. Granule counts at 10 mM Ca²⁺ were similar in WT and KO+Syt7 cells but KO+Syt7 cells secreted more than 2 folds better than WT cells (figure 20-B, C; figure 21 B, C-left panels). The granule counts of Syt7 KO cells and KO+D227N cells were also similar at 10 mM Ca²⁺ but Syt7 KO cells did not secrete. Granule counts in KO+3DN cells are lower than Syt7 KO cells but they could still exhibit secretion. Hence, we conclude that Syt7 acts as a calcium-dependent regulator of CG trafficking and fusion through the second round of secretion in mouse CTLs.

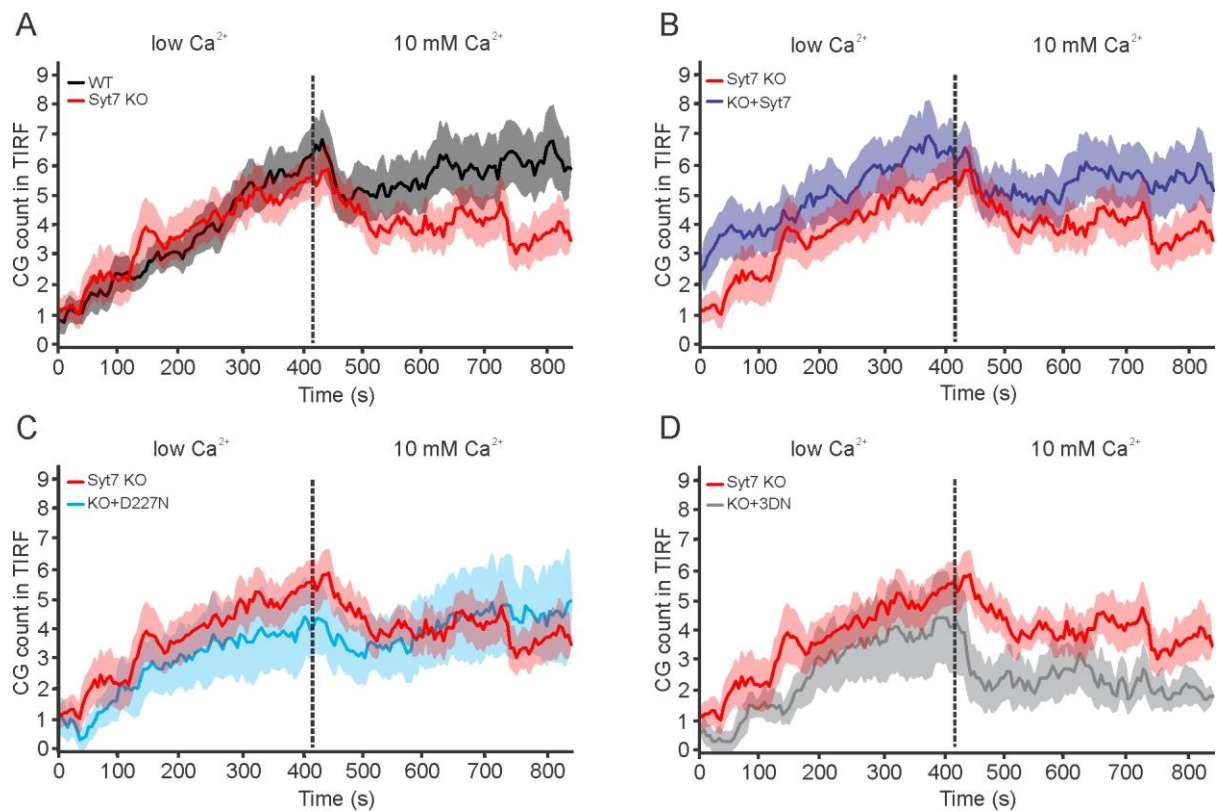


Figure 23: The mean number of granules in TIRF field over time (s) in low and high Ca^{2+} .

(A-D) GranzymeB-positive granules at the IS were counted over time in cells that secreted in our previous TIRF experiments. Granule counts from Syt7 KO cells were compared with granule counts from WT cells (A), KO+Syt7 (B), KO+D227N (C), and KO+3DN (D) cells. Error bars are illustrated as shades around the traces and they represent \pm sem values.

Our results were further validated when we quantified the granule count at the IS from the experiment where cells were measured in low Ca^{2+} for 14 min (Results III.4.1-figure 19). The granule numbers were overlapping throughout the 14 minutes of recording (figure 24). In the second 7 min of recording we saw no decrease or increase in CG numbers as no 10 mM Ca^{2+} was added. This result shows again that Syt7 mediates granule trafficking and fusion and that these functions are dependent on calcium binding.

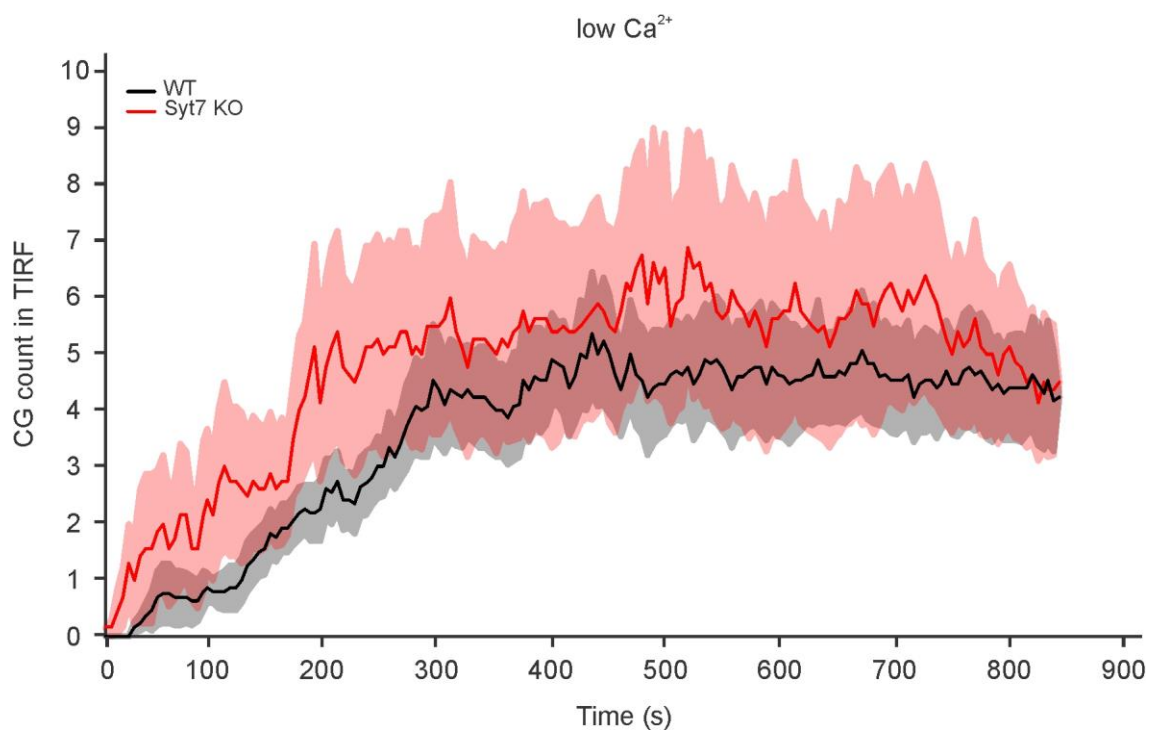


Figure 24: The mean number of CGs in TIRF field over time (s) in low Ca^{2+} only.

Red granules in the TIRF field were counted over the 14 min of recording, in WT and Syt7 KO cells that were kept at low extracellular Ca^{2+} . Error bars are shown as shades around the traces and they represent \pm sem values.

To make sure that the phenotype in Syt7 KO cells is not due to a biogenesis defect, we counted the total number of GranzymeB-positive granules from WT, Syt7 KO, and KO+Syt7 cells. To do so, we overexpressed GranzymeB-mCherry to label CGs and fixed the cells to image them in SIM microscopy. We counted the number of red granular structures in the whole cell using iLastik software. Figure 25 shows that there is no difference in the mean number of GranzymeB-positive granular structures in all three genotypes. Hence, the inability of Syt7 KO cells to regenerate the granule numbers at the IS after the increase in calcium is not due to lack of granules in the cell. From this, we can conclude that Syt7 is necessary for granule replenishment at the synapse in response to elevation in intracellular calcium.

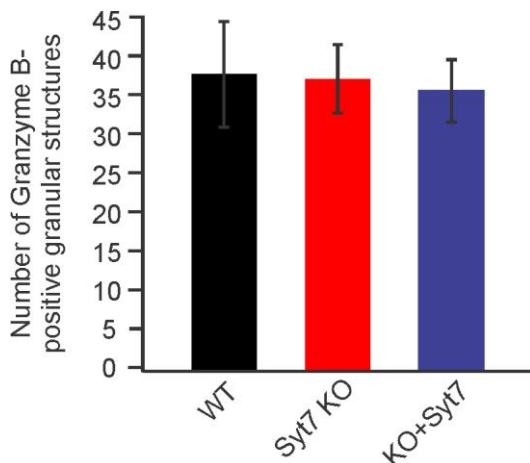


Figure 25: CG count in whole cell.

Day3 activated CTLs from WT, Syt7 KO, and KO+Syt7 cells overexpressing GranzymeB-mCherry were fixed 16 h post-transfection and imaged with the SIM microscope. GranzymeB-positive granular structures were counted in the whole cell. Results are collected from 2 different experiments. Error bars = \pm sem values.

III.7 Syt7 regulates the opening of the fusion pore of cytotoxic granules in mouse CTLs

When we compared secretion between WT cells, Syt7 KO cells and Syt7 overexpression in KO cells, we noticed that the loss of GranzymeB-mCherry fluorescence due to fusion was slower after Syt7 overexpression. We traced the loss of mCherry fluorescence from individual fusing granules from low and high calcium conditions and averaged them in figure 26-A. The fluorescence values were normalized to the starting value to correct for possible differences in granule loading. WT and Syt7 KO cells showed similar responses but granules from Syt7 KO expressing Syt7 demonstrated a slower and less complete loss of GranzymeB-mCherry fluorescence (figure 26-A). The time required for granule fluorescence to decay (to $1-1/e \approx 63.2\%$, tau) of its fluorescence is quantified in figure 26-B and shows that Syt7 overexpression

significantly slowed the loss of GranzymeB-mCherry fluorescence ($\tau = 0.165 \text{ s} \pm 0.0275$ for WT granules; $\tau = 0.138 \text{ s} \pm 0.0156$ for Syt7 KO granules; $\tau = 0.364 \text{ s} \pm 0.045$ for KO+Syt7 granules; mean \pm sem; **, $P < 0.01$; ***, $P < 0.001$) (figure 26-B). Data in figures 26-A and B were averaged from 32 WT, 23 Syt7 KO, and 24 KO+Syt7 fusing granules. Error bars in figures 26-A and B represent sem values. The unpaired two-tailed Student's T-test was carried out to determine P values.

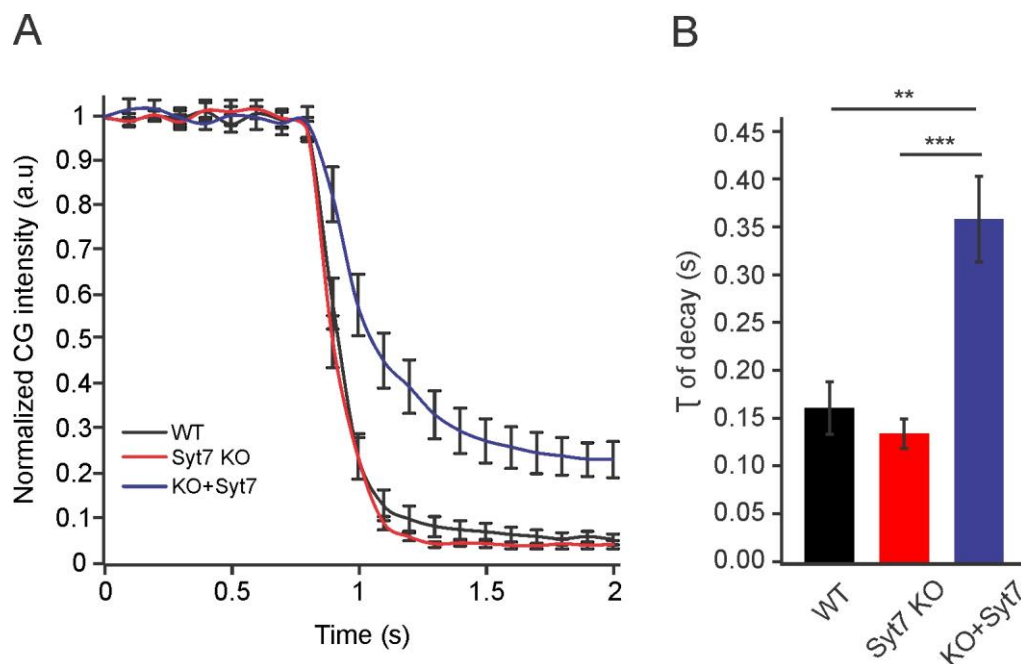


Figure 26: Syt7 overexpression leads to slower emptying of GranzymeB from cytotoxic granules.

(A) The mean normalized fluorescence intensity of GranzymeB-mCherry in fusing granules over time (s). (B) The quantification of the time taken for GranzymeB emptying from fusing CGs. Data were collected from 32 WT, 23 Syt7 KO, and 24 KO+Syt7 fusing granules from 3 different experiments. Error bars = \pm sem values. P values were determined by the unpaired two-tailed Student's T-test.

In order to test for a difference in GranzymeB loading in granules and to characterize the fusion pore formation more critically, we carried out a similar experiment with a pH-sensitive version of GranzymeB, which was tagged with pHuji instead of mCherry. We did this experiment under low calcium conditions only to exclude any effect of high calcium on fusion pore kinetics.

pHuji is a pH-sensitive red fluorescent protein which is quenched in the acidic lumen of the granule (pKa=7.7), and is unquenched when the fusion pore opens and the granule lumen neutralizes (Shen et al., 2014). Figure 27-D shows the dynamics of CG fusion in WT, Syt7 KO, KO+Syt7, KO+D227N, and KO+3DN cells illustrated in the traces of the mean fluorescence values from fusing granules. The fluorescence values were normalized to the starting values to correct for differences in granule loading. We normalized the peaks afterwards to compare the kinetics of pore opening and cargo release. The start of granule fusion is revealed by the increased fluorescence of the fusing granule due to pore opening and lumen neutralization. The release of GranzymeB-pHuji is illustrated by the fast drop of fluorescence intensity.

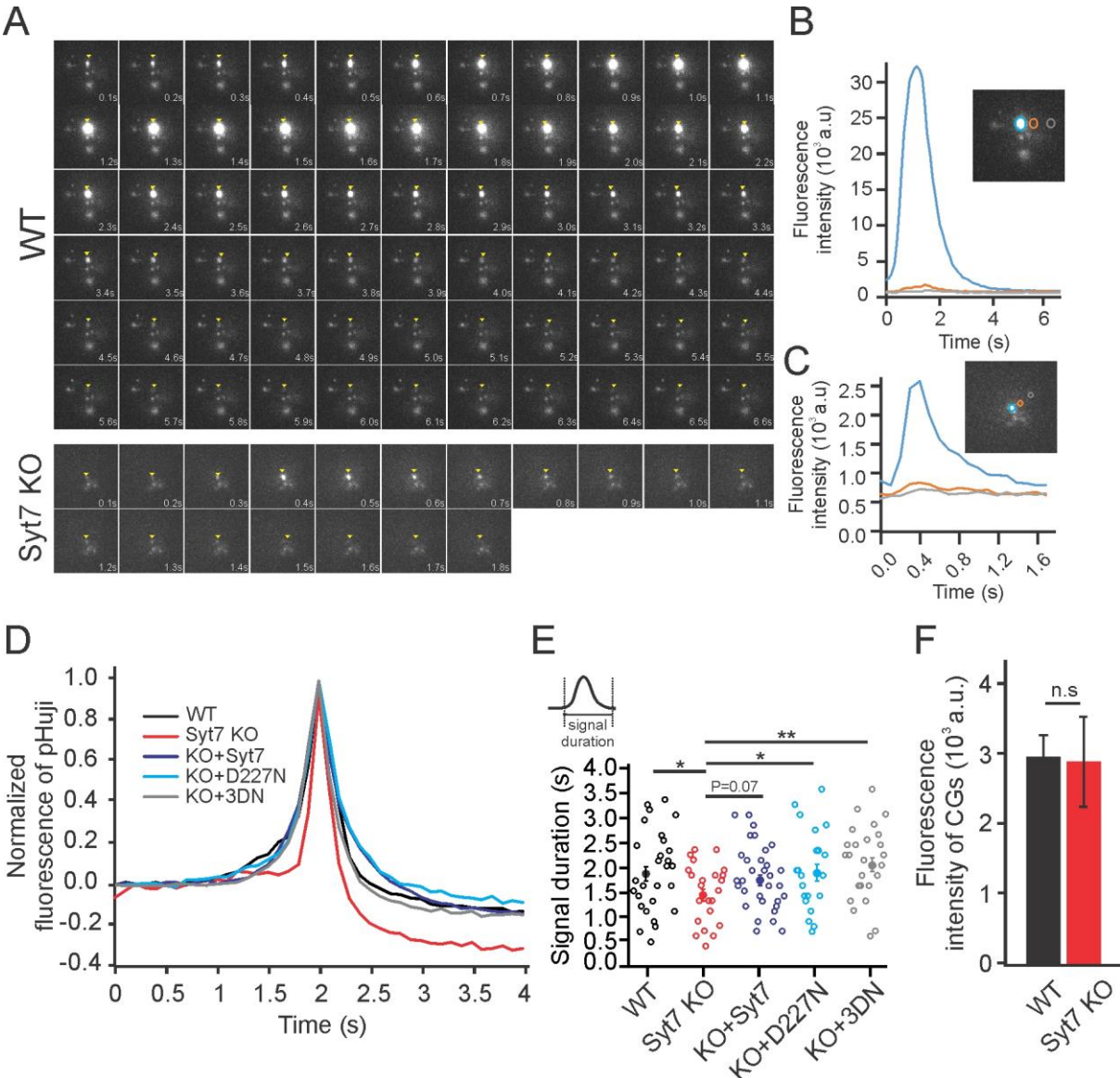


Figure 27: Syt7 regulates the fusion pore expansion.

(A) Representative serial frames of a GranzymeB-pHuji secretion event in WT (upper panel) and Syt7 KO (lower panel) cells. The fusing granule is indicated with a yellow arrow. **(B and C)** Fluorescence intensity change (10^3 a.u) over time (s) in the three regions of interest (ROI) shown in the snapshot of one frame next to each curve. ROIs are drawn around the fusing granule (in blue), next to the granule (in orange), and at a distance from the granule (in gray) to confirm GranzymeB-pHuji release and cloud propagation. **(D)** The mean normalized CG fluorescence intensity (a.u) over time (s) from WT, Syt7 KO, KO+Syt7, KO+D227N, and KO+3DN cells. **(E)** A scatter plot of the signal duration of each fusing granule represented as a single empty circle. A representative drawing of the signal duration is illustrated on top of panel E. The mean signal duration per group is shown as a filled circle in the corresponding color. **(F)** The mean maximal fluorescence intensity (10^3 a.u) from granules treated with ammonium chloride (40mM) in WT and Syt7 KO cells. Error bars = \pm sem values. P values were determined by the unpaired two-tailed Student's T-test (*, $P < 0.05$; **, $P < 0.01$; n.s, non-significant).

Syt7 KO granules (red trace) showed the steepest slopes and the lowest residual fluorescence after fusion indicating the fastest kinetics and the most complete fusion (figure 27-D). We analyzed individual traces and quantified the mean signal duration which is the time (s) taken from the start of increase in fluorescence to the end of release (start of a baseline). We displayed the result as a scatter plot of the signal duration from each fusing granule represented as empty circles (figure 27-E). The mean signal duration \pm sem is shown as a filled circle with error bars for each genotype. The duration of fusion events from Syt7 KO cells were significantly shorter than the other genotypes. The signal duration in Syt7 KO cells were restricted to times less than 2.5 seconds. However, in WT and in KO cells expressing Syt7 (WT or mutant), signal durations were either overlapping with Syt7 KO durations or extending beyond 2.5 seconds. This might indicate that there are two populations of granules, where granules with longer durations are regulated by Syt7 and form the smaller population, and granules with shorter durations are regulated by another synaptotagmin isoform with faster kinetics and form the major population. Figure 27-A shows examples of long and short GranzymeB-pHuji fusion events from WT (upper panel) and Syt7 KO (lower panel) cells in serial frames, where the fusing granule is indicated by a yellow arrow. The WT fusion event (figure 27-A, upper panel) extended over 6 seconds. This was quantified in figure 27-B in which the fluorescence intensities at the site of fusion (blue trace) and near the site of fusion (orange and gray trace) were measured to ensure release and diffusion of GranzymeB-pHuji, respectively (figure 27-B). The fusion event from the Syt7 KO

cell (figure 27-A, lower panel) extended over less than 2 seconds and showed very low fluorescence in comparison to the WT. The change in fluorescence intensity over time was quantified in figure 27-C. The long time course of fusion and accumulation of fluorescence seen in some fusing granules may be due to the restriction of fusion pore expansion after the pore starts to open. In this case, the fluorescence of pHuji starts to increase due to the change in pH of the lumen and the inability of pHuji to diffuse out of the granule due to limited pore size. This gives rise to longer signal duration and higher amplitudes due to the slow diffusion of cargo. We saw this phenotype in a population of granules from WT, KO+Syt7, KO+D227N, and KO+3DN cells. This may indicate that Syt7 restricts fusion pore dilation which may be due to its high affinity for lipid membranes and slow association/dissociation kinetics (Hui et al., 2005; Rhee et al., 2005; Zhang et al., 2010). It was shown previously to be a pore-stabilizing effector protein due to its strong interaction with lipid membranes (Rao et al., 2014; Zhao et al., 2016). The affinity of a Syt isoform to membrane phospholipids may be the major reason for the difference in the kinetics of fusion pore formation (MacDougall et al., 2018), consistent with a role for an alternative synaptotagmin with faster membrane association/dissociation kinetics acting in Syt7 KO cells where we see a faster pore opening and cargo discharge.

The fusion events analyzed in this experiment took place at low calcium during the first 7 min of recording, during which Syt7 appears to not play a significant role (see figure 20-A-E). There was no difference in signal duration between WT, KO+Syt7, KO+D227N, and KO+3DN cells.

To examine whether the shorter signal duration in Syt7 KO granules was due to lower GranzymeB loading, in a separate experiment, we treated the cells with a high concentration of ammonium chloride NH_4Cl (40 mM) which de-quenches pHuji (Lazarenko et al., 2017) (see Methods II.2.12). We measured the maximal fluorescence of pHuji from 56 WT and 26 Syt7 KO granules in epifluorescence mode and quantified it in figure 27-F. Granules from WT and Syt7 KO cells showed the same level of maximal fluorescence when de-quenched indicating that they contain similar amounts of GranzymeB-pHuji in granules (figure 27-F).

The results of this experiment show that Syt7 modulates fusion pore expansion. On the other hand, they support the conclusion that the role of Syt7 in the first phase of fusion is limited.

Data were collected from 28 WT granules, 25 Syt7 KO granules, 32 KO+Syt7 granules, 21 KO+D227N granules, and 25 KO+3DN granules in 3 different experiments. Error bars are equivalent to sem values. P values were determined by the unpaired two-tailed Student's T-test.

III.8 Synaptotagmin 2 in mouse cytotoxic T lymphocytes

Based on our results, an alternative synaptotagmin may regulate secretion in mouse CTLs. The obvious candidate would be Syt2 in spite of its low calcium affinity. Syt2 is homologous to Syt1 (Pinheiro et al., 2016) and it is majorly known for its function in synchronous release of neurotransmitters at the zebrafish neuromuscular junction (NMJ) and the calyx of Held (Pang et al., 2006a; Pang et al., 2006b; Sun et al., 2007; Wen et al., 2010). Secretion at these synapses was shown to be fine-tuned by the duet of Syt2 and Syt7 (Wen et al., 2010; Luo and Südhof, 2017).

Syt2 is expressed in day3 activated CTLs at the RNA level (figure 16). In figure 28, we show the endogenous protein expression level of Syt2 in day3 activated WT and Syt7 KO cells. The quantification of the expression level of Syt2 normalized to GAPDH as a loading control (figure 28-B) shows that Syt2 expression might be slightly enhanced in Syt7 KO cells but this was not significant (figure 28-B). The mean expression level was averaged from 3 western blots.

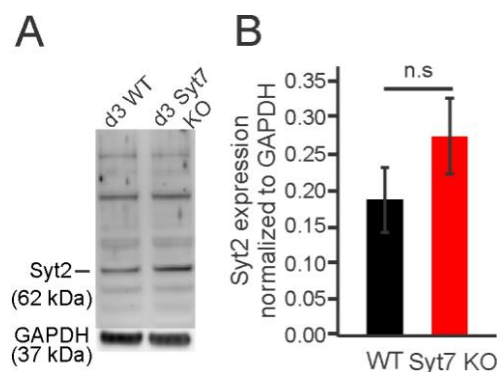


Figure 28: Syt2 protein expression in day3 activated WT and Syt7 KO cells.

(A) A representative western blot showing Syt2 and GAPDH (loading control) expression levels at 62 and 37 kDa, respectively. **(B)** A quantification of Syt2 expression level in WT and Syt7 KO cells normalized to GAPDH. Averages are quantified from 3 experiments. Error bars = \pm sem. P value (n.s; non-significant) was determined by the one tail Student's T test.

Due to the lethality of Syt2 knockout mice (Pang et al., 2006), we decided to downregulate the expression of Syt2 in WT and Syt7 KO CTLs in order to examine the function of Syt2 in these cells. We transfected day2 activated CTLs by electroporation with a combination of two different siRNA sequences that bind to different locations of the Syt2 mRNA and induce its degradation. As a control, we transfected cells with scrambled siRNA sequences. We quantified Syt2 expression level relative to GAPDH at 24 hours and 48 hours after electroporation. A representative western blot and the quantification of the protein level of Syt2 relative to GAPDH are shown in figures 29-A and B.

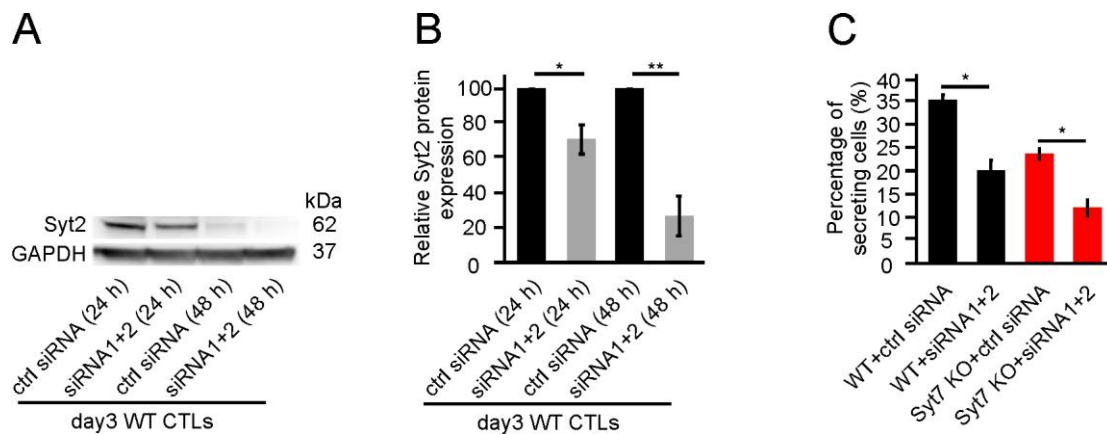


Figure 29: Cytotoxic granule fusion is reduced as Syt2 expression is downregulated by siRNA

(A) A representative western blot showing the downregulation of Syt2 expression upon transfection with a combination of siRNA1 and siRNA2 against Syt2. Cells from control (lanes 1 and 3) and experimental (lanes 2 and 4) conditions were lysed at 24 h and 48 h after transfection. GAPDH was assessed as a loading control. **(B)** A quantification from 3 western blots of Syt2 expression level relative to GAPDH. Values were normalized to controls at 24 h and 48 h respectively. P values (*, $P < 0.05$; **, $P < 0.01$) were determined by the one tailed T test. **(C)** The mean percentage of secreting cells measured in TIRF 24-30 h post-transfection from WT and Syt7 KO cells transfected with control siRNA or siRNA1+2. Data were collected from 2 experiments (121 WT + ctrl siRNA cells, 141 WT + siRNA1+2 cells, 82 Syt7 KO + ctrl siRNA cells, 139 Syt7 KO + siRNA1+2 cells). Error bars represent sem values. The unpaired Student's T test was applied to determine P values (*, $P < 0.05$; n.s, non-significant).

The quantification from three western blot experiments showed that the endogenous expression level of Syt2 decreases significantly by ~ 30 % ($P < 0.05$) after 24 h of transfection and by ~ 75 % ($P < 0.05$) after 48 h of transfection, as compared to controls at 24 h and 48 h respectively.

To test our hypothesis about the function of Syt2, we electroporated day2 WT and Syt7 KO activated CTLs with scrambled control siRNA or siRNA1+2, in combination with GranzymeB-mCherry fusion protein to label cytotoxic granules. We observed secretion of CGs from these cells in TIRF microscopy under low and 10 mM extracellular calcium for 7 minutes each. We carried out our measurements during the 24-30 h time window, where cells were healthy and viable. When we quantified the mean percentage of secreting cells, we found that the secretion probability has significantly decreased by ~ 40% in WT cells ($P = 0.025$) and by ~ 50% ($P = 0.028$) in Syt7 KO cells transfected with siRNA1+2 in comparison to control cells. We found this consistent with the protein expression levels of Syt2 after downregulation measured at 24 h and 48 h in figure 29-B.

Although the system of protein downregulation by siRNA is limited, we could show that Syt2 acts as a main regulator of CG secretion in mouse CTLs.

Data were collected from 2 experiments (121 WT + ctrl siRNA cells, 141 WT + siRNA1+2 cells, 82 Syt7 KO + ctrl siRNA cells, 139 Syt7 KO + siRNA1+2 cells).

IV. DISCUSSION

We have addressed the role of Synaptotagmin7 in CG exocytosis in mouse CTLs. Syt7 has been proposed to be the calcium sensor for lysosomal fusion in fibroblasts (Martinez et al., 2000; Reddy et al., 2001) and for CG fusion in CTLs (Fowler et al., 2007). We determined the expression profile of the synaptotagmin family in day3 activated mouse CTLs (see figure 16) and we found 2 calcium-dependent synaptotagmins: Syt2 and Syt7 (Sugita et al., 2002; Südhof, 2002). CTLs could secrete at low extracellular calcium (100 μ M) (Lyubchenko et al., 2001). Due to the fact that Syt7 is a high affinity calcium sensor and Syt2 is a low affinity calcium sensor (Sugita et al., 2002; MacDougall et al., 2018), in addition to the fact that cytotoxic granules are secretory lysosomes by nature (Peters et al., 1991) and Syt7 was shown to regulate lysosomal fusion (Martinez et al., 2000; Reddy et al., 2001), we hypothesized that Syt7 might be the calcium sensor for cytotoxic granule fusion in mouse CTLs.

We found Syt7 co-localized with cytotoxic granules and on the plasma membrane (see figure 17). Similar localizations of Syt7 were already reported in different types of tissues. It was detected on lysosomes in fibroblasts (Martinez et al., 2000; Reddy et al., 2001) and macrophages (Flannery et al., 2010), on large-dense core vesicles in chromaffin cells and neuroendocrine cell lines (Fukuda et al., 2002; Fukuda et al., 2004; Wang et al., 2005; Rao et al., 2014; Dolai et al., 2016; Rao et al., 2017), and on the plasma membrane in hippocampal neurons (Sugita et al., 2001; Virmani et al., 2003; Weber et al., 2014; Jackman et al., 2016).

We examined secretion with TIRF microscopy in CTLs from Syt7 knockout mice. There was fusion of CGs from cells seeded on coverslips coated with anti-CD3. The result shows that even under low calcium conditions, fusion occurs (see figure 19). Syt7 is not required for fusion, indicating that either another Syt (which must be Syt2) or no Syt is required for fusion.

Surprisingly, upon a change to a higher calcium solution, there was additional fusion in the control cells but not in Syt7 KO cells. We showed that CTLs demonstrate an early and a late phase of cytotoxic granule fusion. Since this fusion was absent when calcium was not increased and did not occur in the absence of Syt7, it appears that Syt7 enables a calcium-dependent late phase of secretion.

Expression of WT Syt7 in Syt7 KO cells rescued the late phase of secretion, confirming its Syt7-dependence, though it did not alter the incidence of CG fusion events in low calcium (see figure 21). The characteristics of single fusion events in TIRF were similar in WT and Syt7 KO cells (see figure 26). However, when WT Syt7 was expressed in KO cells, the significant change in the kinetics of fusion events indicates that Syt7 does alter events, consistent with reports in other types of cells (Jaiswal et al., 2004; Hui et al., 2005; Rhee et al., 2005; Zhang et al., 2010). We saw this effect also in the scatter plot of signal durations (see figure 27-E) where only Syt7-expressing cells (WT, KO+Syt7, KO+D227N, KO+3DN) but not Syt7 KO cells showed additional longer signal durations from fusing granules. These granules with the longer signal durations constituted the minority of fusing granules, revealing that Syt7 might be associated with this population of cytotoxic granules and regulating their cargo release. Our results are similar to what has been shown by Bendahmane et al. (2019) concerning the localization of Syt7 on a sub-population of granules and its role in sustaining CG release and controlling fusion pore expansion (Bendahmane et al., 2019). This group have shown that large-dense core vesicles are either Syt1- or Syt7-associated and that Syt7 is important for maintaining a secretory response upon prolonged cholinergic stimulation. They also demonstrated that the discharge of vesicle cargo is more rapid in Syt1-associated vesicles than in Syt7-associated vesicles (Bendahmane et al., 2019).

We examined the role of calcium binding to Syt7 by mutating the calcium binding aspartates of the C2A domain, considered to be involved in calcium sensing in Syt7 (Segovia et al., 2010; Bacaj et al., 2013; Bacaj et al., 2015). The finding that deletion of one or all three aspartates did not affect secretion in its early phase but compromised CG fusion after stimulation with high calcium supports our conclusion that Syt7 is necessary for regenerating secretion in CTLs (see figure 21). The effect of Syt7 mutation on CG trafficking to the immune synapse (see figure-23 C, D) shows that Syt7 mediates granule replenishment after high calcium stimulation. The function of Syt7 in replenishing granule pools at the synapse was also reported in human pancreatic beta-cells where Syt7 knockdown decreased insulin-secretory granules recruitment to the plasma membrane after stimulation with high glucose (Dolai et al., 2016).

The persistence of secretion in KO cells expressing mutated Syt7 (especially the triple mutant 3DN) (see figure 21) that have lower granule counts than Syt7 KO cells in the second 7 min of recording (see figure 23-D) confirms that Syt7 is calcium sensing CG secretion after calcium stimulation and indicates that it can be mediating this function via its C2B domain.

Our studies of granule numbers at the TIRF field indicate that Syt7 regulates the replenishment of granules at the immune synapse and in this way mediates the late phase of CG fusion. Rescue of Syt7 KO cells with overexpression of WT or mutated Syt7 in these cells led to increased late secretion, consistent with this idea.

Based on our RNA and protein data, the only other calcium sensing Syt in CTLs is Syt2 which has a ~12-fold lower calcium affinity (Sugita et al., 2002). It has been argued that a high affinity sensor is required, but Syt1 has been proposed as a calcium sensor for miniature synaptic potential release in some neurons (Xu et al., 2009), which occurs at much lower calcium concentration than does synaptic transmission. Syt2 is present in CTLs and has a calcium affinity similar to that of Syt1. It may be that a lower calcium affinity is adequate when the calcium increases producing fusion are not transient but last seconds or minutes rather than milliseconds. Due to the lethality of a Syt2 knockout, we used siRNA to reduce the expression level of Syt2. Though the knockdown achieved is less than we would have liked, moderate knockdown was associated with a moderate reduction in fusion in WT and Syt7 KO cells. Based on these data, we propose that Syt2 may be a calcium sensor for CG fusion in mouse CTLs.

IV.1 Cytotoxic granule release is regulated by Syt2 and Syt7

Calcium entry in T cells is mediated mainly by CRAC channels (Feske et al., 2005) which are highly calcium-selective channels but have low unitary conductance (Prakriya and Lewis, 2015). The formation of an immunological synapse induced by anti-CD3 binding to CTLs causes the mobilization of mitochondria to sub-plasma membrane positions which helps in maintaining a low local calcium concentration (Quintana et al., 2011). Knowing that Syt2 is a low affinity calcium sensor which has an EC_{50} of 10-20 μ M (Sugita et al., 2002), the addressed facts may be part of the reasons that explain the slower kinetics of cytotoxic granule release in T cells as compared to synaptic vesicle release in neuronal systems and which makes Syt2 a suitable candidate for calcium sensing in cytotoxic T cells.

According to our data, Syt7 contributes moderately to cytotoxic granule secretion in WT mouse CTLs in response to stimulating the cells with high extracellular calcium (see figure 20). Syt7 mediates this function primarily through replenishing the ‘granule pools’ at the immunological

synapse (see figure 23). The fact that overexpression of Syt7 calcium-binding mutants impairs granule availability at the synapse supports the notion that Syt7 is mediating granule replenishment in a calcium sensitive manner (see figure 23). This function of Syt7 was proposed to occur in hippocampal synapses where synaptic vesicles are replenished after high frequency stimulation (Liu et al., 2014). Liu et al. (2014) further suggested that high frequency stimulation supports Syt7-mediated endocytosis that supports Syt7-associated asynchronous vesicle release (Liu et al., 2014; Rozov et al., 2019). We can't ignore the fact that Syt7 might be promoting granule endocytosis in CTLs especially after showing its plasma membrane localization (see figure 17), but we can not rule out that Syt7 might have been targeted to the membrane due to overexpression.

Our data on granule availability at the IS after WT Syt7 overexpression not only explains the role of Syt7 in granule replenishment after high calcium stimulation, but also shows the calcium-sensing function of Syt7 in regenerated release. We saw this clearly in the 2.5-fold enhancement of secretion at 10 mM Ca^{2+} in rescued cells in comparison to WT cells although the two groups had the same granule count at 10 mM Ca^{2+} (figure 20, 21, 23). This was further validated with the calcium-binding mutants that had comparable granule counts as Syt7 KO cells but exhibited moderate to low secretion in response to calcium elevation (figure 21, 23). The mutations we introduced to Syt7 C2A domain (D227N and 3DN) lie in the calcium-binding loop 3 (CBL3) which has been shown to be the main contributor for the deep penetration of Syt7 into lipid bilayers (Osterberg et al., 2015). This explains why the CG fusion probability was increasingly limited at 10 mM calcium as we moved from a single-aspartate mutation to a triple-aspartate mutation, indicating an essential role of calcium binding to loop 3 in the C2A domain of Syt7 in mediating its function (see figure 21). The dependence of Syt7 on calcium for regenerating granule release was also supported by the fact that WT cells could not secrete when high calcium was not added (see figure 19) although they had comparable granule counts at the IS as Syt7 KO cells (see figure 24). Hence, we have shown that Syt7 is a regulator of regenerated cytotoxic granule release in response to high calcium stimulation.

According to our data on fusion pore expansion, we postulate that there might be two populations of granules, Syt2-associated and Syt7-associated granules (see figure 27). The dynamics of expansion of fusion pores has been shown to depend on the kinetics of interaction of synaptotagmins with membrane lipids (MacDougall et al., 2018). Syt7 is characterized by its high affinity to membrane phospholipids and slow dissociation kinetics from lipid bilayers which

enables more stabilized fusion pores, in contrast to Syt2 and other fast calcium sensors (Syt1 and Syt9) that have lower affinities to membranes and more rapid dilation of fusion pore (Hui et al., 2005; Rhee et al., 2005; Zhang et al., 2010). The lack of difference in signal duration between WT Syt7 overexpression and Syt7 aspartate mutants might be because the C2B domain of Syt7 was intact. It was shown before that the C2B domain of Syt7 acts as a stabilizer of the fusion pore (Segovia et al., 2010), hence we don't see a clear difference between mutants and WT Syt7 overexpression.

V. CONCLUSION and OUTLOOK

In the present study, we show that Syt7 knockout does not prevent CG fusion, showing that Syt7 is not required for fusion. This result indicates a redundancy or a lack of need for a calcium sensor. The result is consistent with the observation that Granzyme could be released by CTLs from Syt7 KO mice, though there were deficits in the immune response (Fowler et al., 2007). We show that the role of Syt7 can take part in the fusion process but is more likely to regulate trafficking of CGs to the immune synapse, in a calcium-dependent manner. The results are consistent with the lack of a difference in CG secretion after anti-CD3 stimulation in WT and Syt7 KO cells (Fowler et al., 2007).

Our results indicate that Syt2 and Syt7 regulate cytotoxic granule fusion in mouse CTLs, though under our conditions, Syt2 is more likely to be the calcium sensor with Syt7 controlling regenerated secretion through CG replenishment. It would be of high interest to confirm our data on Syt2. It is also highly interesting to understand the mechanism behind CG replenishment upon calcium elevation, knowing that CG endocytosis has been shown to be essential for serial killing by Chang et al. (2016). This might be the reason for the decrease in the killing efficiency of Syt7 KO cells as shown by the in-vivo experiments of the Fowler group (Fowler et al., 2007).

BIBLIOGRAPHY

Abbe, E. (1873). *Beiträge zur Theorie des Mikroskops und der mikroskopischen Wahrnehmung*. Arch Mikrosk Anat 9, 413-446.

Arantes, RM., Andrews, NW. (2006). *A Role for Synaptotagmin VII-Regulated Exocytosis of Lysosomes in Neurite Outgrowth from Primary Sympathetic Neurons*. Journal of Neuroscience 26 (17) 4630-4637.

Bacaj, T., Wu, D., Yang, X., Morishita, W., Zhou, P., Xu, W., Malenka, RC., Südhof, TC. (2013). *Synaptotagmin-1 and synaptotagmin-7 trigger synchronous and asynchronous phases of neurotransmitter release*. Neuron 80(4): 947-59.

Bacaj, T., Wu, D., Burré, J., Malenka, RC., Liu, X., Südhof, TC. (2015). *Synaptotagmin-1 and -7 Are Redundantly Essential for Maintaining the Capacity of the Readily-Releasable Pool of Synaptic Vesicles*. PLoS Biol 13(10): e1002267.

Baker, PF., Knight DE. (1978). *Calcium-dependent exocytosis in bovine adrenal medullary cells with leaky plasma membranes*. Nature 276(5688): 620-622.

Barber, CF., Jorquera, RA., Melom, JE., Littleton, JT. (2009) *Postsynaptic regulation of synaptic plasticity by synaptotagmin 4 requires both C2 domains*. J Cell Biol. 187(2):295-310.

Barclay, JW., Morgan, A., Burgoyne, R. (2005). *Calcium-dependent regulation of exocytosis*. Cell Calcium. 38(3-4): 343-53.

Beal, AM., Anikeeva, N., Varma, R., Cameron, TO., Vasiliver-Shamis, G., Norris, PJ., Dustin, ML., Sykulev, Y. (2009). *Kinetics of early T cell receptor signaling regulate the pathway of lytic granule delivery to the secretory domain*. Immunity 31(4):632-42.

Becker, SM., Delamarre, L., Mellman, I., Andrews NW. (2009). *Differential role of the Ca²⁺ sensor synaptotagmin VII in macrophages and dendritic cells*. Immunobiology 214:495–505.

Bendahmane, M., Bohannon, KP., Bradberry, MM., Rao, TC., Schmidtke, MW., Abbineni, PS., Chon, NL., Tran, S., Lin, H., Chapman, ER., Knight, JD, Anantharam, A. (2018). *The synaptotagmin C2B domain calcium binding loops modulate the rate of fusion pore expansion*. Mol Biol Cell. 29(7):773-880.

Bendahmane, M., Kreutzberger, A.J.B., Chapman-Morales, A., Philippe, J.M., Schenk, N., Zhang, S., Kiessling, V., Tamm, L.K., Giovannucci, D.R., Jenkins, P.M., Anantharam, A. (2019). *Synaptotagmin-7 endows a population of chromaffin cell vesicles with enhanced calcium sensing and delayed content release properties*. BioRxiv, <https://doi.org/10.1101/704205>

Bennett, J.M., Reeves, G., Billman, G.E., Sturmburg, J.P. (2018). *Inflammation-Nature's Way to Efficiently Respond to All Types of Challenges: Implications for Understanding and Managing "the Epidemic" of Chronic Diseases*. Front Med (Lausanne). 5:316.

Bhalla, A., Chicka, M.C., Tucker, W.C., Chapman ER (2006). *Ca²⁺-synaptotagmin directly regulates t-SNARE function during reconstituted membrane fusion*. Nat Struct Mol Biol. 13(4):323-30.

Brandt, D.S., Coffman, M.D., Falke, J.J., Knight, J.D. (2012). *Hydrophobic contributions to the membrane docking of synaptotagmin 7 C2A domain: mechanistic contrast between isoforms 1 and 7*. Biochemistry 51(39):7654-7664.

Brose, N., Petrenko, A.G., Südhof, T.C., Jahn, R. (1992). *Synaptotagmin: a calcium sensor on the synaptic vesicle surface*. Science 256(5059):1021-5.

Carr, C.M., Munson, M. (2007). *Tag team action at the synapse*. EMBO Rep. 8(9):834-8.

Chang, C.W., Chiang, C.W., Jackson, M.B. (2017). *Fusion pores and their control of neurotransmitter and hormone release*. J. Gen. Physiol. 149:301–322.

Chapman, E.R., Jahn, R. (1994). *Calcium-dependent interaction of the cytoplasmic region of synaptotagmin with membranes. Autonomous function of a single C2-homologous domain*. J Biol Chem. 269(8):5735-41.

Chen, C., Jonas, P. (2017). *Synaptotagmins: That's Why So Many*. Neuron 94(4):694-696.

Chen, C., Arai, I., Satterfield, R., Young, S.M. Jr., Jonas, P. (2017). *Synaptotagmin 2 Is the Fast Ca²⁺ Sensor at a Central Inhibitory Synapse*. Cell Rep.18(3):723-736.

Chieriegatti, E., Chicka, M.C., Chapman, E.R., Baldini, G. (2004). *SNAP-23 functions in docking/fusion of granules at low Ca²⁺*. Mol Biol Cell.15(4):1918-30.

Corbalan-Garcia, S., Gómez-Fernández, J.C. (2014) *Signaling through C2 domains: more than one lipid target*. Biochim Biophys Acta. 1838(6):1536-47.

Craxton, M. (2010). *A manual collection of Syt, ESyt, Rph3a, Rph3al, Doc2, and Dblc2 genes from 46 metazoan genomes—An open access resource for neuroscience and evolutionary biology*. BMC Genomics. 11:37.

Czibener, C., Sherer, NM., Becker, SM., Pypaert, M., Hui, E., Chapman, ER., Mothes, W., Andrews, NW. (2006). *Ca²⁺ and synaptotagmin VII-dependent delivery of lysosomal membrane to nascent phagosomes*. J. Cell Biol. 174:997–1007.

Davletov, BA., Südhof, TC. (1993). *A single C2 domain from synaptotagmin I is sufficient for high affinity Ca²⁺/phospholipid binding*. J Biol Chem. 268(35):26386-90.

de Saint Basile, G. Ménasché, G., Fischer, A. (2010). *Molecular mechanisms of biogenesis and exocytosis of cytotoxic granules*. Nat Rev Immunol.10(8):568-79.

de Wit, H., Cornelisse, LN., Toonen, RF., Verhage, M. (2006). *Docking of secretory vesicles is syntaxin dependent*. PLoS One 1:e126.

de Wit, H., Walter, AM., Milosevic, I., Gulyás-Kovács, A., Riedel, D., Sørensen, JB., Verhage, M. (2009). *Synaptotagmin-1 docks secretory vesicles to syntaxin-1/SNAP-25 acceptor complexes*. Cell 138(5):935-46.

de Wit, H. (2010). *Molecular mechanism of secretory vesicle docking*. Biochem Soc Trans 38:192–198.

Dieckmann, NMG., Gordon, LF., Asano Y., Stinchcombe JC., Griffiths GM. (2016). *The cytotoxic T lymphocyte immune synapse at a glance*. Journal of Cell Science 129: 2881-2886.

Dolai, S., Xie, L., Zhu, D., Liang, T., Qin, T., Xie, H., Kang, Y., Chapman, ER., Gaisano, HY. 2016. *Synaptotagmin-7 Functions to Replenish Insulin Granules for Exocytosis in Human Islet β -Cells*. Diabetes. 65(7):1962-76.

Dustin, ML., Long, EO. (2010). *Cytotoxic immunological synapses*. Immunol Rev. 235(1):24-34.

Dustin, ML. (2014). *The immunological synapse*. Cancer Immunol Res. 2(11):1023-33.

Earles, CA., Bai, J., Wang, P., Chapman, ER. (2001). *The tandem C2 domains of synaptotagmin contain redundant Ca²⁺ binding sites that cooperate to engage t-SNAREs and trigger exocytosis*. J Cell Biol. 154(6):1117-23.

Fagerberg, L., Hallström, BM., Oksvold, P., Kampf, C., Djureinovic, D., Odeberg, J., Habuka, M., Tahmasebpoor, S., Danielsson, A., Edlund, K., Asplund, A., Sjöstedt, E., Lundberg, E., Szigartyo, CA., Skogs, M., Takanen, JO., Berling, H., Tegel, H., Mulder, J., Nilsson, P., Schwenk, JM., Lindskog, C., Danielsson, F., Mardinoglu, A., Sivertsson, A., von Feilitzen, K., Forsberg, M., Zwahlen, M., Olsson, I., Navani, S., Huss, M., Nielsen, J., Ponten, F., Uhlén, M. (2014). *Analysis of the human tissue-specific expression by genome-wide integration of transcriptomics and antibody-based proteomics*. Mol Cell Proteomics. 13(2):397-406.

Falkowski, MA., Thomas, DD., Messenger, SW., Martin, TF., Groblewski, GE. (2011). *Expression, localization, and functional role for synaptotagmins in pancreatic acinar cells*. Am J Physiol Gastrointest Liver Physiol. 301(2): G306-16.

Feldmann, J., Callebaut, I., Raposo, G., Certain, S., Bacq, D., Dumont, C., Lambert, N., Ouachée-Chardin, M., Chedeville, G., Tamary, H., Minard-Colin, V., Vilmer, E., Blanche, S., Le Deist, F., Fischer, A., de Saint Basile, G. (2003). *Munc13-4 is essential for cytolytic granules fusion and is mutated in a form of familial hemophagocytic lymphohistiocytosis (FHL3)*. Cell.115(4):461-73.

Fernández-Chacón, R., Königstorfer, A., Gerber, SH., García, J., Matos, MF., Stevens, CF., Brose, N., Rizo, J., Rosenmund, C.O, Südhof, TC. (2001). *Synaptotagmin I functions as a calcium regulator of release probability*. Nature 410(6824):41-9.

Feske, S., Prakriya, M., Rao, A., Lewis, RS. (2005). *A severe defect in CRAC Ca²⁺ channel activation and altered K⁺ channel gating in T cells from immunodeficient patients*. J Exp Med. 202(5):651-62.

Fisher, P. (2011) *Immunology Module*, University of California San Francisco. Retrieved from http://missinglink.ucsf.edu/lm/immunology_module/prologue/objectives/obj02.html

Flannery, AR., Czibener, C., Andrews, NW. (2010). *Palmitoylation-dependent association with CD63 targets the Ca²⁺ sensor synaptotagmin VII to lysosomes*. J Cell Biol.191(3):599-613.

Fowler, KT., Andrews, NW., Huleatt, JW. (2007). *Expression and function of synaptotagmin VII in CTLs*. J Immunol. 178(3):1498-1504.

Fooksman, DR., Vardhana, S., Vasiliver-Shamis, G., Liese, J., Blair, DA., Waite, J., Sacristán, C., Victora, GD., Zanin-Zhorov, A., Dustin, ML (2010). *Functional anatomy of T cell activation and synapse formation*. Annu Rev Immunol. 28:79-105.

Fukuda, R., Hirota, K., Fan, F., Jung, YD., Ellis, LM., Semenza, GL. (2002). *Insulin-like growth factor 1 induces hypoxia-inducible factor 1-mediated vascular endothelial growth factor expression, which is dependent on MAP kinase and phosphatidylinositol 3-kinase signaling in colon cancer cells*. J Biol Chem. 277(41): 38205-38211.

Fukuda, M. (2003). *Molecular cloning and characterization of human, rat, and mouse synaptotagmin XV*. Biochem. Biophys. Res. Commun. 306, 64-71.

Fukuda, M., Kanno, E., Satoh, M., Saegusa, C., Yamamoto, A. (2004). *Synaptotagmin VII is targeted to dense-core vesicles and regulates their Ca²⁺-dependent exocytosis in PC12 cells*. J Biol Chem. 279:52677-52684.

Gao, Z., Reavey-Cantwell, J., Young, R. A., Jegier, P. and Wolf, B. A. (2000). *Synaptotagmin III/VII isoforms mediate Ca²⁺-induced insulin secretion in pancreatic islet beta-cells*. J. Biol. Chem. 275,36079-36085.

Gao, Y., Zorman, S., Gundersen, G., Xi, Z., Ma, L., Sirinakis, G., Rothman, JE., Zhang, Y. (2012). *Single reconstituted neuronal SNARE complexes zipper in three distinct stages*. Science. 337(6100):1340-3.

Gaud, G., Lesourne, R., Love, PE. (2018). *Regulatory mechanisms in T cell receptor signaling*. Nature Reviews Immunology 18, 485-497.

Geppert, M., Archer III, B. T., Sudhof, TC. (1991). *Synaptotagmin II: A novel differentially distributed form of synaptotagmin*. J. Biol.Chem. 266, 13548-13552.

Glavan, G., Schliebs, R., Zivin, M. (2009). *Synaptotagmins in neurodegeneration*. Anat Rec (Hoboken) 292(12):1849-62.

Goda, Y., Stevens, CF. (1994). *Two components of transmitter release at a central synapse*. Proc. Natl Acad. Sci. USA, 91, 12942–12946.

Grakoui, A., Bromley, SK., Sumen, C., Davis, MM., Shaw, AS., Allen, PM. and Dustin, ML. (1999). *The immunological synapse: a molecular machine controlling T cell activation*. Science 285, 221-227.

Griffiths, GM., Tsun, A., Stinchcombe, JC. (2010). *The immunological synapse: a focal point for endocytosis and exocytosis*. J Cell Biol. 189(3):399-406.

Grynkiewicz, G., Poenie, M., Tsien, RY. (1985). *A new generation of Ca²⁺ indicators with greatly improved fluorescence properties*. J Biol Chem. 260(6):3440-50.

Gustavsson, N., Lao, Y., Maximov, A., Chuang, JC., Kostromina, E., Repa, JJ., Li. C., Radda, GK., Südhof, TC., Han, W. (2008). *Impaired insulin secretion and glucose intolerance in synaptotagmin-7 null mutant mice*. Proc Natl Acad Sci U S A. 105(10):3992-7.

Gustavsson, N., Wei, SH., Hoang, DN., Lao, Y., Zhang, Q., Radda, GK., Rorsman, P., Südhof, TC., Han, W. (2009). *Synaptotagmin-7 is a principal Ca²⁺ sensor for Ca²⁺ - induced glucagon exocytosis in pancreas*. J Physiol. 587(Pt 6):1169-78.

Haddad, E.K., Wu, X., Hammer III, J.A., Henkart, PA. (2001). *Defective granule exocytosis in Rab27a-deficient lymphocytes from ashen mice*. J. Cell Biol. 152:835–841.

Halimani, M., Pattu, V., Marshall, MR., Chang, HF., Matti, U., Jung, M., Becherer, U., Krause, E., Hoth, M., Schwarz, EC., Rettig, J. (2014). *Syntaxin11 serves as a t-SNARE for the fusion of lytic granules in human cytotoxic T lymphocytes*. Eur J Immunol. 44(2):573-84.

- Han, J., Pluhackova, K., Böckmann, RA. (2017). *The Multifaceted Role of SNARE Proteins in Membrane Fusion*. *Front Physiol.* 8:5.
- Hogan, PG., Lewis, RS., Rao, A. (2010). *Molecular basis of calcium signaling in lymphocytes: STIM and ORAI*. *Annu Rev Immunol.* 28:491-533.
- Hosoi, N., Sakaba, T., Neher, E. (2007). *Quantitative analysis of calcium-dependent vesicle recruitment and its functional role at the calyx of Held synapse*. *J Neurosci.* 27(52):14286-98.
- Hui, E., Bai, J., Wang, P., Sugimori, M., Llinas, RR., Chapman, ER. (2005). *Three distinct kinetic groupings of the synaptotagmin family: candidate sensors for rapid and delayed exocytosis*. *Proc Natl Acad Sci U S A.* 102(14):5210-4.
- Hyrz, KL., Bownik, JM., Goldberg, MP. (2000). *Ionic selectivity of low-affinity ratiometric calcium indicators: mag-Fura-2, Fura-2FF and BTC*. *Cell Calcium.* 27(2):75-86.
- Imig, C., Min, SW., Krinner, S., Arancillo, M., Rosenmund, C., Südhof, T.C., Rhee, J., Brose, N., and Cooper, BH. (2014). *The morphological and molecular nature of synaptic vesicle priming at presynaptic active zones*. *Neuron* 84, 416–431.
- Jackman, SL., Turecek, J., Belinsky, JE., and Regehr, WG. (2016). *The calcium sensor synaptotagmin 7 is required for synaptic facilitation*. *Nature* 529, 88–91.
- Jahn, R., Südhof, TC. (1999). *Membrane fusion and exocytosis*. *Annu Rev Biochem.* 68:863-911.
- Jahn, R., Lang, T., Südhof, TC. (2003). *Membrane fusion*. *Cell.* 112(4):519-33.
- Jahn, R, Scheller, RH. (2006). *SNAREs—engines for membrane fusion*. *Nat Rev Mol Cell Biol* 7:631–643.
- Jaiswal, JK., Chakrabarti, S., Andrews, NW., Simon, SM. (2004). *Synaptotagmin VII restricts fusion pore expansion during lysosomal exocytosis*. *PLoS Biol.* 2(8): E233.
- Janeway, CA. Jr, Travers, P., Walport, M., et al. (2001). *Immunobiology: The Immune System in Health and Disease 5th edition: T cell-mediated cytotoxicity*. New York: Garland Science
- Kabanova, A., Zurli, V., Baldari, CT. (2018). *Signals Controlling Lytic Granule Polarization at the Cytotoxic Immune Synapse*. *Front Immunol.* 9:307.
- Katz, B., Miledi, R. (1965). *The effect of calcium on acetylcholine release from motor nerve terminals*. *Proc R Soc Lond B Biol Sci.* 161:496-503.

Karatekin, E., Tran, VS., Huet, S., Fanget, I., Cribier, S., Henry, JP. (2008). *A 20-nm step toward the cell membrane preceding exocytosis may correspond to docking of tethered granules*. *Biophys J.* 94(7):2891-905.

Kloepper, TH., Kienle, CN., Fasshauer, D. (2007). *An elaborate classification of SNARE proteins sheds light on the conservation of the eukaryotic endomembrane system*. *Mol Biol Cell.* 18(9):3463-71.

Lancki, DW., Weiss, A., Fitch, FW. (1987). *Requirements for triggering of lysis by cytolytic T lymphocyte clones*. *J. Immunol.*, 138:3646-3653

Lazarenko, LM., Babenko, LP., Bubnov, RV., Demchenko, OM., Zotsenko, VM., Boyko, NV., et al. *Imunobiotics are the novel biotech drugs with antibacterial and Immunomodulatory properties*. *Mikrobiol Z.* 79(1):66–75

Leong, AS., Cooper, K., Leong, FJ. (2003). *Manual of diagnostic antibodies for immunohistology*. 2nd edition, Greenwich Medical Media ISBN 1 84110 100 1.

Lewis, RS. (2001). *Calcium signaling mechanisms in T lymphocytes*. *Annu Rev Immunol.* 19:497-521.

Li, Y., Wang, P., Xu, J., Gorelick, F., Yamazaki, H., Andrews, N., Desir, GV. (2007). *Regulation of insulin secretion and GLUT4 trafficking by the calcium sensor synaptotagmin VII*. *Biochem Biophys Res Commun.* 2007 Oct 26;362(3):658-64.

Liou, J., Fivaz, M., Inoue, T., Meyer, T. (2007). *Live-cell imaging reveals sequential oligomerization and local plasma membrane targeting of stromal interaction molecule 1 after Ca²⁺ store depletion*. *Proc Natl Acad Sci U S A.* 104(22):9301-9306.

Littleton, JT., Bai, J., Vyas, B., Desai, R., Baltus, AE., Garment, MB., Carlson, SD., Ganetzky, B., Chapman, ER. (2001). *Synaptotagmin mutants reveal essential functions for the C2B domain in Ca²⁺-triggered fusion and recycling of synaptic vesicles in vivo*. *J Neurosci.* 21(5):1421-33.

Liu, C., Bickford, LS., Held RG., Nyitrai, H., Südhof, TC., Kaeser, PS. (2014). *The active zone protein family ELKS supports Ca²⁺ influx at nerve terminals of inhibitory hippocampal neurons*. *J. Neurosci.* 34: 12289-12303.

Liu, H., Bai, H., Hui, E., Yang, L., Evans, CS., Wang, Z., Kwon, SE., Chapman, ER. (2014). *Synaptotagmin 7 functions as a Ca²⁺-sensor for synaptic vesicle replenishment*. *Elife.*3:e01524.

Luo, F., Südhof, TC. (2017). *Synaptotagmin-7-Mediated Asynchronous Release Boosts High-Fidelity Synchronous Transmission at a Central Synapse*. *Neuron.*94(4):826-839.e3

Lyubchenko, TA., Wurth, GA., Zweifach, A. (2001). *Role of calcium influx in cytotoxic T lymphocyte lytic granule exocytosis during target cell killing*. *Immunity* 15(5):847-59.

- MacDougall, DD., Lin, Z., Chon, NL., Jackman, SL., Lin, H., Knight, JD., Anantharam, A. (2018). *The high-affinity calcium sensor synaptotagmin-7 serves multiple roles in regulated exocytosis*. J Gen Physiol. 150(6):783-807.
- Martinez, I., Chakrabarti, S., Hellevik, T., Morehead, J., Fowler, K., Andrews, NW. (2000). *Synaptotagmin VII regulates Ca²⁺-dependent exocytosis of lysosomes in fibroblasts*. J Cell Biol. 148(6):1141-49.
- Martínez-Lostao, L., Anel, A., Pardo, J. (2015). *How Do Cytotoxic Lymphocytes Kill Cancer Cells?* Clin Cancer Res. 21(22):5047-56.
- Matsuoka, H., Harada, K., Nakamura, J., Fukuda, M., Inoue, M. (2011). *Differential distribution of synaptotagmin-1, -4, -7, and -9 in rat adrenal chromaffin cells*. Cell Tissue Res. 344:41–50.
- Mattheyses, AL., Simon, SM., Rappoport, JZ. (2010). *Imaging with total internal reflection fluorescence microscopy for the cell biologist*. J Cell Sci.123(Pt 21):3621-8.
- Matti, U., Pattu, V., Halimani, M., Schirra, C., Krause, E., Liu, Y., Weins, L., Chang, HF., Guzman, R., Olausson, J., Freichel, M., Schmitz, F., Pasche, M., Becherer, U., Bruns, D., Rettig, J. (2013). *Synaptobrevin2 is the v-SNARE required for cytotoxic T-lymphocyte lytic granule fusion*. Nat Commun. 4:1439.
- Maximov, A., Lao, Y., Li, H., Chen, X., Rizo, J., Sørensen, JB., Südhof, TC. (2008). *Genetic analysis of synaptotagmin-7 function in synaptic vesicle exocytosis*. Proc Natl Acad Sci U S A.105(10):3986-91.
- McIlwain, DR., Berger, T., Mak, TW. (2013). *Caspase functions in cell death and disease*. Cold Spring Harb Perspect Biol. 5(4): a008656.
- Medzhitov, R., Janeway, C Jr. (2000). *Innate immune recognition: mechanisms and pathways*. Immunol Rev. 173:89-97.
- Michaut, M., De Blas, G., Tomes, CN., Yunes, R., Fukuda, M., Mayorga, LS. (2001). *Synaptotagmin VI participates in the acrosome reaction of human spermatozoa*. Dev Biol. 235(2):521-9.
- Ming, M., Schirra, C., Becherer, U., Stevens, DR., Rettig, J. (2015). *Behavior and Properties of Mature Lytic Granules at the Immunological Synapse of Human Cytotoxic T Lymphocytes*. PLoS One. 10(8): e0135994.
- Molnar, C., Gair, J. (2013). *Concepts of Biology-1st Canadian Edition*. Rice University.
- Murphy, K., Reiner, S (2002). *The lineage decisions of helper T cells*. Nat Rev Immunol. 2:933–44.

Nalefski, EA., Wisner, MA., Chen, JZ., Sprang, SR., Fukuda, M., Mikoshiba, K., Falke, JJ. (2001). *C2 domains from different Ca²⁺ signaling pathways display functional and mechanistic diversity*. *Biochemistry* 40:3089-3100

Ockenga W., (2012). *Total Internal Reflection Fluorescence (TIRF) Microscopy* Retrieved from <https://www.leica-microsystems.com/science-lab/total-internal-reflection-fluorescence-tirf-microscopy>.

Olsen, SJ., Tarte, K., Sherman, W., Hale, EE., Weisse, MT., Orazi, A., Klein, B., Chang, Y. (1998). *Evidence against KSHV infection in the pathogenesis of multiple myeloma*. *Virus Res.* 57(2):197-202.

Osińska, I., Popko, K., Demkow, U. (2014). *Perforin: an important player in immune response*. *Cent Eur J Immunol.* 39(1):109-15.

Osterberg, JR., Chon, NL., Boo, A., Maynard, FA., Lin, H., Knight, JD. (2015). *Membrane Docking of the Synaptotagmin 7 C2A Domain: Electron Paramagnetic Resonance Measurements Show Contributions from Two Membrane Binding Loops*. *Biochemistry.* 54(37):5684-95.

Palfreyman, M., Jorgensen, E. (2010). *Roles of SNARE Proteins in Synaptic Vesicle Fusion*. 10.1007/1-59745-481-8_3.

Pang, ZP., Sun, J., Rizo, J., Maximov, A., Südhof, TC. (2006a). *Genetic analysis of synaptotagmin 2 in spontaneous and Ca²⁺-triggered neurotransmitter release*. *EMBO J.* 25(10):2039-50.

Pang, ZP., Melicoff, E., Padgett, D., Liu, Y., Teich, AF., Dickey, BF., Lin, W., Adachi, R., Südhof, TC. (2006b). *Synaptotagmin-2 is essential for survival and contributes to Ca²⁺ triggering of neurotransmitter release in central and neuromuscular synapses*. *J Neurosci.* 26(52):13493-504.

Pattu, V., Halimani, M., Ming, M., Schirra, C., Hahn, U., Bzeih, H., Chang, HF., Weins, L., Krause, E., Rettig, J. (2013). *In the crosshairs: investigating lytic granules by high-resolution microscopy and electrophysiology*. *Front Immunol.* 4:411.

Peters, PJ., Borst, J., Oorschot, V., Fukuda, M., Krähenbühl, O., Tschopp, J., Slot, JW., Geuze, HJ. (1991). *Cytotoxic T lymphocyte granules are secretory lysosomes, containing both perforin and granzymes*. *J Exp Med.* 173(5):1099-109.

Pinheiro, PS., Houy, S., Sørensen, JB. (2016). *C2-domain containing calcium sensors in neuroendocrine secretion*. *J Neurochem.* 139(6):943-958.

Prakriya, M., Lewis, RS. (2015). *Store-Operated Calcium Channels*. *Physiol Rev.* 95(4):1383-436.

- Qu, B., Al-Ansary, D., Kummerow, C., Hoth, M., Schwarz, EC. (2011). *ORAI-mediated calcium influx in T cell proliferation, apoptosis and tolerance*. Cell Calcium. 50(3):261-9.
- Quintana, A., Pasche, M., Junker, C., Al-Ansary, D., Rieger, H., Kummerow, C., Nuñez, L., Villalobos, C., Meraner, P., Becherer, U., Rettig, J., Niemeyer, BA., Hoth, M. (2011). *Calcium microdomains at the immunological synapse: how ORAI channels, mitochondria and calcium pumps generate local calcium signals for efficient T-cell activation*. EMBO J. 30(19):3895-912.
- Rao, TC., Passmore, DR., Peleman, AR., Das, M., Chapman, ER., Anantharam, A. (2014). *Distinct fusion properties of synaptotagmin-1 and synaptotagmin-7 bearing dense core granules*. Mol Biol Cell. 25(16):2416-27.
- Rao, TC., Santana Rodriguez, Z., Bradberry, MM., Ranski, AH., Dahl, PJ., Schmidtke, MW., Jenkins, PM., Axelrod, D., Chapman, ER., Giovannucci, DR., Anantharam, A. (2017). *Synaptotagmin isoforms confer distinct activation kinetics and dynamics to chromaffin cell granules*. J. Gen. Physiol. 149:763–780.
- Reddy, A., Caler, EV., Andrews, NW. (2001). *Plasma membrane repair is mediated by Ca²⁺-regulated exocytosis of lysosomes*. Cell. 106(2):157-69.
- Rhee, JS., Li, LY., Shin, OH., Rah, JC., Rizo, J., Südhof, TC., Rosenmund, C. (2005). *Augmenting neurotransmitter release by enhancing the apparent Ca²⁺ affinity of synaptotagmin 1*. Proc Natl Acad Sci U S A. 102(51):18664-9.
- Rozov, A., Bolshakov, AP., Valiullina-Rakhmatullina, F. (2019). *The Ever-Growing Puzzle of Asynchronous Release*. Front Cell Neurosci.13:28.
- Sakaba, T., Neher, E. (2001). *Calmodulin mediates rapid recruitment of fast-releasing synaptic vesicles at a calyx-type synapse*. Neuron. 32(6):1119-31.
- Segovia, M., Alés, E., Montes, MA., Bonifas, I., Jemal, I., Lindau, M., Maximov, A., Südhof, TC., Alvarez de Toledo, G. (2010). *Push-and-pull regulation of the fusion pore by synaptotagmin-7*. Proc Natl Acad Sci U S A.107(44):19032-7.
- Shaw, PJ., Feske, S. (2012). *Regulation of lymphocyte function by ORAI and STIM proteins in infection and autoimmunity*. J Physiol. 590(17):4157-67.
- Shedlock, DJ., Shen, H. (2003). *Requirement for CD4 T Cell help in generating functional CD8 T cell memory*. Sci Just. 300:337–9.
- Shen, Y., Rosendale, M., Campbell, RE., Perrais, D. (2014). *pHuji, a pH-sensitive red fluorescent protein for imaging of exo- and endocytosis*. J Cell Biol. 207(3):419-32.
- Simon, SM., Llinás, RR. (1985). *Compartmentalization of the submembrane calcium activity during calcium influx and its significance in transmitter release*. Biophys J 48:485–498.

Stinchcombe, JC., Barral, DC., Mules, EH., Booth, S., Hume, AN., Machesky, LM., Seabra, MC., Griffiths, GM. (2001). *Rab27a is required for regulated secretion in cytotoxic T lymphocytes*. J Cell Biol. 152(4):825-34.

Südhof, TC., Rizo, J. (2011). *Synaptic vesicle exocytosis*. Cold Spring Harb Perspect Biol. 3(12). pii: a005637.

Südhof, TC. (2002). *Synaptotagmins: why so many?* J Biol Chem. 277(10):7629-32.

Südhof, TC. (2004). *The synaptic vesicle cycle*. Annu Rev Neurosci. 27:509-47.

Sugita, S., Han, W., Butz, S., Liu, X., Fernández-Chacón, R., Lao, Y., Südhof, TC. (2001). *Synaptotagmin VII as a plasma membrane Ca²⁺ sensor in exocytosis*. Neuron 30(2):459-73.

Sugita, S., Shin, OH., Han, W., Lao, Y., Südhof, TC. (2002). *Synaptotagmins form a hierarchy of exocytotic Ca²⁺ sensors with distinct Ca²⁺ affinities*. EMBO J. 21(3):270-80.

Sun, J-, Pang, ZP., Qin, D., Fahim, AT., Adachi, R., Südhof, TC. (2007). *A dual-Ca²⁺-sensor model for neurotransmitter release in a central synapse*. Nature. 450(7170):676-82.

Sutton, RB., Davletov, BA., Berghuis, AM., Südhof, TC., Sprang, SR. (1995). *Structure of the first C2 domain of synaptotagmin I: a novel Ca²⁺/phospholipid-binding fold*. Cell. 80(6):929-38.

Sutton, RB., Fasshauer, D., Jahn, R., Brunger, AT. (1998). *Crystal structure of a SNARE complex involved in synaptic exocytosis at 2.4 Å resolution*. Nature.395(6700):347-53.

Sutton, RB., Ernst, JA., Brunger, AT. (1999). *Crystal structure of the cytosolic C2A-C2B domains of synaptotagmin III. Implications for Ca²⁺-independent snare complex interaction*. J Cell Biol. 147(3):589-98.

Toonen, RF., Kochubey, O., de Wit, H., Gulyas-Kovacs, A., Konijnenburg, B., Sørensen, JB., Klingauf, J., Verhage M. (2006). *Dissecting docking and tethering of secretory vesicles at the target membrane*. EMBO J. 25(16):3725-37.

Ubach, J., Zhang, X., Shao, X., Südhof, TC., Rizo, J. (1998). *Ca²⁺ binding to synaptotagmin: how many Ca²⁺ ions bind to the tip of a C2-domain?* EMBO J. 17(14):3921-30.

Verhage, M., Sørensen, JB. (2008). *Vesicle docking in regulated exocytosis*. Traffic. ;9(9):1414-24.

Vig, M., Kinet, JP. (2009). *Calcium signaling in immune cells*. Nat Immunol. 10(1):21-7.

- Virmani, T., Han, W., Liu, X., Südhof, TC., Kavalali, ET. (2003). *Synaptotagmin 7 splice variants differentially regulate synaptic vesicle recycling*. EMBO J. 22(20):5347-57.
- Voets, T., Toonen, RF., Brian, EC., de Wit, H., Moser, T., Rettig, J., Südhof, TC., Neher, E., Verhage, M. (2001). *Munc18-1 promotes large dense-core vesicle docking*. Neuron. 31(4):581-91.
- Voleti, R., Tomchick, DR., Südhof, TC., Rizo, J. (2017). *Exceptionally tight membrane-binding may explain the key role of the synaptotagmin-7 C2A domain in asynchronous neurotransmitter release*. Proc Natl Acad Sci U S A. 114(40): E8518-E8527.
- Voskoboinik, I., Thia, MC., Trapani, JA. (2005). *A functional analysis of the putative polymorphisms A91V and N252S and 22 missense perforin mutations associated with familial hemophagocytic lymphohistiocytosis*. Blood. 105(12):4700-6.
- Wang, P., Chicka, MC., Bhalla, A., Richards, DA., Chapman, ER. (2005). *Synaptotagmin VII is targeted to secretory organelles in PC12 cells, where it functions as a high-affinity calcium sensor*. Mol Cell Biol. 25(19):8693-702.
- Wang, C., Wang, Y., Hu, M., Chai, Z., Wu, Q., Huang, R., Han, W., Zhang, CX., Zhou, Z. (2016). *Synaptotagmin-11 inhibits clathrin-mediated and bulk endocytosis*. EMBO Rep. 17(1):47-63.
- Wang, T., Li, L., Hong, W. (2017). *SNARE proteins in membrane trafficking*. Traffic. 18(12):767-775.
- Weber, JP., Toft-Bertelsen, TL., Mohrmann, R., Delgado-Martinez, I., Sørensen, JB. (2014). *Synaptotagmin-7 is an asynchronous calcium sensor for synaptic transmission in neurons expressing SNAP-23*. PLoS One. 9(11): e114033.
- Wei, D., Cao, X. (2018). *Cytotoxic Pathways in Allogeneic Hematopoietic Cell Transplantation*. Front. Immunol 9.
- Wen, H., Linhoff, MW., McGinley, MJ., Li, GL., Corson, GM., Mandel, G., Brehm, P. (2010). *Distinct roles for two synaptotagmin isoforms in synchronous and asynchronous transmitter release at zebrafish neuromuscular junction*. Proc Natl Acad Sci U S A. 107(31):13906-11.
- Wu, B., Wie, S., Petersen, N., Ali, Y., Wang, X., Bacaj, T., Rorsman, P., Hong, W., Südhof, TC., Han, W. (2015). *Synaptotagmin-7 phosphorylation mediates GLP-1-dependent potentiation of insulin secretion from β -cells*. Proc Natl Acad Sci U S A. 112(32):9996-10001.
- Wu, Z., Thiyagarajan, S., O'Shaughnessy, B., Karatekin, E. (2017). *Regulation of Exocytotic Fusion Pores by SNARE Protein Transmembrane Domains*. Front Mol Neurosci. 10:315.

Xu, J., Mashimo, T., Südhof, TC. (2007). *Synaptotagmin-1, -2, and -9: Ca²⁺ sensors for fast release that specify distinct presynaptic properties in subsets of neurons*. Neuron. 54(4):567-81.

Xu, J., Pang, ZP., Shin, OH., Südhof, TC. (2009). *Synaptotagmin-1 functions as a Ca²⁺ sensor for spontaneous release*. Nat Neurosci.12(6):759-66.

Yoshihara, M., Adolfsen, B., Littleton, JT. (2003). *Is synaptotagmin the calcium sensor?* Curr Opin Neurobiol. 13(3):315-23.

Zhang, SL., Yu, Y., Roos, J., Kozak, JA., Deerinck, TJ., Ellisman, MH., Stauderman, KA., Cahalan, MD. (2005). *STIM1 is a Ca²⁺ sensor that activates CRAC channels and migrates from the Ca²⁺ store to the plasma membrane*. Nature. 437(7060):902-5.

Zhang, Z., Hui, E, Chapman, ER., Jackson, M.B.. (2010). *Regulation of exocytosis and fusion pores by synaptotagmin-effector interactions*. Mol. Biol. Cell. 21:2821–2831.

Zhang, Z., Wu, Y., Wang, Z., Dunning, F.M., Rehfuss, J., Ramanan, D., Chapman, ER., Jackson, M.B. (2011). *Release mode of large and small dense-core vesicles specified by different synaptotagmin isoforms in PC12 cells*. Mol. Biol. Cell. 22:2324–2336.

Zhao, H., Ito, Y., Chappel, J., Andrews, NW., Teitelbaum, SL., Ross, FP. (2008). *Synaptotagmin VII regulates bone remodeling by modulating osteoclast and osteoblast secretion*. Dev. Cell. 14:914–925.

Zhao, WD., Hamid, E., Shin, W., Wen, PJ., Krystofiak, ES., Villarreal, SA., Chiang, HC., Kachar, B., Wu, LG. (2016). *Hemi-fused structure mediates and controls fusion and fission in live cells*. Nature. 534:548–552.

Zhou, X., Friedmann, K.S., Lyrmann, H., Zhou, Y., Schoppmeyer, R., Knörck, A., Mang, S., Hoxha, C., Angenendt, A., Backes, C.S., Mangerich, C., Zhao, R., Cappello, S., Schwär, G., Hässig, C., Neef, M., Bufe, B., Zufall, F., Kruse, K., Niemeyer, B.A., Lis, A., Qu, B., Kummerow, C., Schwarz, E.C., Hoth, M. (2018). *A calcium optimum for cytotoxic T lymphocyte and natural killer cell cytotoxicity*. J Physiol. 596(14):2681-2698.

Zucker, RS. (1996). *Exocytosis: a molecular and physiological perspective*. Neuron. 17:1049–1055.

Zucker, RS., Regehr, WG. (2002). *Short-term synaptic plasticity*. Annu. Rev. Physiol. 64:355–405.

Resume

Marwa Sleiman

Place of birth: Saida, Lebanon

Date of birth: 08.08.1988

Education

2014-2019	Saarland University	PhD in Immunology
2011-2012	Lebanese University	Master 2 in Molecular Immunology
2010-2011	Lebanese University	Master 1 in Biochemistry
2007-2010	Lebanese University	Bachelor of Science

Publications

Sleiman, M. et al. (2020) Cytotoxic Granule Trafficking and Fusion in Synaptotagmin7-Deficient Cytotoxic T Lymphocytes. *Front. Immunol.* doi: 10.3389/fimmu.2020.01080

Chitirala, P., Sleiman, M. et al. (2019) Cytotoxic granule exocytosis from human cytotoxic T lymphocytes is mediated by VAMP7. *Front. Immunol.* | doi: 10.3389/fimmu.2019.01855

Chang, HF., Sleiman, M. et al. (2017). Preparing the lethal hit: interplay between exo- and endocytic pathways in cytotoxic T lymphocytes. *Cell Mol Life Sci.* 74(3):399-408

Sleiman, M. et al. (2017). Simultaneous Membrane Capacitance Measurements and TIRF Microscopy to Study Granule Trafficking at Immune Synapses. *Methods Mol Biol-Springer Nature.* 1584:157-169.